

AD-A162 520

AIR PARCEL MOTION AT THE VANDENBERG HYDROGEN FLARE
STACKS(U) NAVAL POSTGRADUATE SCHOOL MONTEREY CA
G E SCHACHER ET AL OCT 85 NPS-61-86-005

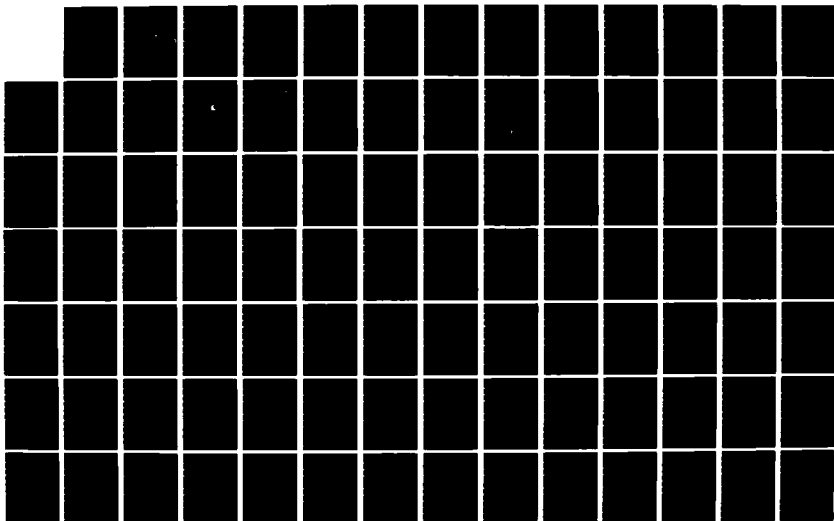
1/2

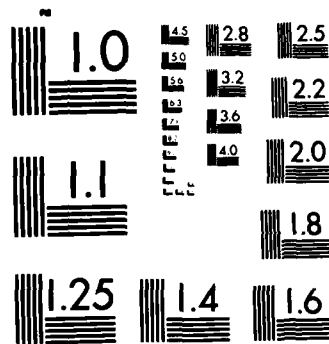
UNCLASSIFIED

MIPR-FV6168500914

F/G 19/1

NL





MICROCOPY RESOLUTION TEST CHART
NATIONAL BUREAU OF STANDARDS 1963-A

AD-A162 520

NAVAL POSTGRADUATE SCHOOL

Monterey, California



DTIC
ELECTE
DEC 24 1985
S D

AIR PARCEL MOTION AT THE VANDENBERG
HYDROGEN FLARE STACKS

by

Gordon E. Schacher and Charles E. Skupniewicz

October 1985

Approved for public release; distribution unlimited

Prepared for: STG/SAFC
Vandenberg AFB, CA 93437

DTIC FILE COPY

NAVAL POSTGRADUATE SCHOOL
Monterey, California


Commodore R. H. Shumaker
Superintendent


D. A. Schrady
Provost

The work reported herein was supported in part by STG/SAFC,
Vandenberg AFB, California


Reproduction of all or part of this report is authorized.

This report was prepared by:



G. E. SCHACHER
Professor of Physics


C. E. SKUPNIEWICZ
Atmospheric Scientist

Approved by:


G. E. SCHACHER
Chairman, Dept. of Physics

Released by:


J. N. DYER
Dean of Science and Engineering

UNCLASSIFIED

SECURITY CLASSIFICATION OF THIS PAGE (When Data Entered)

REPORT DOCUMENTATION PAGE		READ INSTRUCTIONS BEFORE COMPLETING FORM
1. REPORT NUMBER NPS-61-86-005	2. GOVT ACCESSION NO. AD-A162	3. RECIPIENT'S CATALOG NUMBER 520
4. TITLE (and Subtitle) Air Parcel Motion at the Vandenberg Hydrogen Flare Stacks		5. TYPE OF REPORT & PERIOD COVERED Dec. 1984 - Oct. 1985
7. AUTHOR(s) Gordon E. Schacher and Charles E. Skupniewicz		6. PERFORMING ORG. REPORT NUMBER
9. PERFORMING ORGANIZATION NAME AND ADDRESS		8. CONTRACT OR GRANT NUMBER(s)
11. CONTROLLING OFFICE NAME AND ADDRESS 6595 STG/SAFC ATTN: LT R. G. Johnson Bldg. 8500, Vandenberg AFB, CA 93437		10. PROGRAM ELEMENT, PROJECT, TASK AREA & WORK UNIT NUMBERS MIPR NUMBER FY6168500914
14. MONITORING AGENCY NAME & ADDRESS (if different from Controlling Office)		12. REPORT DATE October 1985
		13. NUMBER OF PAGES 119
		15. SECURITY CLASS. (of this report) UNCLASSIFIED
		15a. DECLASSIFICATION/DOWNGRADING SCHEDULE
16. DISTRIBUTION STATEMENT (of this Report) Distribution unlimited		
17. DISTRIBUTION STATEMENT (of the abstract entered in Block 20, if different from Report)		
18. SUPPLEMENTARY NOTES		
19. KEY WORDS (Continue on reverse side if necessary and identify by block number) Turbulence, Complex Terrain, Plume Motion		
20. ABSTRACT (Continue on reverse side if necessary and identify by block number) Three months of flow and turbulence data obtained at the Vandenberg AFB hydrogen flare stack site has been used to simulate the behavior of the plume. Time series analyses have been used to determine air parcel trajectories. Turbulence in the area is sufficient to carry air parcels to ground level. The spatial persistence of the trajectory end and function of time spent near the average position have been determined as functions of conditions. The results have been prepared and methodologies outlined to enable heat deposition calculation to be performed.		

DD FORM 1 JAN 73 1473

EDITION OF 1 NOV 68 IS OBSOLETE
S/N 0102-LF-014-6601

UNCLASSIFIED

SECURITY CLASSIFICATION OF THIS PAGE (When Data Entered)

INDEX

	<u>PAGE</u>
I. Introduction	1
II. Location	3
III. Equipment	8
IV. Calculation of Air Parcel Motion	12
V. Background Meteorology	16
1. Correlation with Tower 301	16
2. Wind direction probability, orographic effects	18
3. Mean wind elevation angle	25
VI. Displacement Calculations	29
1. Air parcel trajectory profiles	31
2. Maximum displacement	36
VII. Trajectory End Statistics	50
1. Persistence	50
2. Fraction of time	65
VIII. Spectral Analysis	77
IX. Wind Climatology	86
X. Heat Deposition Calculations	95
1. General considerations	95
2. Use of fraction of time	98
3. Use of persistence	99
4. Non-Uniform heat deposition	101
XI. Summary	105

ACKNOWLEDGMENT

Lts Robert Johnson and Paul Mueller have rendered a great deal of assistance in this project. Lt Johnson's efforts in helping us get the project underway and coordinating NPS and Vandenberg work were indispensable. We thank Drs. Soren Larsen and Torben Mikkelsen for many valuable discussions, especially Dr. Mikkelsen's work on spectral analysis.



Accession For	
NTIS CRA&I	<input checked="checked" type="checkbox"/>
DTIC TAB	<input type="checkbox"/>
Unannounced	<input type="checkbox"/>
Justification	
By	
Distribution /	
Availability Codes	
Dist	Avail and/or Special
A-1	

LIST OF FIGURE

	<u>PAGE</u>
Figure 1. Placement of flare stacks and location of area where a hazard may exist at the Vandenberg AFB Space Shuttle launch site.	5
Figure 2. Horizontal view of the flare stack site, showing elevation of the stacks, hydrogen storage dewar, and terrain.	6
Figure 3. Rough schematic of the Space Shuttle launch site and surrounding terrain, showing location of meteorological tower 301.	7
Figure 4. Structure used to mount the bivariate anemometer on top of the flare stacks.	11
Figure 5. Idealized behavior of the motion of the flare stack plume between successive time steps. The apparent advection is unrealistically large.	15
Figure 6. Wind direction difference (WD flare-WD 301) as a function of the wind direction at 301.	17
Figure 7. Number of 10 min data files that were obtained during the flare stack experiment as a function of wind speed and direction.	20
Figure 8. Probability of the wind being from a particular direction at the flare stacks within each 60 deg range.	21
Figure 9. Probability of the wind being from a particular direction at meteorological tower 301 within each 60 deg range.	23
Figure 10. Mean wind elevation angle as a function of wind direction.	27
Figure 11. Polar plot of the magnitude of the elevation angle. The dashed line shows the zero elevation wind directions.	28
Figure 12. Illustration of the calculation of the displacements of the air parcels that make up a plume.	30

Figure 13.	Second-by-second vertical air parcel trajectory profiles for 25, 50 and 95 ft.	32
Figure 14.	Percent occurrence of a given maximum vertical displacement, and cumulative percent for various wind speeds.	46
Figure 15.	Percent occurrence of maximum vertical and horizontal displacements.	47
Figure 16.	Cumulative percent occurrence, percent of occurrences within a given maximum displacement, for vertical and horizontal displacements.	48
Figure 17.	Percent of occurrences within 1 m and 2 m maximum vertical displacement as a function of wind direction range.	49
Figure 18.	Probability that the trajectory end will remain within a given distance for the specified time period.	53
Figure 19.	Probability that the trajectory end will remain within a given distance for the specified time period. Data is presented for the four wind speed ranges.	54
Figure 20.	Persistence probability data for various time periods versus the 5 sec and 10 sec probability data.	55
Figure 21.	5 sec persistence probability data for 2 m and 3 m versus the 1 m probability data.	56
Figure 22.	5sec-1m and 20sec-8m persistence probability data versus the 10sec-4m probability data.	57
Figure 23.	Persistence time probability universal curves to relate probabilities for various distances.	61
Figure 24.	Persistence time probability universal curves to relate probabilities for various times.	62
Figure 25.	Persistence time probability universal curves to relate 5sec-1m and 20sec-8m probabilities to 10sec-4m.	63
Figure 26.	10m-4sec persistence time probabilities as a function of wind direction range.	64

Figure 27. Fraction of the time that the plume end remains within a given displacement of its average position for the four averaging times. Two wind speed ranges are shown.	68
Figure 28. Fraction of the time the plume end remains within a given displacement of its average position for 10 and 120 sec averaging times for vertical and horizontal displacement.	69
Figure 29. Fraction of time data (dots) and superimposed error function fit (crosses).	74
Figure 30. Displacement standard deviations as a function of wind direction range.	76
Figure 31. Schematic of a single turbulence eddy superimposed on the mean flow and the assumed sinusoidal behavior of the vertical velocity.	78
Figure 32. Response of the plume to an idealized eddy for two different sized eddies.	79
Figure 33. Schematic power spectral density of vertical velocity and the area used to determine the mean-square vertical velocity at frequency f .	83
Figure 34. Conversion of a power spectrum into a displacement function. The dashed line is the power spectrum and the solid line the resulting displacement.	84
Figure 35. Example of power spectral density plots of vertical velocity.	85
Figure 36. Fractional occurrence of the wind as a function of wind direction for each month.	88
Figure 37. Probability that a south wind, when it occurs, will be at a particular time of day (non-normalized).	91
Figure 38. Flare stack wind direction as a function of time-of-day.	94
Figure 39. Geometrical picture of overlap between plume and hazard areas and overlap area versus center separation.	100

LIST OF TABLES

	PAGE
Table 1. Percent occurrence of a given maximum displacement as a function of wind speed and wind direction.	38
Table 2. Persistence time probabilities for 10sec-4m displacement.	65
Table 3. Error function and corrections to the error function fit to the fraction of time data as a function of the function of the standard deviation.	71
Table 4. Fraction of time standard deviations as a function of wind speed and wind direction.	75

I. INTRODUCTION

During the pre-launch and launch phases of the Space Shuttle, liquid hydrogen flows from a storage dewar to the main engine tanks. This operation may last for several hours, during which time a considerable amount of hydrogen gas is boiled off. This gas could be a safety hazard if allowed to accumulate in the area, thus it is disposed of by burning. At Vandenberg AFB (VBG) this is accomplished by two flare stacks which are in the immediate launch site area. The area is small enough that the flames from the flare stacks could represent a hazard to personnel and structures. The purpose of the work reported here is to determine if a significant hazard could exist.

One would normally assume that a gas as light as hydrogen would rise quickly when released from a stack. However, because hydrogen is so light, momentum transfer between it and the ambient air flowing past a stack will control the gas motion and it can be transported away from the stack imbedded in the surrounding flow. A flare one or two hundred feet long, moving nearly horizontally could be produced.

As a first step to understanding the flares, it is necessary to understand the air flow, both mean and turbulence, at the site. The flare stacks are located in a region of complex topography which makes it very difficult to predict either the mean flow or turbulence. The only reasonable approach to the problem is to measure these parameters. It is expected that air motion will depend dramatically on the local conditions, which means that the

measurements should be made under as wide a range of conditions as possible. Also, a significant amount of data for each condition should be obtained so that statistically significant probabilities for the air motion can be determined. During the course of this experiment, several months of data from two different sensor arrays were obtained, and a wide range of meteorological conditions were experienced.

It must be emphasized that this work does not determine the motion of the hydrogen flare but of the motion of the air at the flare stacks. A significant modeling effort is required to accurately determine the motion of the flare from these data. However, it is a reasonable approximation to assume the flare follows the ambient flow for wind speeds that are not too small.

This report describes the location, the equipment used, the analysis techniques, the assumptions made in the analyses, and the results. Details of the computer programs used in the analyses can be obtained from the authors.

II. LOCATION

The flare stack facility contains two stacks, 50 ft and 90 ft high. A top view of the locality, including nearby structures and critical areas, is shown in Figure 1. An elevation view of the immediate locality, viewed from the south, is shown in Figure 2. These figures do not do justice to the complexity of the area. The site is on the side of a hill that extends to the east and rises several hundred feet. Immediately to the north the hill is cut by a major canyon that extends to the east, and another lesser canyon is to the south. The area is on the edge of a ridge of coastal hills, which rise to almost 2000 feet within 2 miles. Figure 3 is a rough drawing of the area, attempting to represent the major features which will have a significant affect on the flow.

Refering to Figure 1, we see that the liquid hydrogen storage dewar is within 200 ft of the stacks. Also within 200 to 300 ft are the facilities for handling the hydrogen and the fuel unloading area. These are critical impact areas. The launch site is somewhat further away, 500 to 600 ft, with the closest structure being the MST building, a distance of 500 ft in its rolled back position. All of these critical areas are included in a wind direction arc from 000 to 110 deg.

Flow from the east could produce an impact on the hydrogen handling and storage area. From this direction, the flow is down the hillside and is expected to follow the terrain. This could

carry the flare down toward the critical area, so it is important to determine the mean declination of the flow for these conditions.

Another significant hazard is that the flare from the 50 ft high southerly stack impacting on the 90 ft high northerly stack. The wind direction for which this can occur is approximately 160 deg.

The location of the meteorological tower, 301, which will provide operational information for the Shuttle facility, is shown on Figure 3. This tower is in a more exposed location than the flare stack facility and the wind conditions are expected to be different there. Thus, a part of this study is to relate the winds at the two sites so that 301 data can be used to assess conditions at the flare stacks. Air flow patterns for the area, which will be explained later in this report, are also shown in Figure 3.

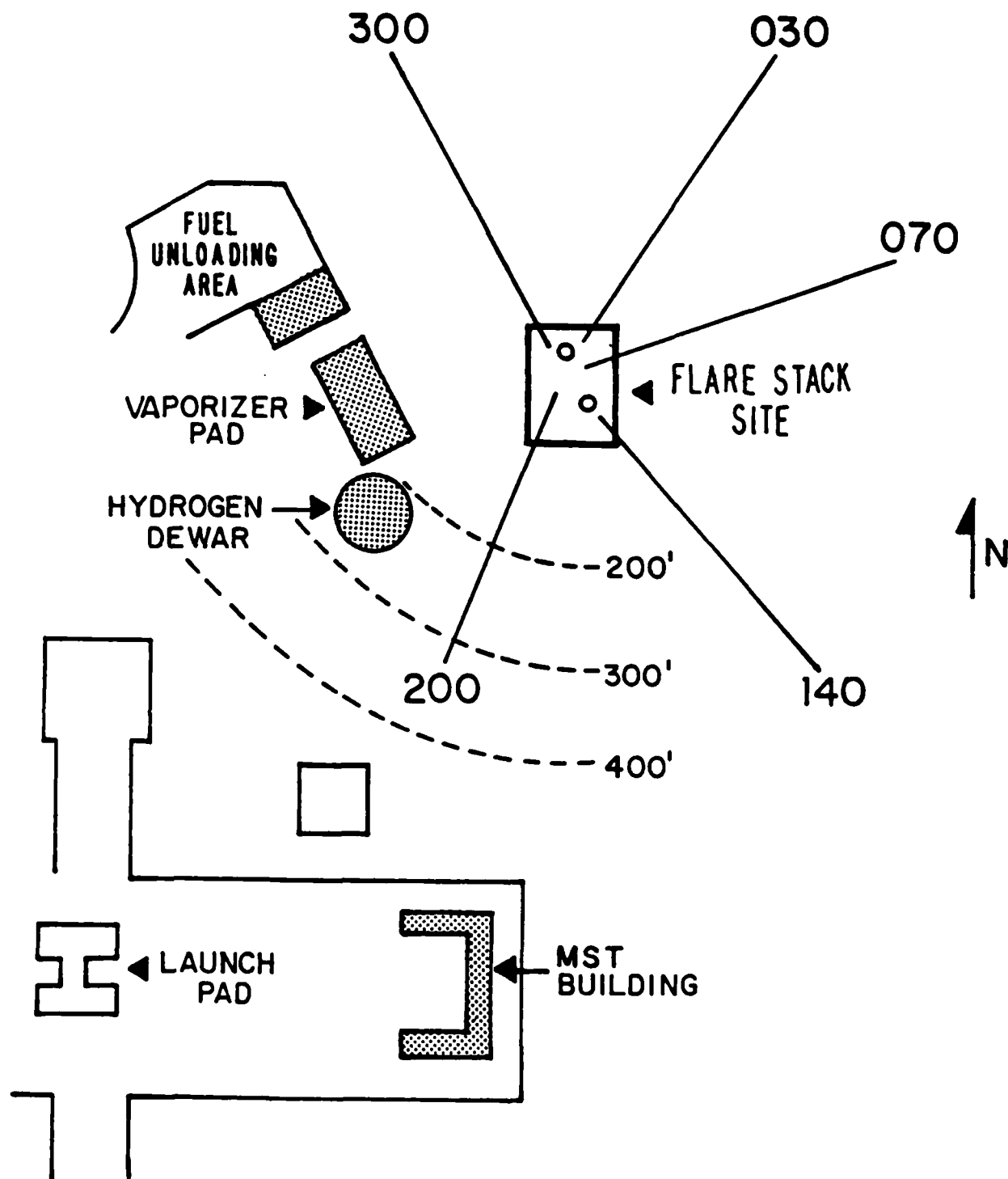


Figure 1. Placement of flare stacks and location of area where a hazard may exist at the Vandenberg AFB Space Shuttle launch site. The wind direction ranges used in the analyses are shown.

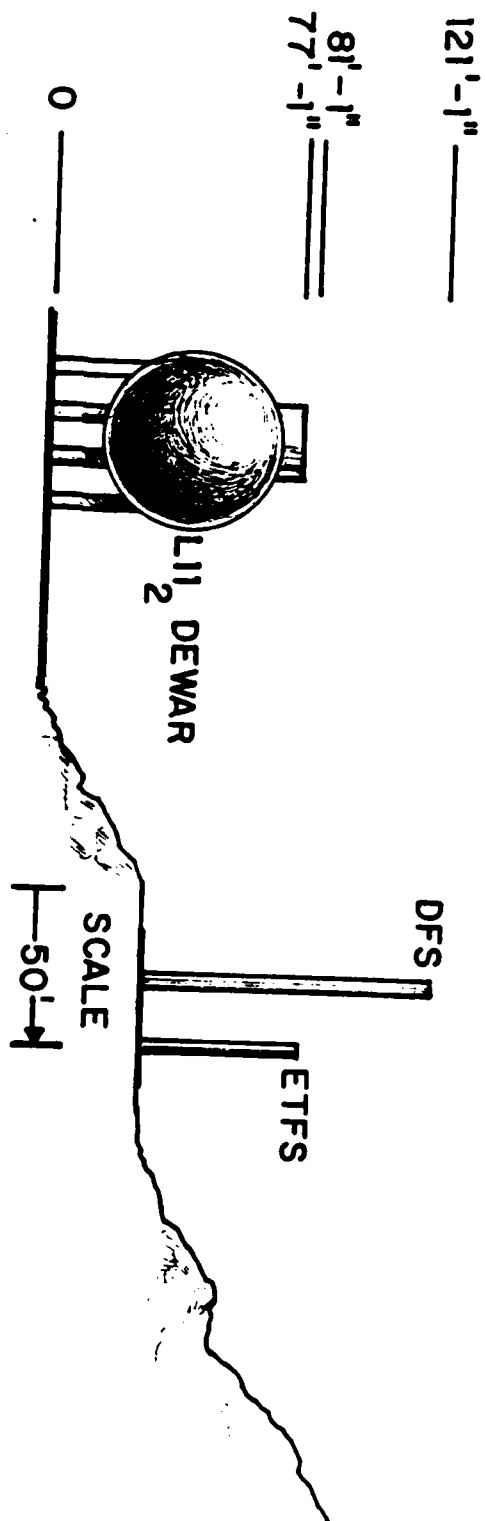


Figure 2. Horizontal view of the flare stack site, showing elevation of the stacks, hydrogen storage dewar, and terrain.

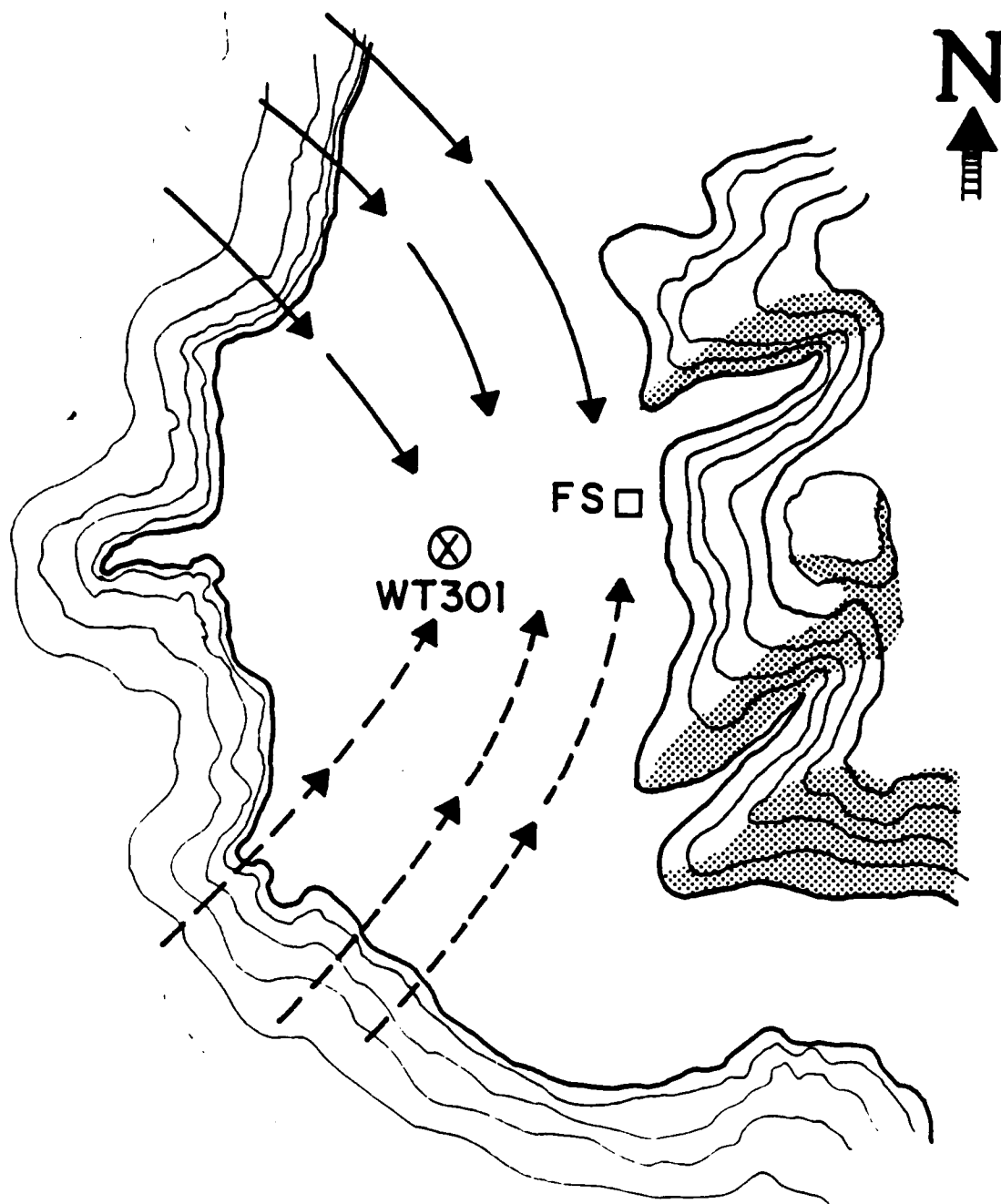


Figure 3. Rough schematic of the Space Shuttle launch site and surrounding terrain, showing location of meteorological tower 301. The solid and dashed lines show turning of the wind by the terrain for Northwest and Southwest winds respectively.

III. EQUIPMENT

For this study, it is important to determine the vector wind so bivane anemometers were used as sensors. They were Gill, model 21003 manufactured by R.M. Young. The sensors contain two potentiometers, one for elevation and one for azimuth, and a generator attached to the propeller for speed indication. The read-outs manufactured by the company were not used. In their place, we constructed a transducer which fed signals to a computer controlled data acquisition system. The computer used was a Hewlett Packard 86 and the data acquisition system a Hewlett Packard 3421.

Each signal was sampled at a 1 sec rate. Due to the large amount of processing needed, it was not possible to do it on site so that all of the data was recorded. There were three sensors and three signals from each sensor, which required a considerable amount of data storage. The computer converted all signals to their meteorological units and all data were stored on Innovative Data Technology 1050 9-track, 1600 bpi, magnetic tape. The storage volume was sufficient to allow two weeks of continuous operation before changing tapes.

All equipment was placed in sealed plastic shelters for environmental protection. Fans circulated filtered ambient air to provide cooling.

Two sampler arrays were used, both utilizing three sensors. In the first, all three sensors were at a height of approximately

54 ft, arranged in a roughly triangular array. One corner of the triangle was at the top of the 50 ft stack and the legs were 55, 70, and 75 ft. The legs were aligned to be along the predominant wind directions and along the maximum threat direction. The second was a vertical array, with sensors at 25, 50, and 95 ft. The top sensor in the vertical array was on the 90 ft stack. The other two sensors were on a mast displaced horizontally by about 20 ft so the array was not truly vertical. The displacement was necessary because of the physical layout at the site and because the large size of the 90 ft stack caused considerable flow distortion near it.

Mounting sensors on top of the stacks was not a simple task. It was necessary to have the sensors above the top of the stacks to be out of the region of flow distortion. The height above the stack top was 4 ft. The mounting arrangement is shown in Figure 4. The only way to construct the mount so that it wouldn't be a danger to service was to mount the sensor on a retractable mast which was mounted to the outside of the safety railing.

Because vertical wind speeds are so small, misalignment of the sensor in the vertical can introduce significant errors since a fraction of the horizontal wind speed would be mixed into the vertical. The sensors have a bubble leveler on their base but it cannot be used for the sensors on top of the stacks due to inaccessability. Alignment was done with a theodolite placed 100 to 200 ft away from the sensor. By careful leveling of the theodolite, it was possible to align the sensor to within 2 deg.

Construction of the bivanes was such that the alignment of the elevation potentiometers was not known. In order to calibrate the elevation signal, a device was constructed which allowed the vane to be locked into a 30 deg up or 30 deg down orientation. With the vane so locked, the output voltages from the potentiometers were read to establish the calibration.

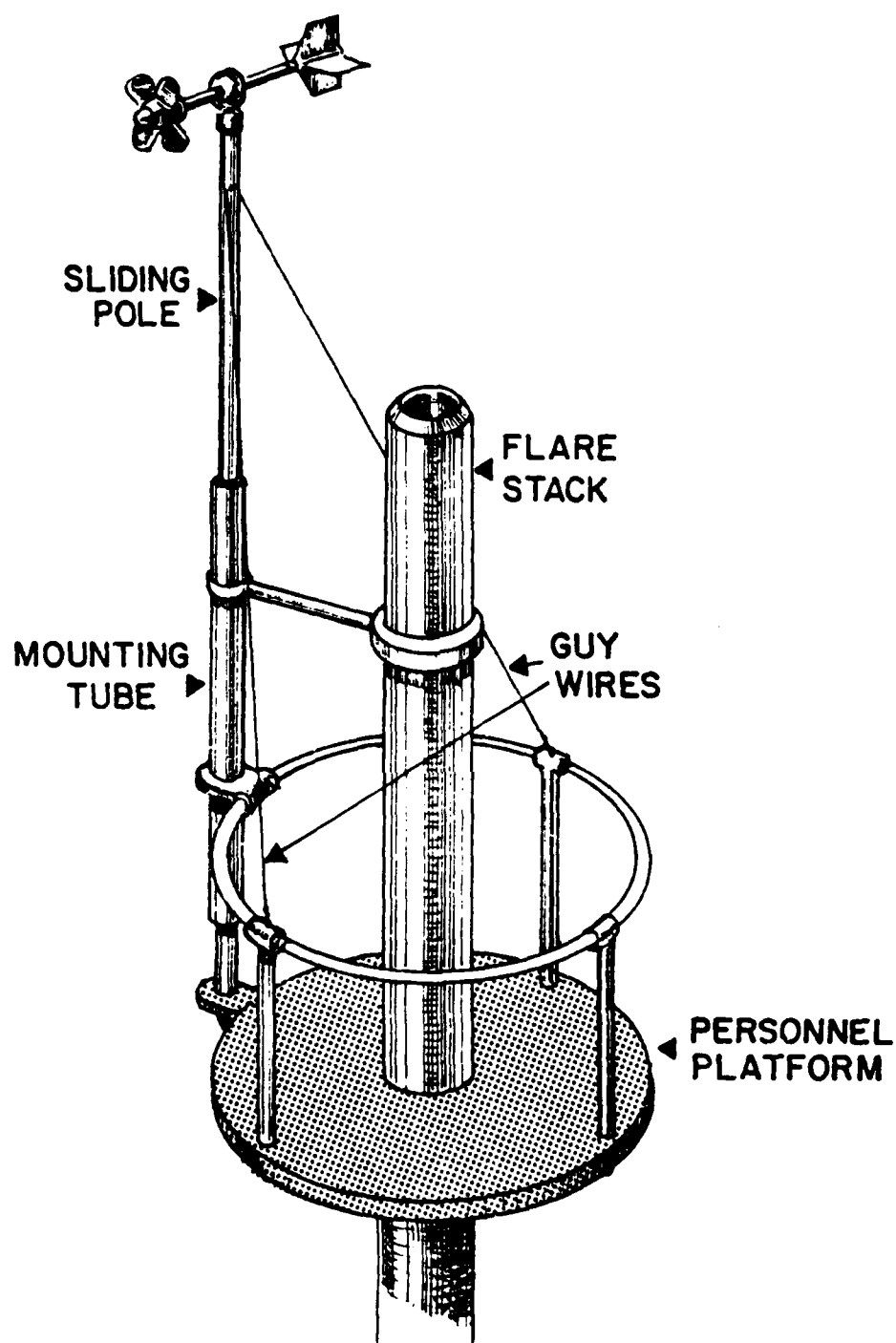


Figure 4. Structure used to mount the bivane anemometer on top of the flare stacks.

IV. CALCULATION OF AIR PARCEL MOTION

As described in the previous section, the wind records consist of the wind speed, elevation angle, and azimuthal angle sampled every 1 sec. We use these data to calculate the positions of air parcels that are separated in time by one second (separated in space by the wind speed) and originate from the top of the stacks. The location in space of an air parcel is updated each second by displacing it with the wind vector. Only the transverse displacements are determined, with horizontal and vertical components treated separately. Displacements along the flow direction are not determined, for reasons that are explained below.

We assume that the mean flow follows the terrain so that it maintains the air parcels at a height above the ground equal to the stack height. For almost all calculations the mean flow is determined from 10 min averages. Deviations of parcel motions from the mean flow will be caused by turbulence. The ultimate purpose of this study is to determine the hazard from the hydrogen flame. For this purpose one must answer questions such as: Will the flame (air parcels) reach the ground? How much heat will be deposited at an impact point? In order to answer the first question one must know the probability that turbulence can cause vertical displacement away from the mean flow of sufficient magnitude to impact the ground. Heat deposition depends on the residence time at a point, which depends on the

rates and magnitudes of transverse motion, both vertical and horizontal. Obviously, on the average air parcels follow the mean flow and it is not necessary to specifically treat that motion here. Transverse displacements off the mean flow are the quantities of interest.

In the analyses we have performed, the most important assumption is that of homogeneity. The analyses use the wind records from a single point. From these records the behavior of the air parcels both at and at distances away from the stacks are calculated. Since the air motion at a distance from the stack is not measured, homogeneity must be assumed. This assumption is reasonable as long as the distance from the measurement point is not too large. If the calculation of the location of an air parcel places it near the ground, the assumption begins to break down due to the suppression of vertical motion near the ground. Thus, calculations to determine the probability that the parcel reaches the ground will be a conservative estimate. Note that assuming homogeneity means that all air parcels undergo the same displacement at a time step.

There is a limit to how long an air parcel should be followed because the purpose is to approximate flare behavior and the flare is of limited lifetime. As the hydrogen gas moves downstream, air is entrained and combustion takes place. When a sufficient amount of burning has occurred, the entrained air and hydrogen gas will be at a high temperature, bouyancy will take

over, and the flare will rise. When this occurs the model we are using ceases to be appropriate and the calculation should cease. The distance from the stack where this will occur depends on the wind speed. We have assumed a maximum flare length of 50 m so that the maximum time a parcel is followed is

$$T_{\text{par}} = 50/U, \quad (1)$$

where U is the wind speed in m/sec. When U is small, equation 1 will give an unrealistically long time since the plume will begin to rise after a fairly short distance. This difficulty is avoided by never following an air parcel for longer than 10 sec. The use of both a maximum length and a maximum time leads to a peculiar result. For a 10 m/sec wind speed, one is dealing with an air trajectory that is 50 m long and has a lifetime of 5 sec. For a 2 m/sec wind speed, the values are 20 m and 10 sec. This leads to some peculiarities in the results which will be discussed later in the report.

An illustration of the assumed behavior of the plume is presented in Figure 5 by showing the location of the plume at two successive time steps. (The advection is unrealistically large in the figure in order to better illustrate the motion.) Note that there is no determination made of the size of the plume as it expands due to diffusion and heating. Only the location of the center of mass of each air parcel is calculated.

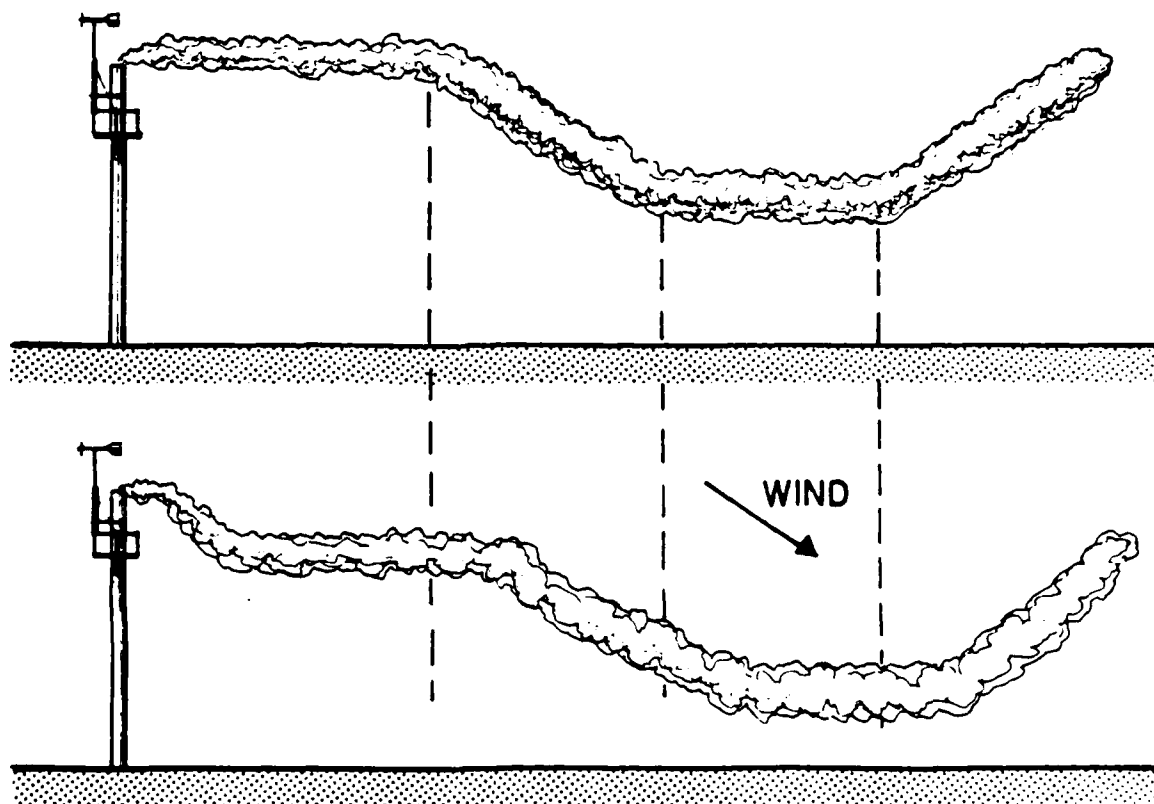


Figure 5. Idealized behavior of the motion of the flare stack plume between successive time steps. The apparent advection is unrealistically large.

V. BACKGROUND METEOROLOGY

It is important to set the analyses presented here within the framework of the meteorology of the Vandenberg area. For example, our analyses show what happens when south winds occur, but it also is important to know how often and under what condition such winds occur. This section provides such information.

1. Correlation with Tower 301

The principal quantity of interest in assessing the flare stack hazard is the wind direction since it determines where the impact will occur. During shuttle operations, wind measurements at the flare stack site will not be available; all wind information will be provided by the 301 meteorological tower, which is about 3/4 mile away. This part of the analysis is to simply determine the correlation between the directions at the flare stack site and tower 301. The difference, $WD(\text{flare stack}) - WD(301)$, is determined as a function of $WD(301)$. No attempt has been made to determine the dependence on any other parameters.

The difference in the wind direction at the flare stack and at 301 is plotted as a function of the 301 wind direction in Figure 6. No sorting on wind speed was done because the scatter in the data obscured any wind speed dependence, which is thus assumed to be small.

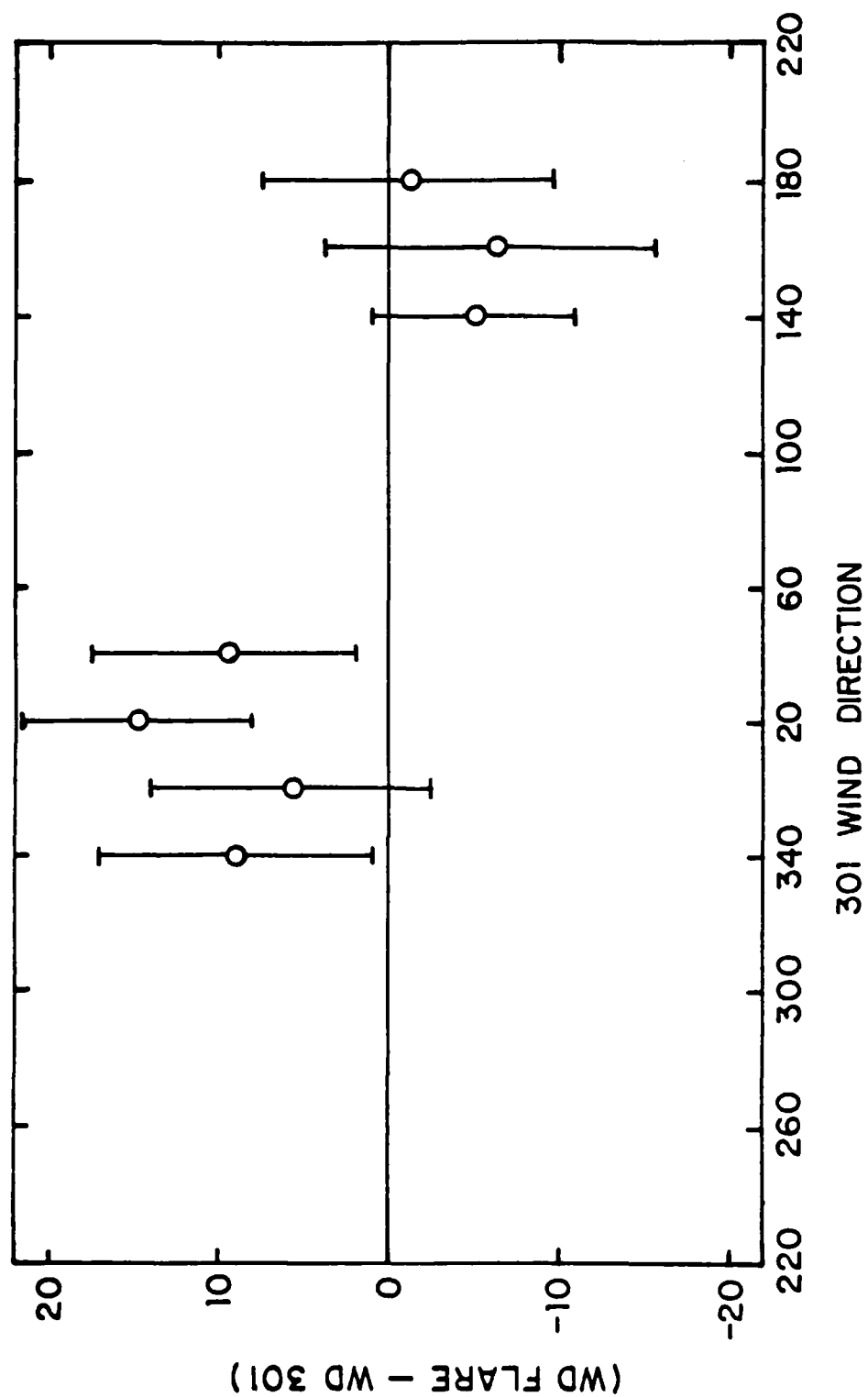


Figure 6. Wind direction difference (WD flare-WD 301) as a function of the wind direction at 301.

The only conclusions that can be obtained from the graph is that the wind is turned clockwise when coming from the north and counterclockwise when from the south. Turned means the rotation of the 301 wind direction to obtain the flare stack wind direction. The effect is not large, the turning being approximately

Northerly wind	10 deg
Southerly wind	5 deg

The effect is illustrated in Figure 3. Note that the figure shows two different flows, differentiated by solid and dashed lines, not one flow with convergence. The most obvious reason for the turning of the wind is the influence of the nearby hills. The flow is channeled by the hills into a general North-South direction.

2. Wind Direction Probability, Orographic Effects

The general direction of the wind is controlled by synoptic and mesoscale influences, with local effects being a perturbation. Orographic effects are due to nearby terrain features and may steer the flow into preferred directions. The procedure is to find the direction probabilities due to non-local forcing and then to separate out the orographically preferred directions.

The preferred directions are determined by finding the probability distribution of the wind direction within direction ranges. The ranges are:

A	0-60, 60-120, 120-180, 180-240, 240-300, 300-0
B	30-90, 90-150, 150-210, 210-270, 270-330, 330-30

Each range is divided into twelve 5 deg wide bins. For a 10 min period, twenty 30 sec average wind directions are calculated and the bin into which each falls is determined. The resulting statistics give the probability distribution for the wind direction within each range (for each general flow condition). Two sets of ranges are used to remove ambiguity caused by the methodology, which will be fully discussed below.

The affect of the topography on the wind is most easily seen in the wind direction probability since the most dramatic effect is steering of the wind into preferred directions. Finding topographically induced directions must be done carefully since synoptic and mesoscale influences also exhibit preferred directions which must be separated in the analysis. The probabilities of the wind being from various directions, due to all influences, are shown in Figure 7. The data plotted are the number of data files recorded for various wind speed-wind direction categories.

Figure 7 shows several effects. When the winds are light, < 2 m/sec, there is little direction preference. Light winds can be caused by any forcing, or combination, and unless the cause is known, no conclusions can be drawn. At the other end of the wind speed scale, winds 7-10 m/sec show a strong preference for a northerly direction. Strong winds are due to a strong synoptic pressure gradient and are much less frequent than lower winds. Note that strong winds do blow out of the south but this does not occur often.

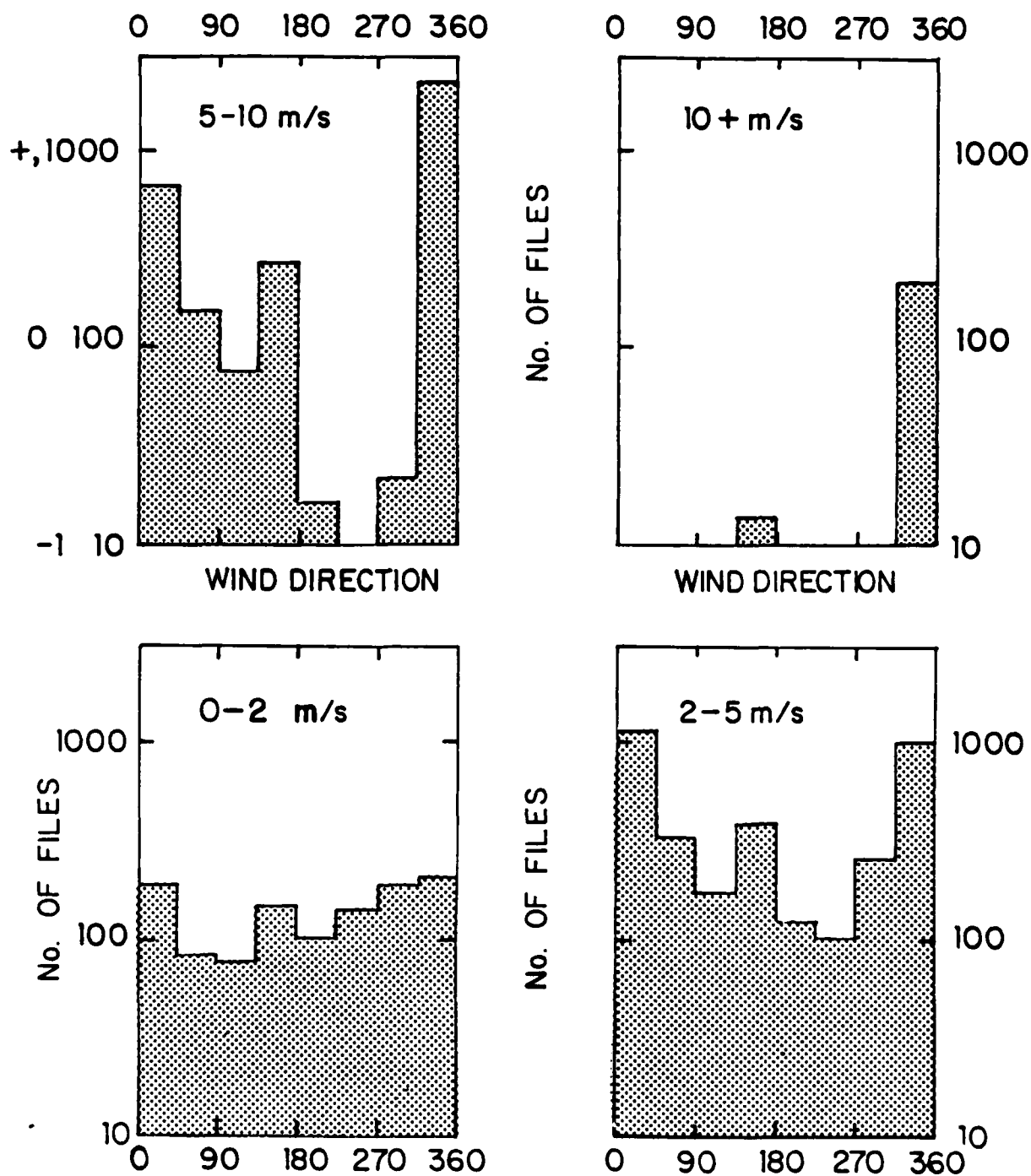


Figure 7. Number of 10 min data files that were obtained during the flare stack experiment as a function of wind speed and direction.

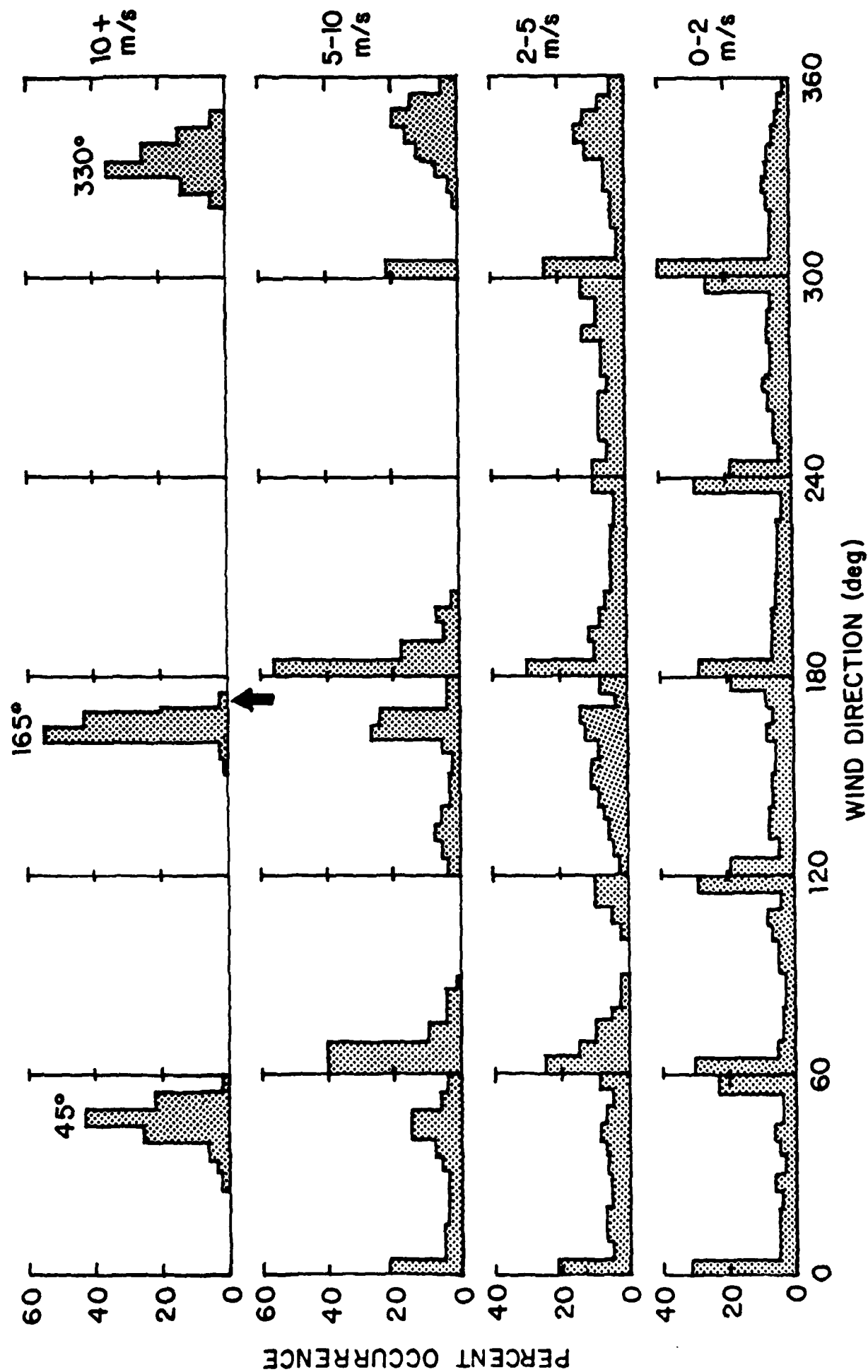


Figure 8a. Probability of the wind being from a particular direction at the flare stacks within each 60 deg range. The arrow shows the South to North flare stack direction.

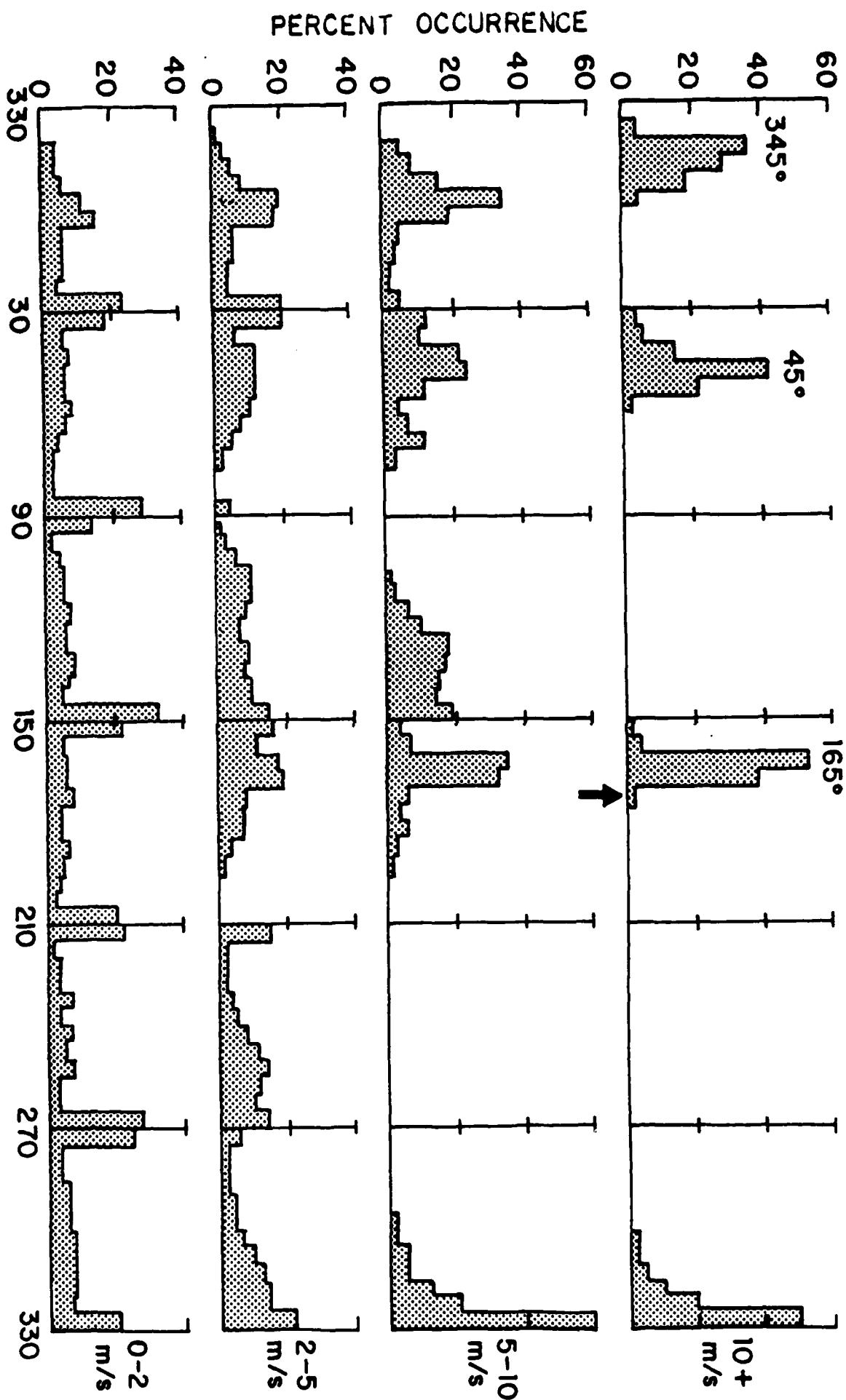


Figure 8b. Probability of the wind being from a particular direction at the flare stacks within each 60 deg range. Ranges shifted by 30 deg.

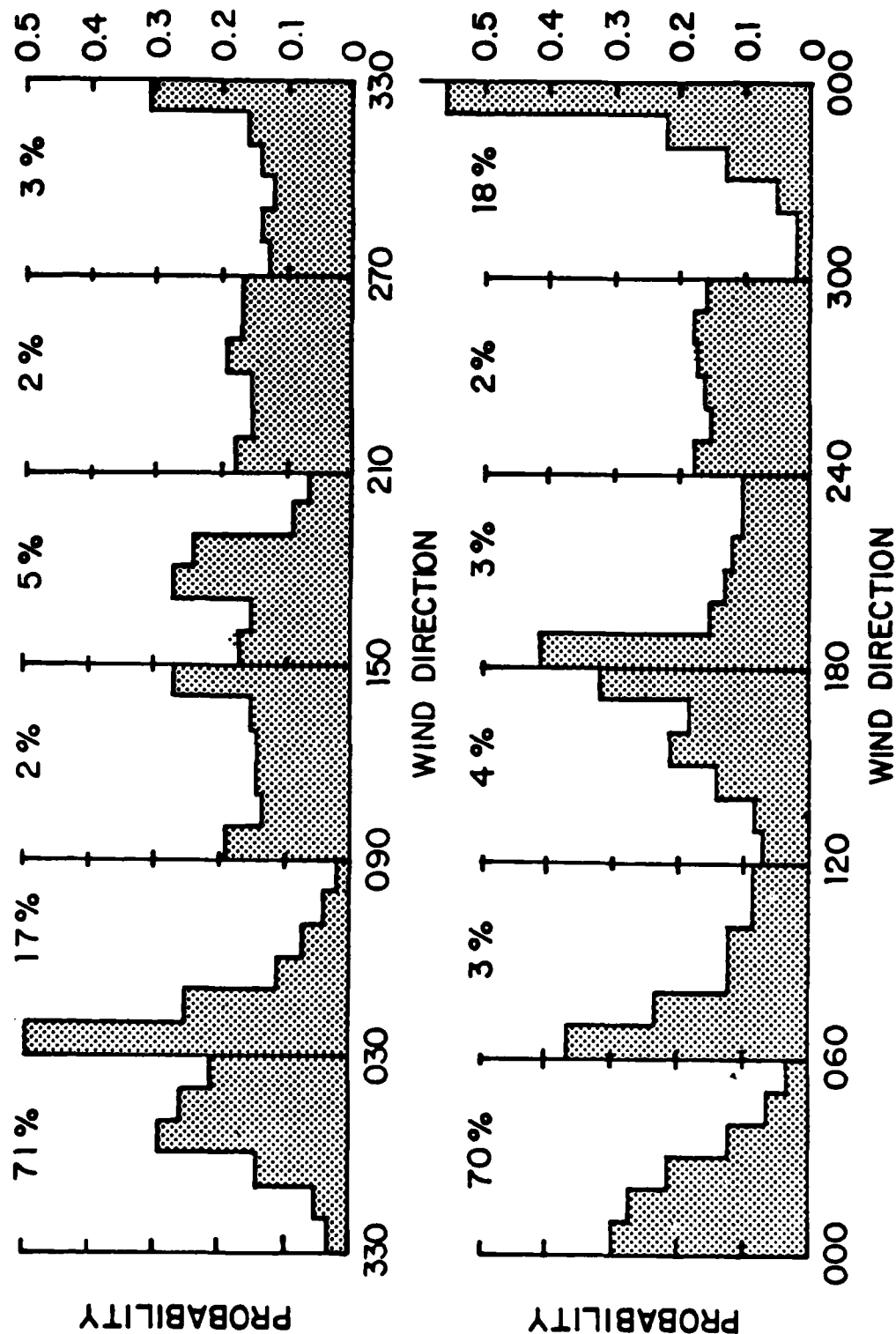


Figure 9. Probability of the wind being from a particular direction at meteorological tower 301 within each 60 deg range. The percentages shown are the fraction of the total data contained in that range.

Moderate winds, 2-10 m/sec, show an increasing preference for northerlies as the speed increases but southerlies and north-easterlies are frequent. The wind seldom blows from the South-West with any strength.

The local orographic effects are illustrated in Figures 8, where the wind-direction probabilities within 60 deg range bins are shown. This analysis suffers from one flaw: if the wind direction is highly variable and the mean is near the edge of a range, fluctuations out of the range cause an excess of data points in the range edge bins. This effect is seen in the figures for low wind speed where highly variable winds occur. The edge bin appears to be a preferred direction but, in reality, is only an artifact of the method. In order to eliminate this problem, the analysis was done twice, with the ranges rotated 30 deg for the second analysis (Figure 8b).

As the wind speed increases, preferred directions appear. The most aparent directions are 45 deg, 165 deg and 345 deg. (The reason for the peak showing up at 330 deg in the rotated range analysis is not known.) Note that 165 and 345 deg are reciprocals and that this direction is roughly parallel to the hill line adjacent to the site. This suggests that the peak is due to steering of the flow by the adjacent hillside. The peak at 45 deg is probably due to channeling of land-breeze flow by the canyon to the North-East.

It must be emphasized that these data are from about a 3 month period. The amount of data is extensive and the

statistical validity is good. However, when dealing with the atmosphere, a full year can be anomalous. Therefore, when using these results to predict effects for a different time, caution is warranted.

Note that the direction from the south flare stack to the north stack is 172 deg, very close to the preferred direction peak at 165 deg.

It is not wise to conclude that a peak in the flare stack wind probabilities is due to the immediate topography without first making sure that the same peaks don't show up in tower 301 data. Thus, plots of direction probabilities within the same 60 deg ranges are shown in Figure 9 for tower 301. Note that here the bins are 10 deg wide. The results are for 1 full year of data and are not segmented by wind speed. Also shown in the figure is the percent of time that the wind was within each range. There are no edge effects such as for the flare stack data.

Figure 8 shows a strong preference for north winds but not the peaks that were located for the flare stack site. The results are not conclusive due to the lack of wind speed segmentation, but the flare stack results appear to be site specific, due to the immediately adjacent topography.

3. Mean Wind Elevation Angle

Air flow can be expected to roughly follow the terrain, so that the elevation angle should be a function of wind direction. At the flare stack site, winds from the East should show

downslope flow, an average declination, winds from the West an average elevation, etc. For this analysis the wind direction is divided into 8 ranges, 45 deg wide, starting at 0 deg. Within each wind direction range, the mean elevation angle is determined as a simple average of the 10 min average values for those cases where the wind was within that range.

The elevation angles for 10 min average winds are shown in Figure 10. The results are presented as a function of wind speed. Up-slope and down-slope elevations occur as expected, with maximum elevation and declination angles of approximately 5.5 deg. This compares closely to the mean slope angle at the site of about 7.5 deg. There is no consistent dependence on wind speed. The dashed line is a hand drawn curve through the data points, drawn in such a way that the maximum elevation and declination angles are the same and to be symmetric with a one-half cycle period of 180 deg.

These results are also presented in Figure 11, which is a polar plot of magnitude of the elevation angle using the values from the dashed line in Figure 10. The dashed line in Figure 11 shows the wind directions for which zero elevation occur.

The elevation angle results confirm the reasonableness of our assumption that the mean flow follows the terrain. Actually this statement should be modified to state "follows the mean slope of the terrain". We have no evidence that the flow follows the details of the steps in the terrain (see Figure 2) nor would we expect it to do so.

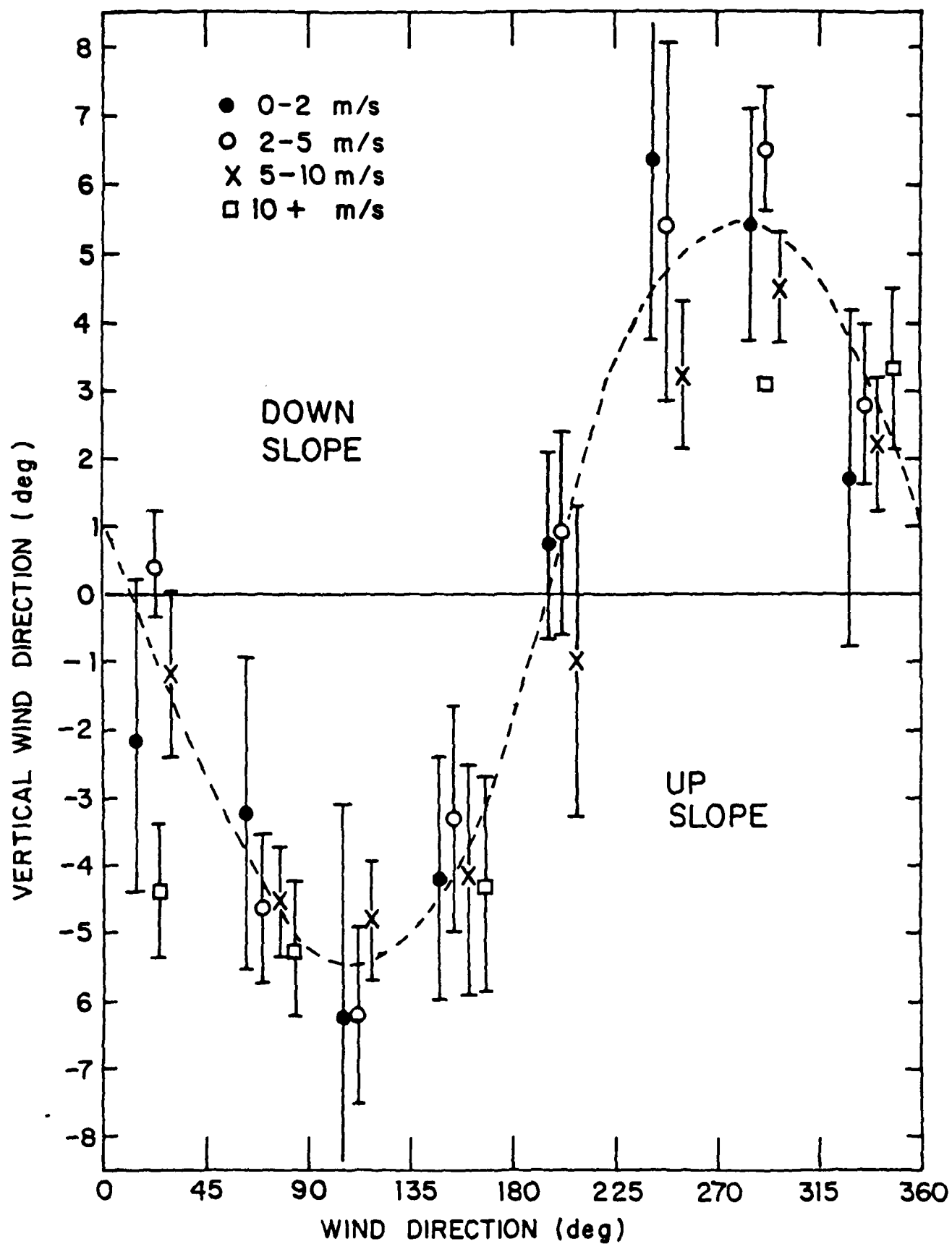


Figure 10. Mean wind elevation angle as a function of wind direction.

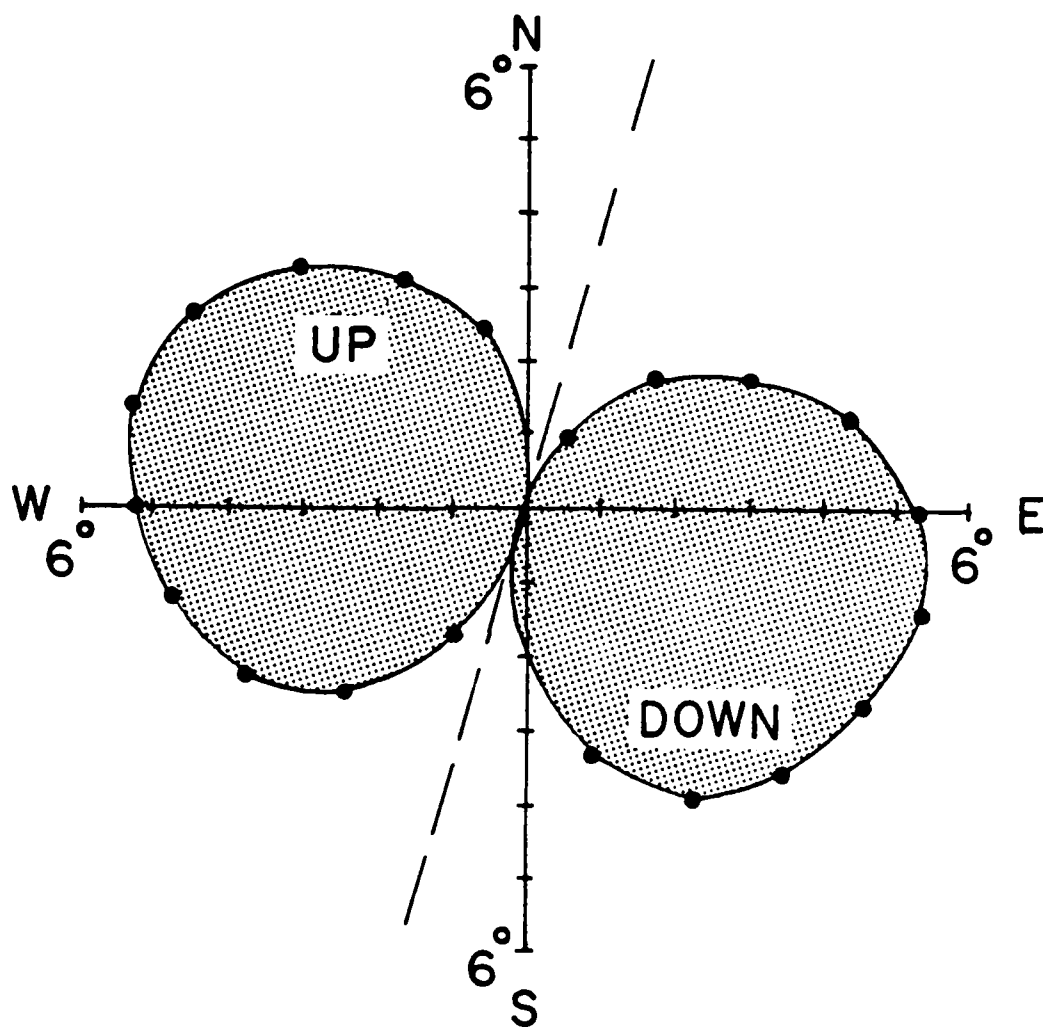


Figure 11. Polar plot of the magnitude of the elevation angle. The dashed line shows the zero elevation wind directions.

VI. DISPLACEMENT CALCULATIONS

Displacement is defined to be the distance an air parcel is away from the position it would have if it followed the mean wind. The displacements of each air parcel along the length of the trajectory are calculated from the sum of the differences between the instantaneous and average wind directions for the life of the parcel. The calculation is performed for both the horizontal and vertical directions.

The displacements of all one-second-separated air parcels along a trajectory are calculated. This gives a snapshot picture of the configuration of the locations of the air parcel centers of mass, one snapshot each second. Since the calculation of displacement is one of the key tools in these analyses, an idealized example is shown in Figure 12 for clarity. The figure includes an idealized vertical wind speed record and trajectory configuration for two elapsed times.

All displacement data is segmented into both wind direction and wind speed ranges. They are:

Direction

300-030 030-070 070-140 140-200 200-300

Speed

0-2, 2-5, 5-10, 10+ m/sec

The direction ranges are shown in Figure 1, and are chosen to segment into corridors where significant hazards can occur. The wind speed ranges are chosen only because they seem reasonable.

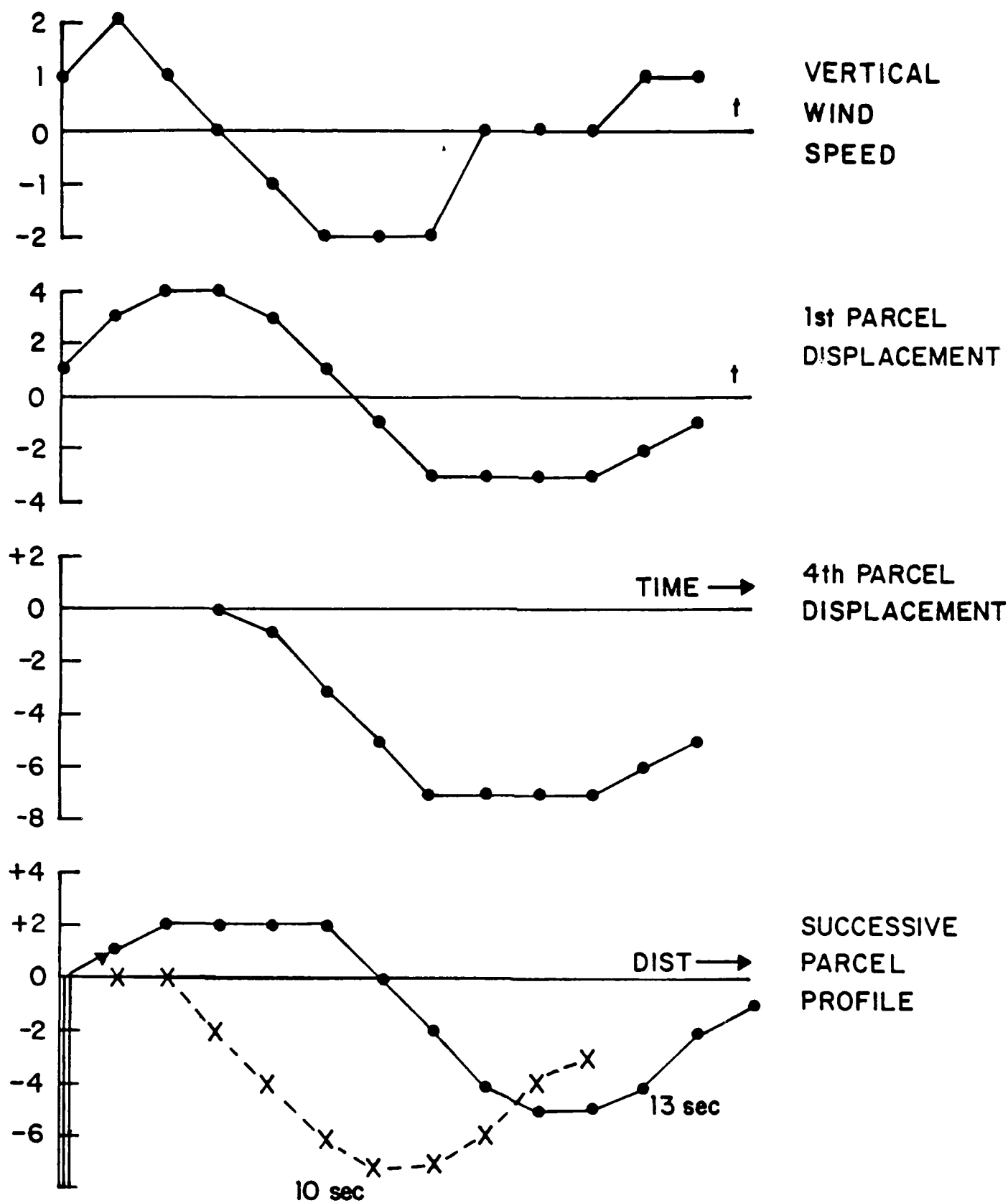


Figure 12. Illustration of the calculation of the displacements of the air parcels that make up a plume.

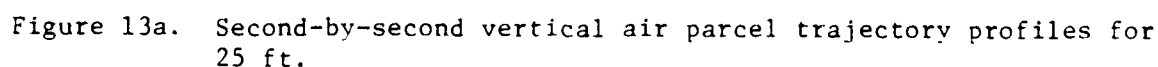
1. Air Parcel Trajectory Profiles

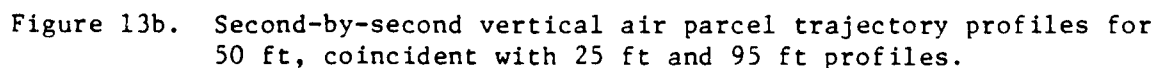
It is instructive to examine Figures 13a-d, which show second-by-second vertical trajectory profiles for all three sensors in the vertical array. The data are from 1857 on 4/9/85. The 10 min average wind direction was from the North, and the mean speeds and vertical speeds were (m/sec):

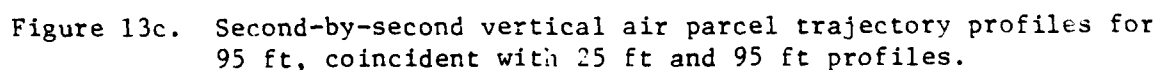
<u>Height</u>	<u>Mean Speed</u>	<u>Vertical Speed</u>
25 ft	5.0	-0.2
50 ft	5.8	-1.3
100 ft	6.1	0.5

The wind speed increases with height, as expected, and the mean vertical speed is not the same at all heights. The large differences in mean vertical speed and the large values of the speed are unusual. Such values would only be found in very complex terrain and for short averaging periods.

Some explanation is in order if the figures are to be understood. The numbers in each line are the vertical displacements of all successive air parcels that make up the plume trajectory. The parcels are separated in time along the trajectory by one-second and in space by the magnitude of the wind speed. Successive lines of data are separated in time by one second so that they show the progression of the shape of the plume simulation with time. 999 replaces a number for the parcel displacement when travel time times the wind speed exceeds 90 m. (for illustrative purposes 90 m was used in place of 50 m for the maximum plume length for these figures.)







[illegible]

Figure 13d. Second-by-second vertical air parcel trajectory profiles for 95 ft. The time period was chosen to illustrate large downward displacements.

The first three of the figures present data for 25 ft, 50 ft, and 95 ft that are coincident in time, line by line. The figures allow one to look for correlations in the vertical wind fluctuations at the three heights. The data in the fourth figure is from the 95 ft height and the same 10 min time period but not coincident in time with the other data.

The data presented was chosen because large negative displacements are included. Figure 13d has the largest displacements of the 10 min period. Large negative displacements were chosen because they represent a hazard at ground level. The following conclusions can be drawn from these displacement profiles:

1. Displacements for air parcel trajectories for all heights are of sufficient magnitude to reach ground level.
 2. Displacements from 50 ft can exceed those from 95 ft for near coincident excursions.
 3. Displacements from the three heights are not in phase, but closely related.
 4. Air parcels undergo large changes in displacement in short time periods (for 95 ft, -8 m to +12 m in 5 sec).
- The plume end commonly moves vertically at 2 m/sec.

2. Maximum Displacement

The hazard from the flame depends on whether or not it reaches the ground or a sensitive structure. If the plume were to follow the mean flow, and if the mean flow follows the terrain, the plume would never reach the ground. The probability

distribution for the vertical displacement can give the probability for reaching the ground.

For this determination, we are specifically interested in the probability that any point along the trajectory will reach the ground. Thus for each one-second snapshot of the plume, the maximum displacement at any point along the plume is found. Then, the probability distributions for these maxima are determined. The calculation is done for both horizontal and vertical maximum displacement for comparison purposes. Only downward vertical displacements are considered.

The maximum displacement of any air parcel that makes up a trajectory is highly variable with time. In fact, any parameter that depends on atmospheric turbulence will be predictable only in a probabilistic sense. This means that only average behavior can be predicted and that the standard deviation about the average will be large. Fortunately, we are not interested in the details of the air motion but in the probability that certain motions can occur.

The percent occurrences of maximum displacement are listed in Table 1. The data are the percent occurrence for the displacement being in a particular range; e.g. 17% for 2 m means that 17% of the trajectories had values greater than or equal to 1 m and less than 2 m. These data are also directly plotted in the first part of Figure 14. This plot is difficult to decipher because the data are so crowded. A more useful format, cumulative percentage, is shown in the second part of the figure.

Table 1a Percent Occurrence of Maximum Horizontal Displacement for 25 ft

<Direction> u(m/s)	Maximum Displacement(m)															
	2	4	6	8	10	12	14	16	18	20	22	24	26	28	30	40+
<300-030>																
0-2	32	26	16	10	6	3	2	1	1							4
2-5	12	19	16	12	9	7	6	4	3	3	2	2	1	1	1	1
5-10	16	26	20	14	9	6	4	2	1	1	1	1				0
10+	28	31	22	12	5	2	1									0
<030-070>																
0-2	32	30	17	8	3	2	1	1								5
2-5	20	27	19	13	8	4	3	2	1	1	1					1
5-10	14	26	19	13	9	6	4	3	2	1	1	1				0
10+																
<070-140>																
0-2	29	26	16	9	5	4	2	1	1	1						5
2-5	28	33	21	10	5	2	1									0
5-10	14	25	19	14	10	7	4	3	2	1						0
10+																
<140-200>																
0-2	37	30	16	7	3	2	1	1								3
2-5	22	24	17	13	8	6	4	2	2	1						0
5-10	23	29	19	12	7	4	3	1	1							0
10+																
<200-300>																
0-2	23	23	18	12	8	5	3	2	1	1						3
2-5	15	18	15	12	9	7	5	4	3	2	2	1	2	1	1	1
5-10																
10+																

Maximum Displacement(m)

<Direction> u(m/s)	1	2	3	4	5	6	7	8	9	10	11	12	13	14	15	20+
<300-030>																
0-2	50	24	13	6	3	2	1									0
2-5	27	20	15	11	8	5	4	3	2	1	1	1	1			0
5-10	25	21	17	12	9	6	4	2	2	1	1					0
10+	29	28	19	13	6	3	1									0
<030-070>																
0-2	55	19	10	6	3	3	2	1	1	1						0
2-5	40	23	14	8	5	4	2	1	1	1						0
5-10	25	22	17	12	8	5	3	2	2	1	1	1				0
10+																
<070-140>																
0-2	53	22	11	7	3	2	1	1								0
2-5	50	26	13	6	3	1	1									0
5-10	27	22	17	12	8	5	4	2	1	1						0
10+																
<140-200>																
0-2	60	24	11	4	1	1										0
2-5	40	25	15	9	5	3	2	1								0
5-10	35	26	17	10	6	3	1	1								0
10+																
<200-300>																
0-2	40	24	15	9	6	3	2	1	1							0
2-5	29	19	15	10	8	5	4	3	2	2	1	1	1			0
5-10																
10+																

Table 1b Percent Occurrence of Maximum Vertical Displacement for 25 ft

Table 1c Percent Occurrence of Maximum Horizontal Displacement for 50 ft

<Direction> u(m/s)	Maximum Displacement(m)															
	2	4	6	8	10	12	14	16	18	20	22	24	26	28	30	40+
<300-030>																
0-2	29	26	17	10	6	4	2	1	1							4
2-5	14	19	15	11	9	6	5	4	3	2	2	2	1	1	1	3
5-10	18	26	18	12	8	5	3	2	2	1	1	1				2
10+	28	33	20	10	5	2	1									1
<030-070>																
0-2	25	24	17	12	8	4	3	2	1	1						4
2-5	17	22	16	11	8	6	4	3	3	2	1	1	1	1		3
5-10	18	26	18	12	8	5	3	2	2	1	1	1				3
10+																
<070-140>																
0-2	31	24	15	10	6	4	2	1	1	1						5
2-5	30	29	16	9	5	3	2	1	1	1						2
5-10	27	31	18	10	6	4	2	1	1	1						1
10+																
<140-200>																
0-2	29	26	16	9	6	3	2	2	1	1						4
2-5	23	26	18	12	7	5	3	2	1	1	1					1
5-10	27	29	18	11	7	4	2	1	1							0
10+	54	31	10	3	1											0
<200-300>																
0-2	25	24	17	12	8	5	2	1	1							4
2-5	16	22	17	13	9	6	4	3	2	1	1	1	1	1		4
5-10	6	15	11	9	7	6	3	3	4	3	4	4	7	7	4	9
10+	13	22	22	12	11	7	5	3	3							2*

Maximum Displacement(m)																
<Direction> u(m/s)	1	2	3	4	5	6	7	8	9	10	11	12	13	14	15	20+
<300-030>																
0-2	43	24	15	8	5	2	1	1								0
2-5	29	18	13	10	7	5	4	3	2	2	2	1	1	1	1	1
5-10	28	21	15	11	7	5	3	2	2	1	1	1	1	1	1	1
10+	31	25	18	12	7	4	2	1	1							0
<030-070>																
0-2	45	22	13	8	5	3	2	1	1							0
2-5	35	19	19	9	6	5	3	3	2	2	1	1	1	1		0
5-10	35	22	22	9	6	4	3	2	2	1	1	1				0
10+																
<070-140>																
0-2	53	22	11	6	4	2	1	1								0
2-5	43	21	13	8	6	4	2	1	1	1						0
5-10	33	22	15	10	7	5	4	2	2	1	1					0
10+																
<140-200>																
0-2	49	24	13	7	4	2	1	1								0
2-5	37	21	14	10	7	4	3	2	1							0
5-10	33	21	15	11	8	5	3	2	1							0
10+	48	28	13	6	3	2	1	1								0
<200-300>																
0-2	37	22	15	10	7	4	2	1	1							0
2-5	31	19	15	11	8	6	4	3	2	1	1					0
5-10	27	19	17	14	10	6	3	2	1	1	1					0
10+	17	17	14	11	7	9	6	8	6	4	1	1				0 *

Table 1d Percent Occurrence of Maximum Vertical Displacement for 50 ft

Table 1e Percent Occurrence of Maximum Horizontal Displacement for 95 ft

<Direction> u(m/s)	Maximum Displacement(m)																40+
	2	4	6	8	10	12	14	16	18	20	22	24	26	28	30		
<300-030>																	
0-2	31	27	17	11	6	3	1	1								4	
2-5	15	21	17	13	9	7	5	3	3	2	2	1	1	1	1	1	
5-10	19	26	18	12	8	5	3	2	2	1	1	1	1			0	
10+	31	33	20	10	5	2	1									0	
<030-070>																	
0-2	23	22	17	11	7	5	3	2	1	1	1					7	
2-5	20	24	17	12	8	6	4	3	2	2	1	1				0	
5-10	17	25	18	12	8	6	4	3	2	1	1	1	1			0	
10+	22	30	24	14	6	2	1	1	1							0	
<070-140>																	
0-2	29	26	16	10	6	3	2	1	1							6	
2-5	31	32	17	9	5	2	1	1	1							0	
5-10	32	32	17	9	5	3	1	1								0	
10+																	
<140-200>																	
0-2	30	25	16	9	5	3	2	1	1	1	1					7	
2-5	25	26	17	11	7	4	3	2	1	1	1	1				1	
5-10	30	29	17	10	6	3	2	1	1							0	
10+	59	30	8	2	1											0	
<200-300>																	
0-2	24	24	18	12	8	5	3	2	1	1						3	
2-5	16	22	17	13	9	7	5	3	2	2	1	1	1	1		1	
5-10	11	26	18	14	10	10	4	3	2	1	1					0 *	
10+																	

<Direction> u(m/s)	Maximum Displacement(m)															
	1	2	3	4	5	6	7	8	9	10	11	12	13	14	15	20+
<300-030>																
0-2	42	24	15	8	5	3	2	1	1							0
2-5	28	18	14	10	8	6	4	3	2	2	1	1	1	1	1	1
5-10	26	20	15	11	8	5	4	3	2	1	1	1	1	1	1	1
10+	30	26	19	12	7	3	2	1								0
<030-070>																
0-2	47	21	13	7	5	3	2	1	1							0
2-5	39	20	13	8	5	4	3	2	2	1	1	1	1	1		0
5-10	31	20	14	9	6	5	4	3	2	2	1	1	1	1		0
10+	39	27	16	8	4	2	2	1	1	1						0
<070-140>																
0-2	47	23	13	7	4	3	1	1	1							0
2-5	43	24	15	8	5	3	1	1								0
5-10	35	21	15	9	6	5	3	2	1	1	1					0
10+																
<140-200>																
0-2	53	24	11	5	3	2	1									0
2-5	38	20	13	9	7	5	3	2	1	1	1					0
5-10	33	22	15	10	7	5	3	2	1	1	1					0
10+	55	27	11	4	2	1										0
<200-300>																
0-2	36	22	15	11	7	4	2	1	1	1						0
2-5	26	17	14	11	9	7	5	4	3	2	1	1	1			0
5-10	18	15	17	15	14	8	4	4	2	2	1					0
10+																

Table 1f Percent Occurrence of Maximum Vertical Displacement for 95 ft

Cumulative percentage is the percent of time the maximum displacement is less than a particular value. This format nicely separates the data.

Figure 14-17 are used to illustrate trends in the data, the dependence on various parameters. The complete data are presented only in the table.

The dependence on wind speed is shown in Figure 14. A larger percentage at low displacements means that large displacements are less probable. Thus, the wind speed dependence shows that 0-2, 10+, 5-10, 2-5 m/sec is the succession from minimum to maximum displacements. One expects displacement to be less for greater wind speed since turbulence intensity, $\sigma\theta$, is known to be less. It is peculiar that 0-2 m/sec has the least displacement. This is due to the processing methodology that utilizes both a maximum time and a maximum length for the allowed trajectory. At 2 m/sec the length is restricted by the 10 sec maximum time to 20 m. The trajectory is longer for greater wind speeds, producing a greater possible transverse displacement. Note that Figures 13 show that the maximum displacement usually occurs at the end of the plume.

Figures 15 and 16 show both vertical and horizontal displacements, 15 is percent occurrence and 16 is cumulative percent. The horizontal displacements are considerably larger than the vertical. This is due to the non-isotropy of turbulence near the ground. The length scales of the turbulence which will

drive the trajectory to ground level are the order of the height of the stacks. These scales will be suppressed in the vertical but not in the horizontal direction.

The dependence of the maximum vertical displacement on wind direction is shown in Figure 17. The figures for each wind direction range contain two sets of data. The lower set is the cumulative percent for 1 m, the upper set for 2 m or less. Range bin 4 is shaded to illustrate that the trajectory length used for this range was less than for others (50 ft to 90 ft stack). The figures contain data for trajectories for emission heights of 25 ft 50 ft and 95 ft. The results are not dramatic but some trends are apparent:

1. Displacements are greater for range 5 (200-300 deg).
2. Displacements are less for range 4 (140-200 deg).
3. There is a slight tendency for lesser displacement when winds are from the East.

The most striking fact to be gained from these data is that large displacements do occur. For moderate winds, 2-10 m/sec, vertical displacements of 10 m or greater occur at least 5% of the time. In a 10 min period, this means that ground level will be reached for more than 30 sec.

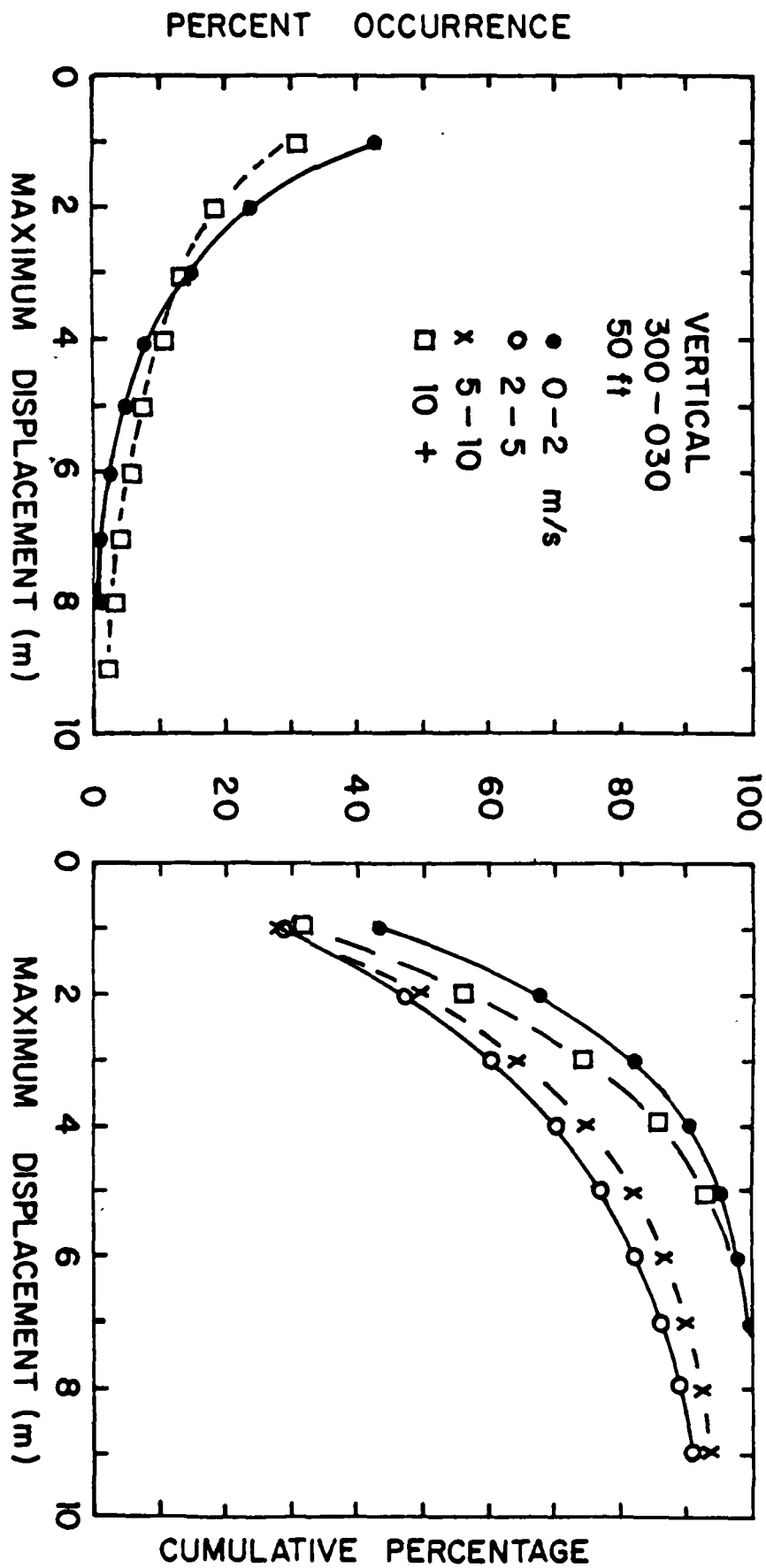


Figure 14. Percent occurrence of a given maximum vertical displacement, and cumulative percent for various wind speeds, (right figure is cumulative percent). Cumulative percent is the percent of occurrences within a displacement.

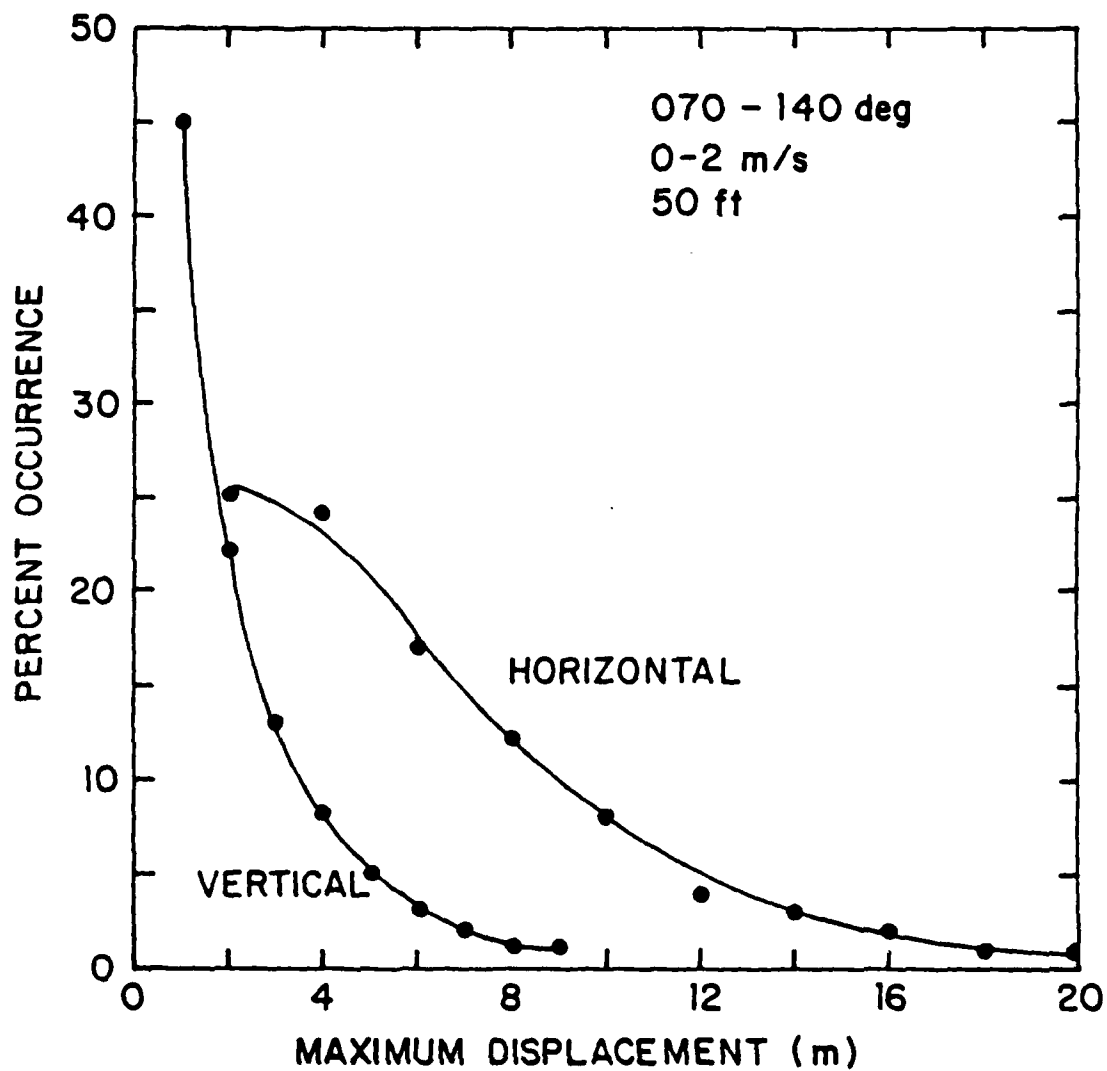


Figure 15. Percent occurrence of maximum vertical and horizontal displacements.

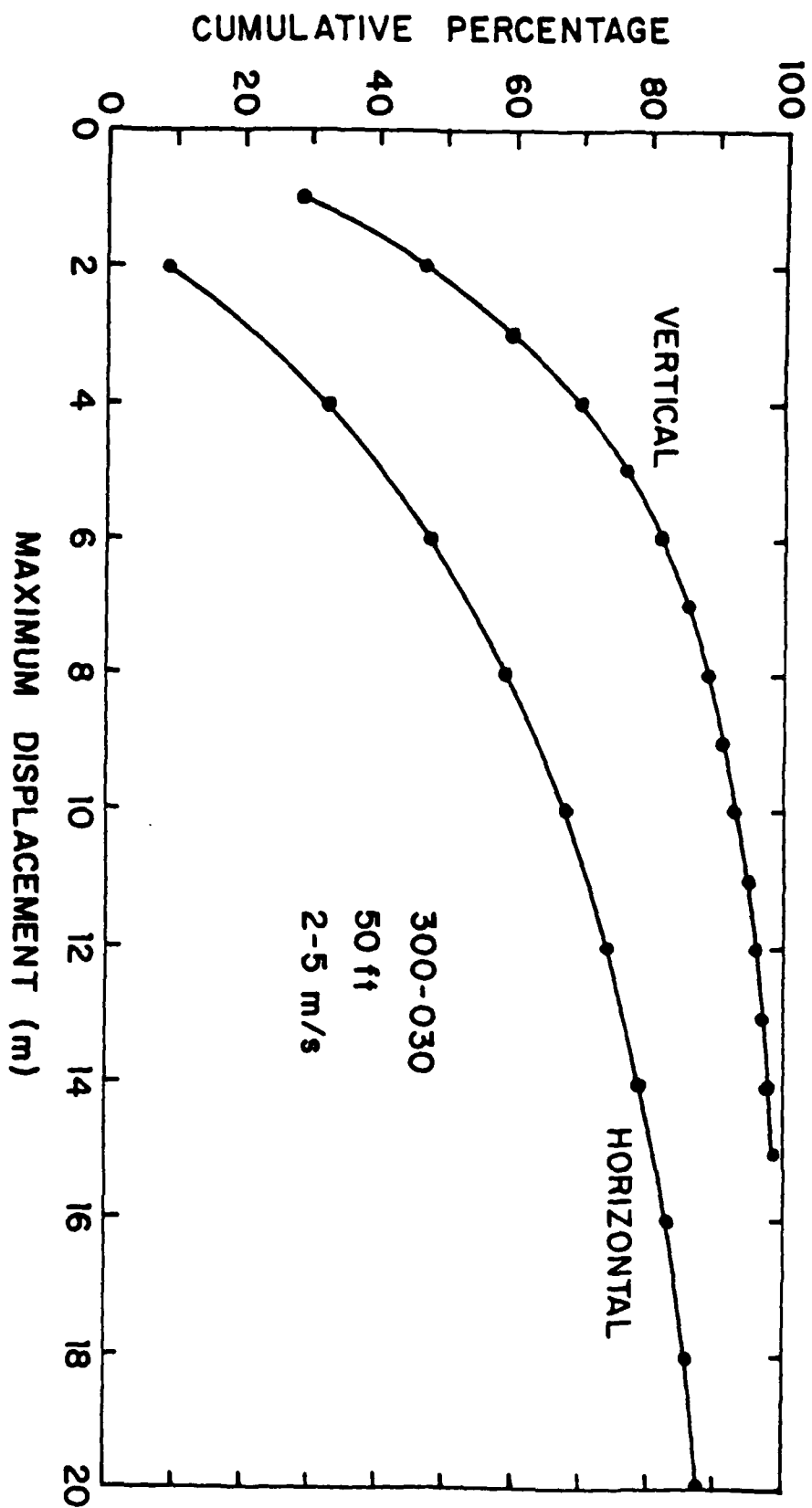


Figure 16. Cumulative percent occurrence, percent of occurrences within a given maximum displacement, for vertical and horizontal displacements.

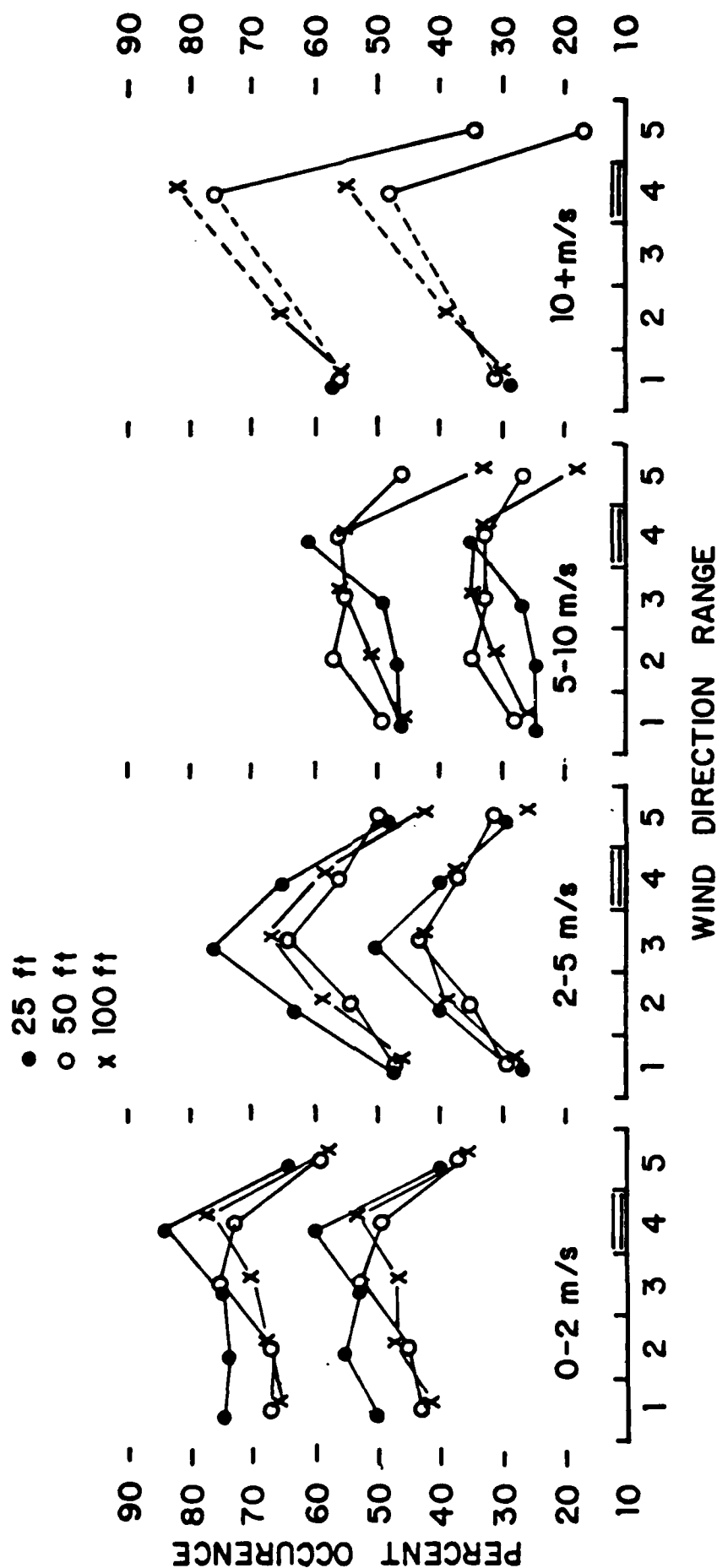


Figure 17. Percent of occurrences within 1 m and 2 m maximum vertical displacement as a function of wind direction range. The lower group of data in each range is for 1 m displacement, the upper 2 m. Ranges are 1: 300-030, 2: 030-090, 3: 090-140, 4: 140-200, 5: 200-300.

VII. TRAJECTORY END STATISTICS

All of the results presented in this section are based on the displacement calculations described earlier. We specifically consider the transverse motion, both vertical and horizontal of the end of the plume. In a later section we describe how these results can be used to perform heat deposition calculations.

1. Persistence

The damage the flare can do depends on both where it impacts and how long it remains on that point. If the flame were to remain on a critical point for a considerable length of time the heat deposited, and damage, could be great. Persistence is simply defined to be the length of time the end of the plume remains at a point. Persistence is determined for both horizontal and vertical motions, which are assumed independent. The correlation between the two is not determined.

Note, the calculation is performed for the motion of the end of the plume for all cases except when the wind direction is such that the flame from the 50 ft south stack could impact on the 90 ft north stack. In that case, the movement of the plume at the position of the 90 ft stack is calculated.

In the calculation of persistence, it is necessary to specify a threshold distance within which the plume end is assumed to be at the starting point. Several threshold distances are used and the persistence calculated for each. They are

Persistence Distance Thresholds

1, 2, 3, 4, 5, 6, 7, 8, 9, 10+ m

The persistence calculation proceeds as follows:

1. Calculate the displacements of the end of the air parcel trajectories for each 1 second time step.
2. Choose a distance threshold for which the persistence will be determined and a starting time.
3. Take the displacement at the starting time as the initial point and determine how long the displacement remains within the chosen distance threshold of that point.
4. Perform the calculation for all distance thresholds and possible starting times in the 10 min. record.

A set of persistence times is generated in this manner for all of the distance thresholds listed above. Each 10 min. record yields a maximum of 599 times.

The persistence times are grouped into time bins and the probability distribution for persistence time determined. The time bins used were

Persistence Time Bins

1, 2, 3, 4, 5, 6, 7, 8, 9, 10+ sec

These bins are too small for large distance thresholds because for those cases persistence tends to be long. Thus, for thresholds greater than 3 m the time bins are increased by a factor of two and for greater than 7 m by a factor of four.

The probability distribution calculated is the probability that the plume will remain within the given distance for the time indicated. We use this form because the quantity of interest is the total heat deposited, which depends on the length of time the flame remains at a point.

The data set to be presented for persistence is very large. The number of data entries is $(10 \text{ times}) \times (10 \text{ distances}) \times (5 \text{ wind direction ranges}) \times (4 \text{ wind speed ranges}) = 2000$, and this number is needed for both vertical and horizontal displacements, for each sensor height (3). The grand total is 12,000, a rather excessive number. Fortunately, there seems to be little dependence on emission height so this division can be neglected. In fact, averaging the results for the various heights helps to smooth the data.

It has been necessary to expend a large amount of effort to reduce the quantity of data to be utilized. A technique has been found to reduce the results to one small table and three sets of curves. Before presenting these simplified results, it is useful to briefly describe the basic behavior that was found for persistence.

The probabilities that the trajectory end remains within a given distance for a specified time period, when the wind is from 300 to 030 deg at 0-2 m/s, are shown in Figure 18. The first part of the figure shows the probabilities as functions of time for three distances and the second part as functions of distance for several times. The behavior is as expected. The probability increases with increasing distance and decreases with increasing

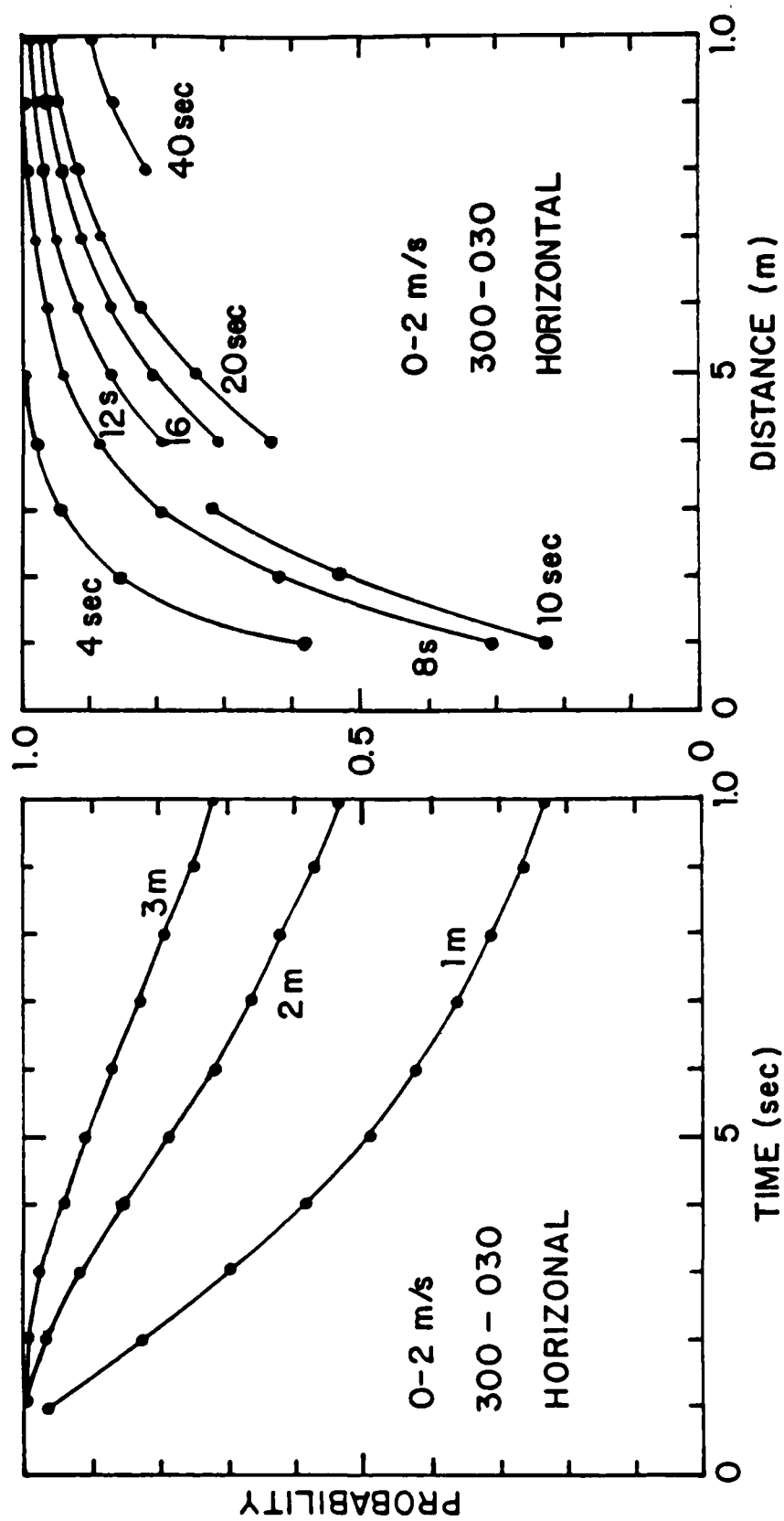


Figure 18. Probability that the trajectory end will remain within a given distance for the specified time period.

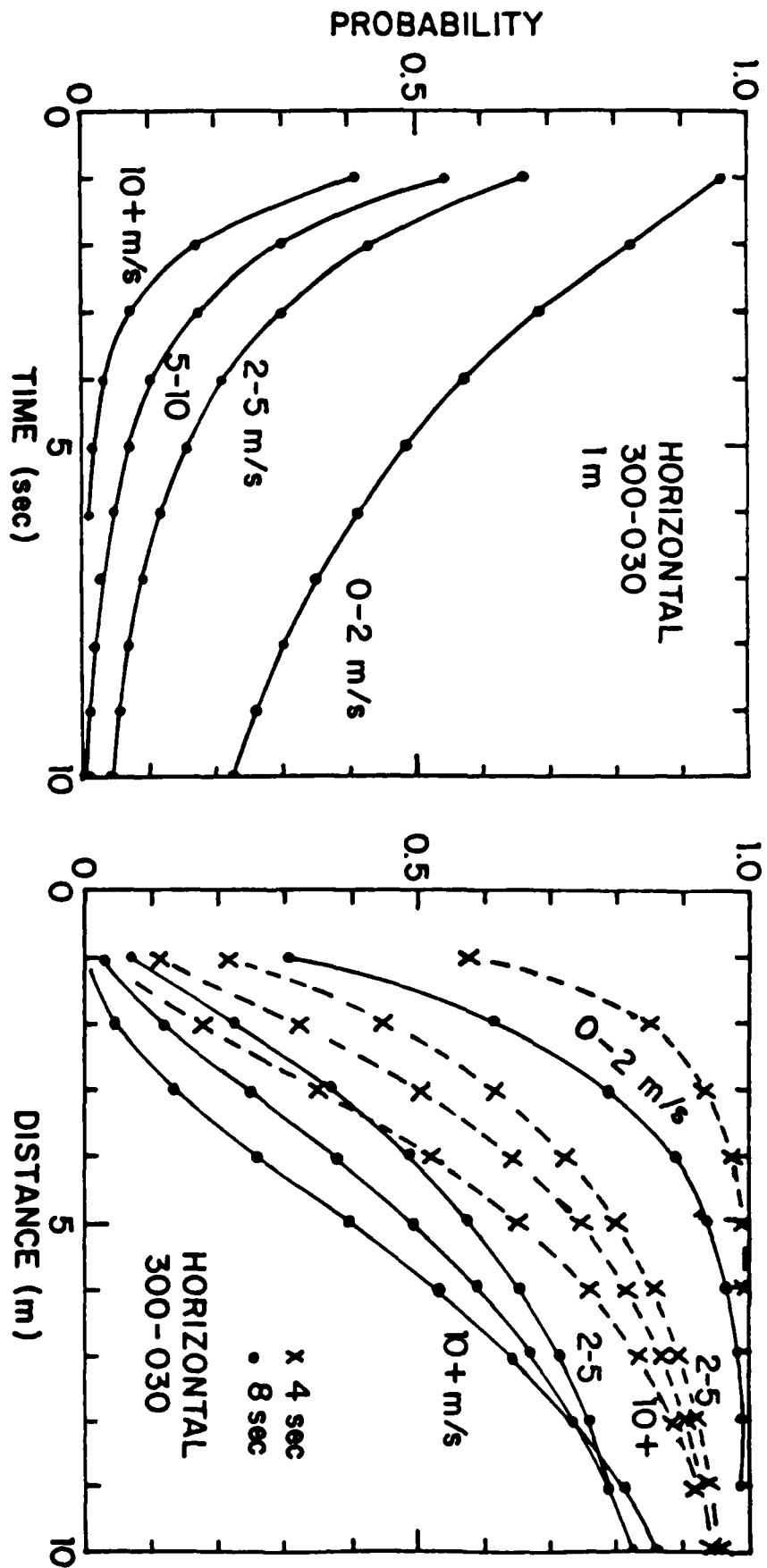


Figure 19. Probability that the trajectory end will remain within a given distance for the specified time period. Data is presented for the four wind speed ranges. In the right figure the 5-10 m/sec curve is not labeled.

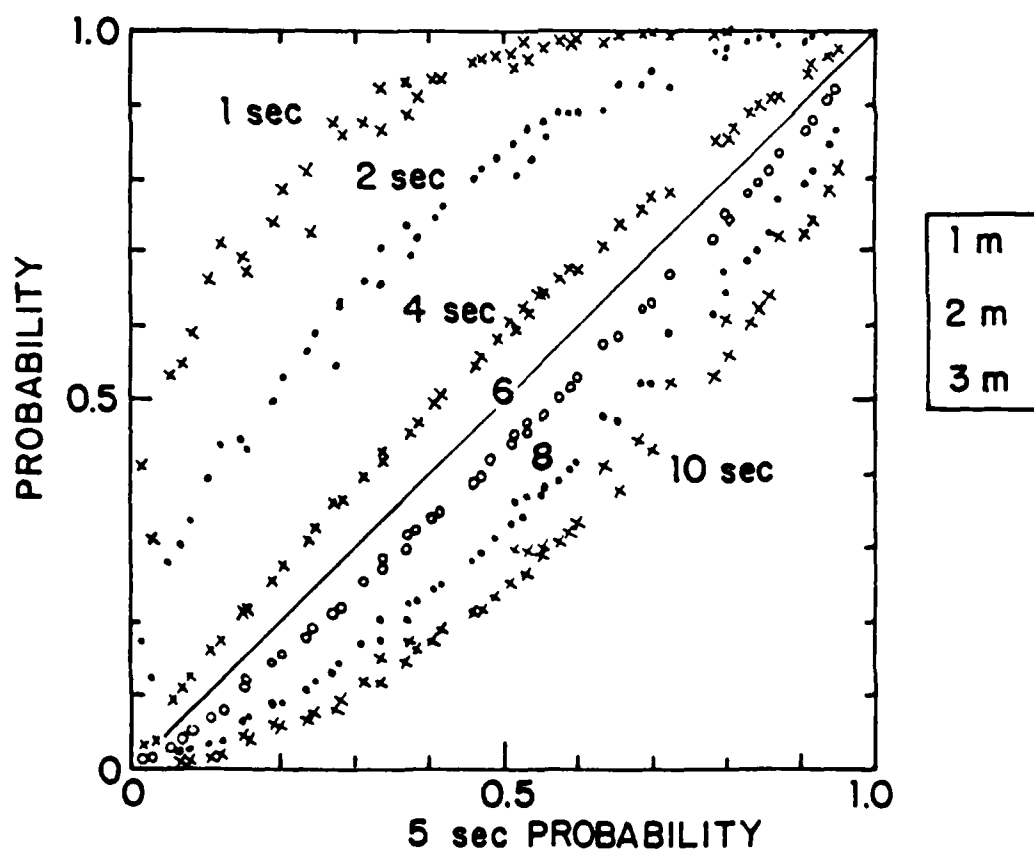
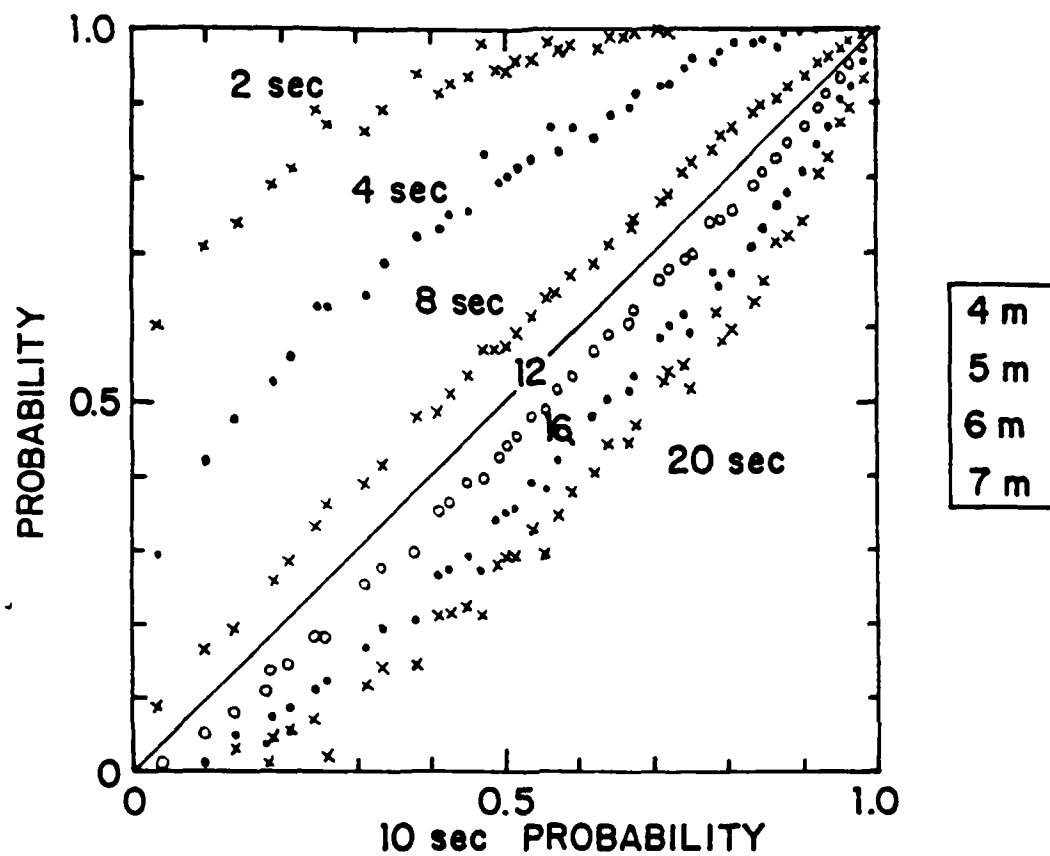


Figure 20. Persistence probability data for various time periods versus the 5 sec and 10 sec probability data.

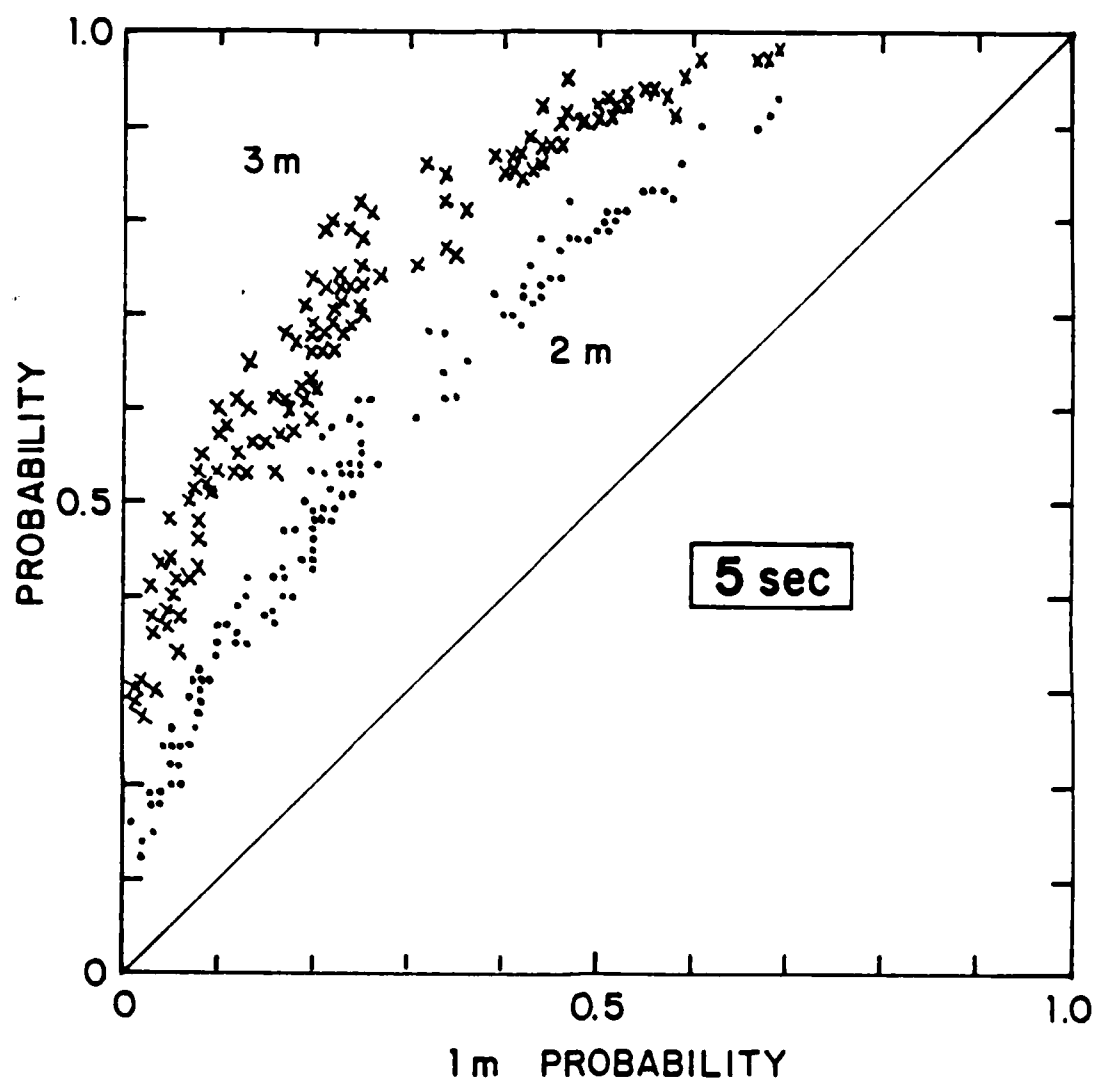


Figure 21. 5 sec persistence probability data for 2 m and 3 m versus the 1 m probability data.

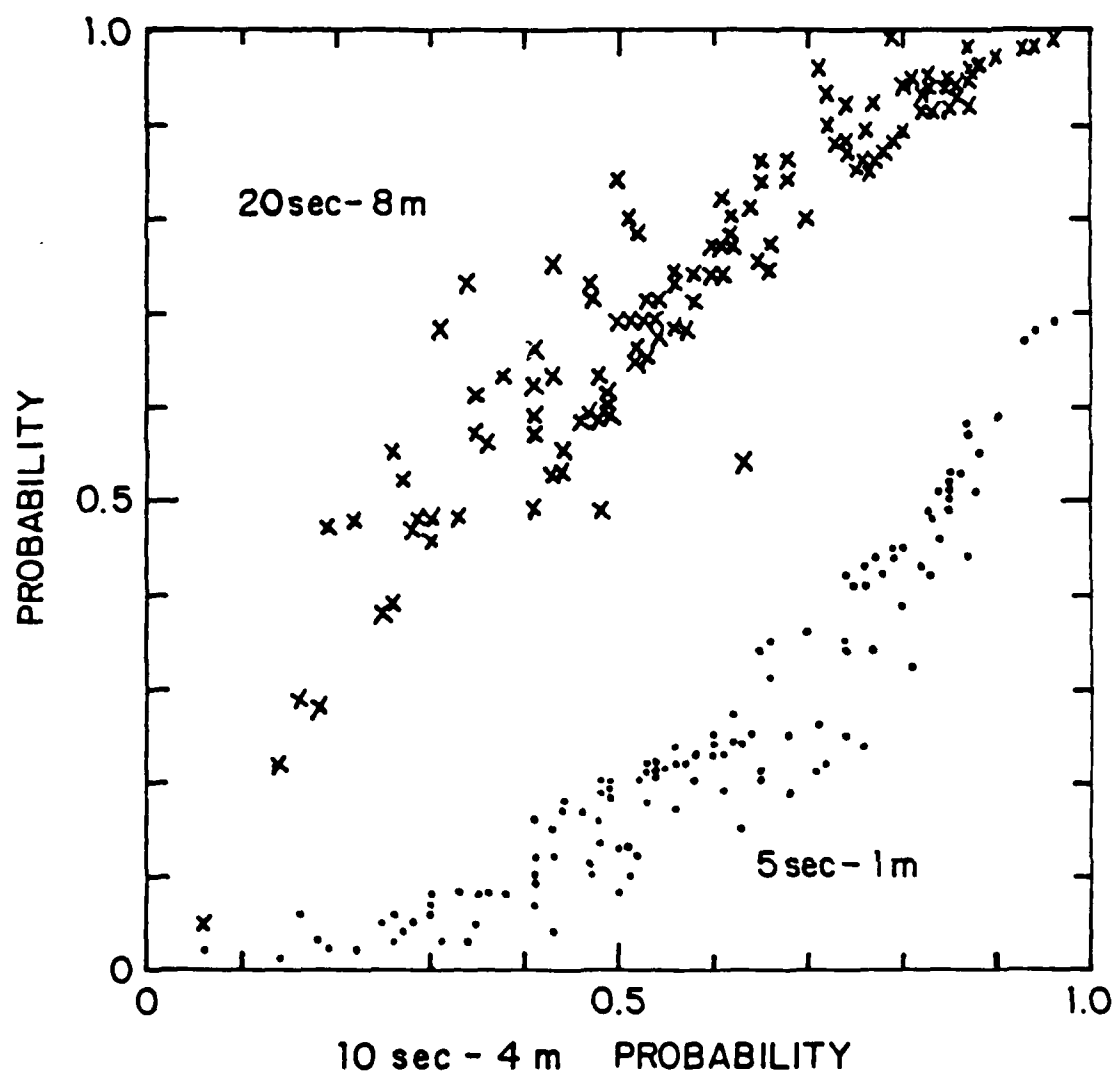


Figure 22. 5sec-1m and 20sec-8m persistence probability data versus the 10sec-4m probability data.

time. Obviously, the plume will remain within a larger distance for a longer time, and if the time is long the plume can be expected to move out of range.

Figure 19 show the same information for the four wind speed ranges. The persistence continually decreases with increasing wind speed.

Note that the character of the curves is quite smooth and that the shapes appear to follow a consistent pattern. This opens the possibility that universal relations can be found to express the results. It is not obvious that this can actually be done so Figures 20, 21, and 22 are used to illustrate that the procedure works.

Recall that the data makes use of both distance and time bins, with 1 to 10 sec being used for 1, 2, and 3 m, 2 to 20 sec for 4, 5, 6, and 7 m, and 4 to 40 sec for 8, 9, and 10 m. Figure 20 shows that universal curves exist to relate the 5 sec probabilities to those for all other times for the smaller distances, and also shows similar results for 10 sec for the intermediate distances. Note that these data are for all wind speeds and directions, for both horizontal and vertical displacements, and for all applicable distances.

Figure 21 shows that 5 sec probabilities for 1, 2, and 3 m can be related. Similar results for 10 sec and 20 sec are not shown. Figure 22 shows that the 5 sec and 20 sec results can be related to the 10 sec results.

The end result is that all data for a given wind speed-wind direction category can be found from the 10sec-4m probability. The curves which are used to do this are found in Figures 23, 24, and 25 and the 10sec-4m data in Table 2.

The following is a description of how these results are used.

1. If a 10 sec-4 m probability is needed use the table directly.
2. If a 10 sec probability for some other distance is needed, use the 10 sec curves from Figure 23 to correct the number from the table.
3. If another time/distance is needed within the 2-20 sec 4-7 m group, first use Figure 23 to correct to the proper distance the Figure 24 to correct for the time. The order is important.
4. For another time group, 1-10 sec or 4-40 sec, first use Figure 25 to correct the 10 sec data to either 5 sec or 20 sec then proceed with the appropriate curves as described above.

In order to check initial use of the curves, the following values should be obtained for horizontal displacement, 300-030 deg, 2-5 m/sec:

10sec-4m : 0.44	→	10sec-7m : 0.64
↓		
5sec-1m : 0.12	→	5sec-3m : 0.55
↓		↓
2sec-1m : 0.46		10sec-3m : 0.28

The numbers in parentheses by the arrows indicate the curves (figures) which were used to obtain the desired probability. Again we emphasize that the 25-23-24 order is important. If a different wind speed-wind direction range, or vertical rather than horizontal is desired a new entry from Table 2 must be used.

One may object to the above described procedure because it can not exactly reproduce the original data. This is obvious since Figures 20, 21, and 22 show some scatter in the data. Smoothing the scattered data is desirable. There will be natural fluctuations in any measurements since one is dealing with a fluctuating medium. It is not possible to predict the results of any particular measurement (except by luck), only average behavior can be predicted. Thus, the only appropriate approach is to apply some technique to smooth the results. This is what the curves do.

Finally, there is some dependence on wind direction and the vertical persistence is consistently slightly larger than the horizontal. This is shown in Figure 26. The 10 sec-4 m probabilities from Table 2 are plotted as a function of wind direction range, with separate curves for each wind speed range. The persistence is greatest for range 3, 070-140 deg, and smallest for winds from the West, 200-300 deg. The shaded range, 140-200 deg, is the one for which a different trajectory length was used, with no apparent affect on the data.

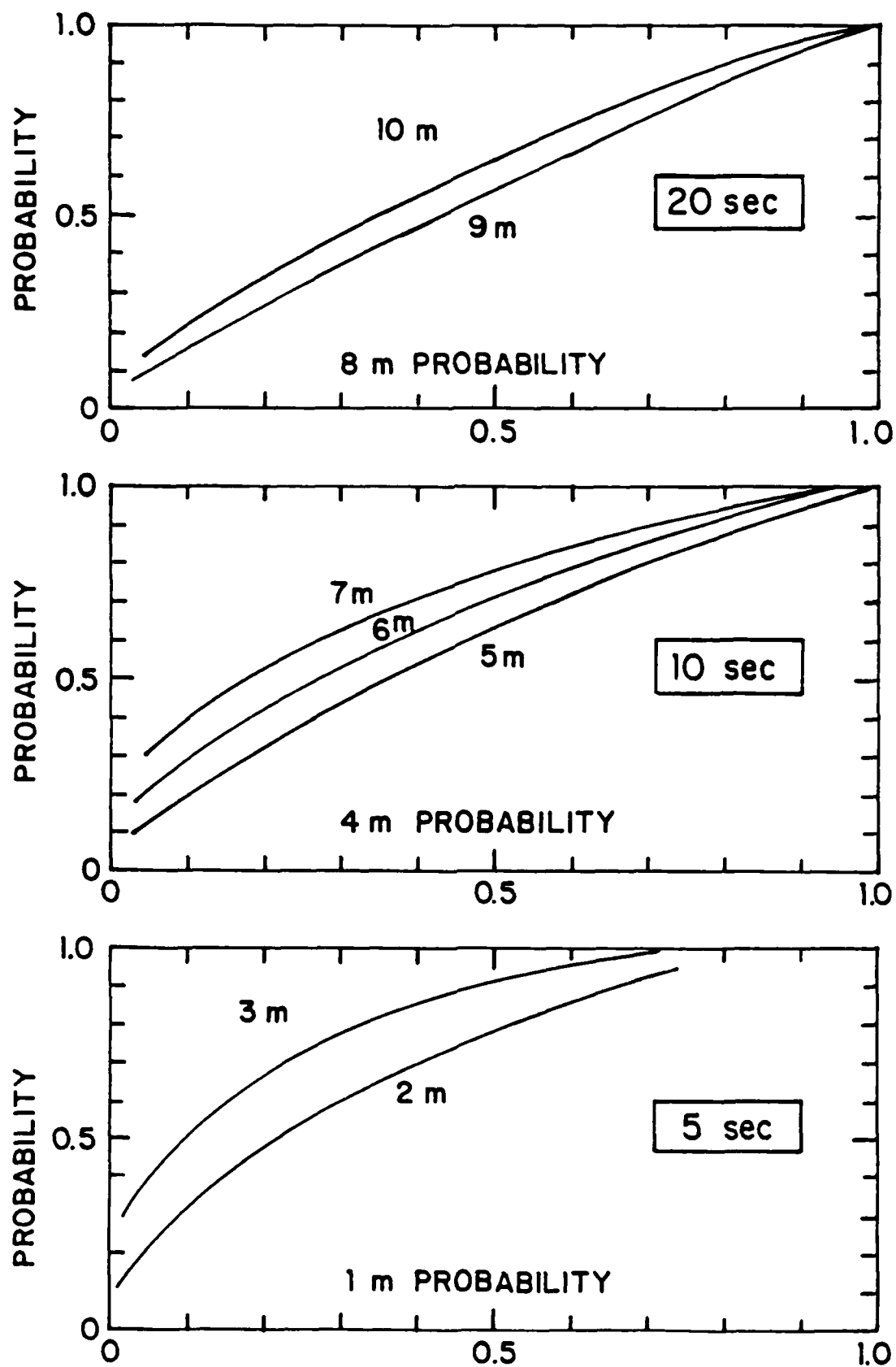


Figure 23. Persistence time probability universal curves to relate probabilities for various distances.

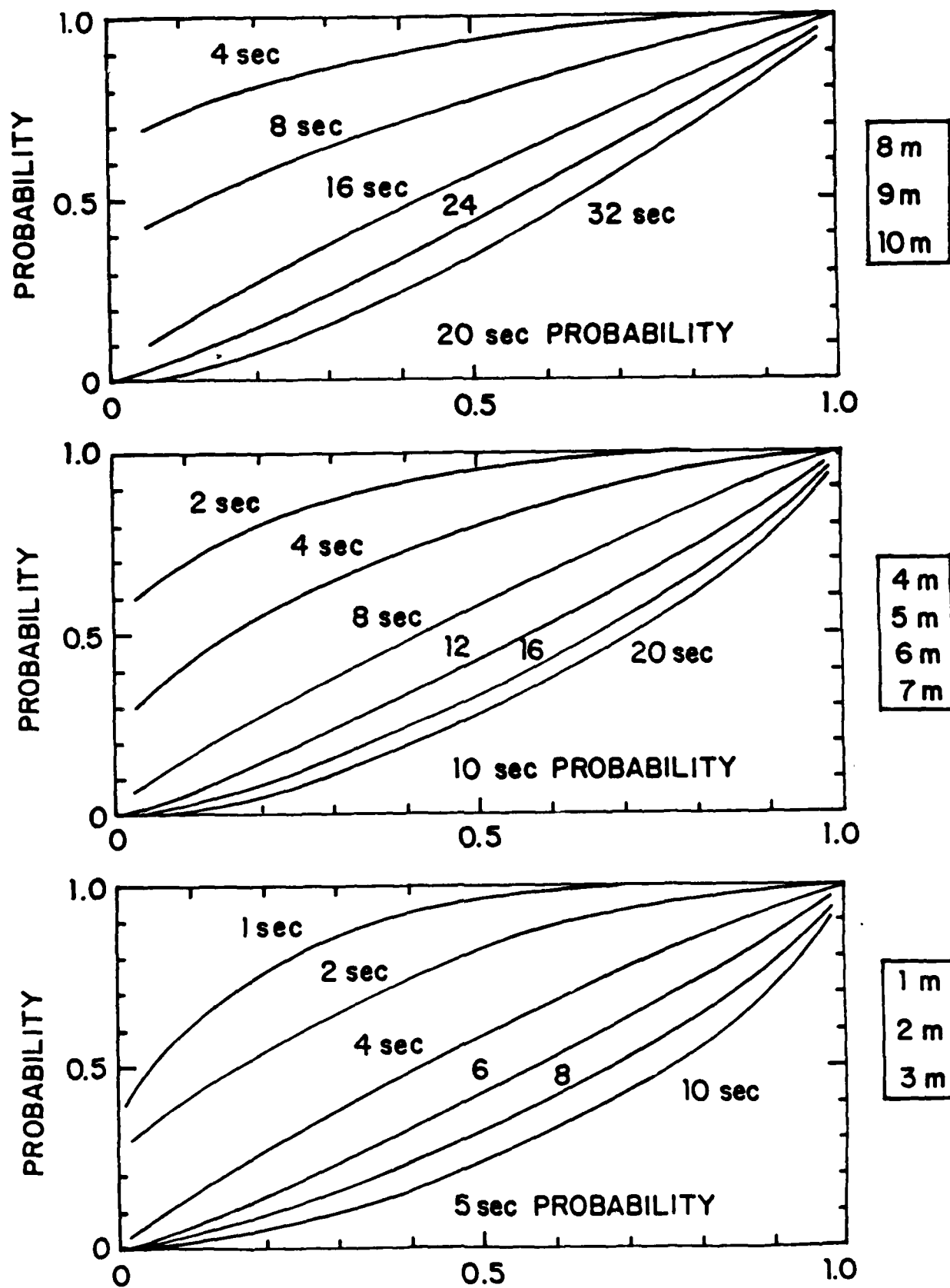


Figure 24. Persistence time probability universal curves to relate probabilities for various times.

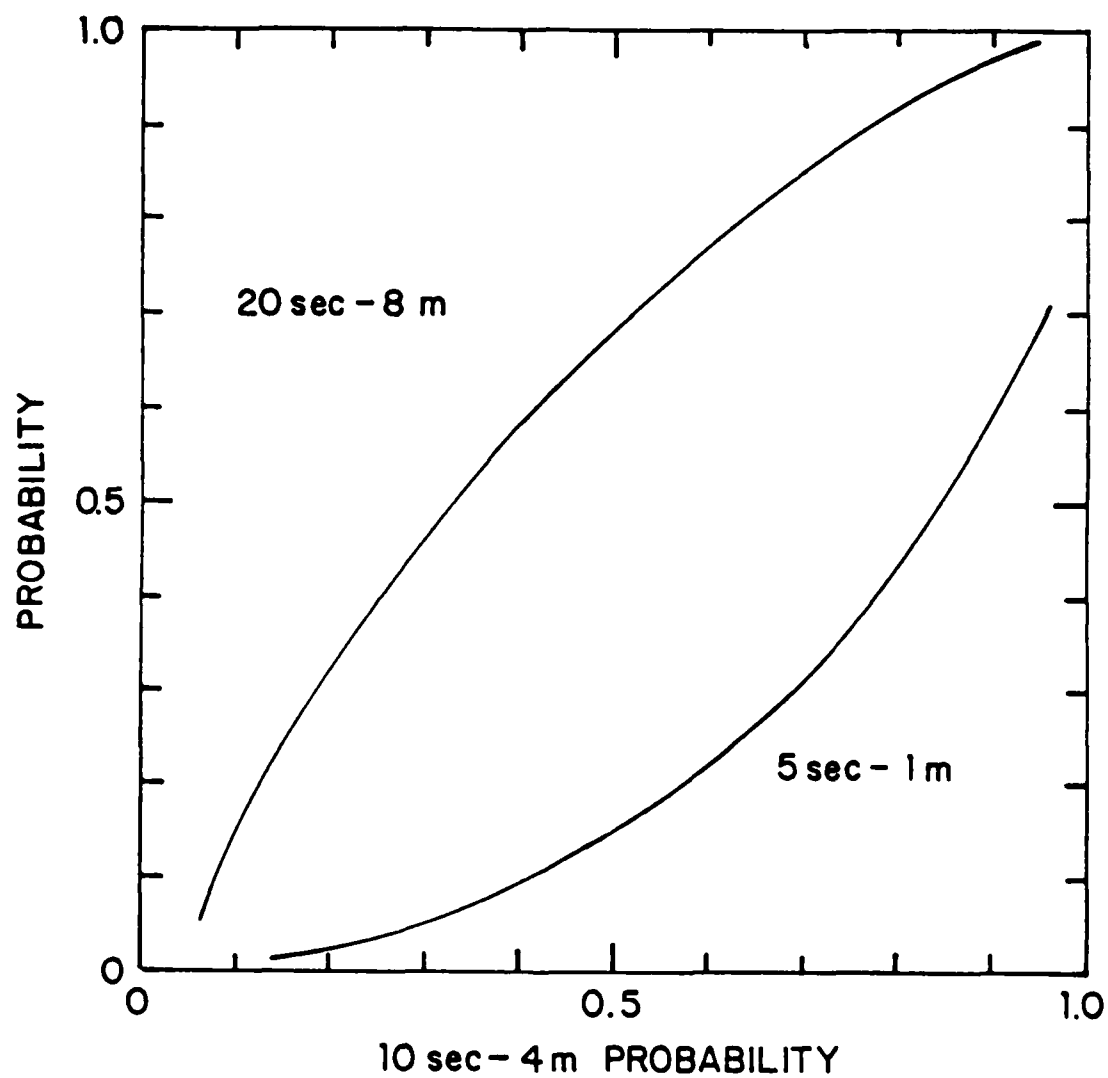


Figure 25. Persistence time probability universal curves to relate 5sec-1m and 20sec-8m probabilities to 10sec-4m.

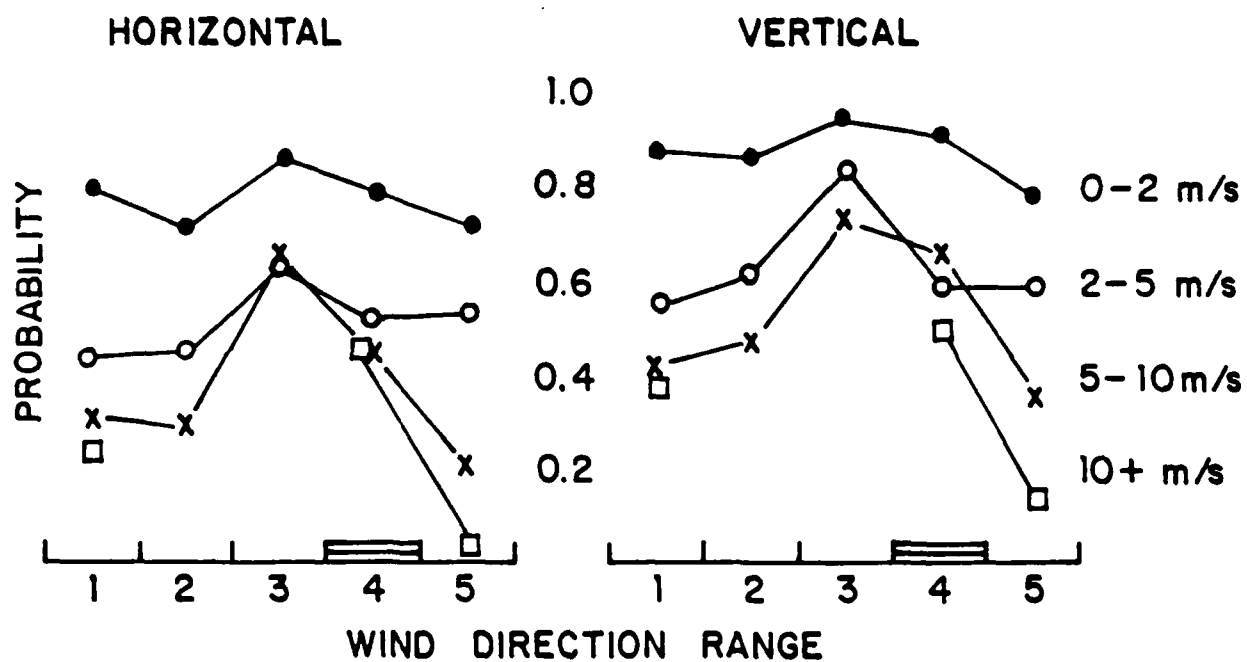


Figure 26. 10m-4sec persistence time probabilities as a function of wind direction range.

	<u>300-030</u>	<u>030-070</u>	<u>070-140</u>	<u>140-200</u>	<u>200-300</u>
<u>U(m/s)</u>	Horizontal				
0-2	0.79	0.76	0.85	0.78	0.71
2-5	0.44	0.45	0.63	0.52	0.53
5-10	0.31	0.30	0.65	0.50	0.21
10+	0.29			0.51	0.03
	Vertical				
0-2	0.87	0.86	0.94	0.91	0.78
2-5	0.55	0.61	0.83	0.59	0.59
5-10	0.43	0.48	0.74	0.66	0.36
10+	0.38			0.50	0.14

Table 2 Persistence time probabilities for 10 sec - 4m displacement.

2. Fraction of Time

Persistence time does not assess the situation where the plume moves rapidly back and forth across a point with small displacement. In this instance, the persistence time is short but the total heat deposited, summed over a longer time period, could be large. It would be difficult to determine the rate at which the plume moves and correlate it with the persistence. A quantity as useful as the rate is the fraction of time the flame remains at or near a location. The point along the trajectory used for this calculation is the same as for persistence: the plume end or the distance from the 50 ft to 90 ft stack.

A 10 min record is divided into equal time intervals, and the fraction determined for each of these intervals. Unless the short term average wind is statistically stationary over the full record, the results will depend on the interval used. Five time intervals are used:

10 sec, 20 sec, 30 sec, 1 min, 2 min

As with the persistence determination, distance thresholds are used for determining the fraction of time spent near the average displacement. The following set of distance thresholds is used for both horizontal and vertical motion:

1, 2, 3, 4, 5, 6, 7, 8, 9, 10 + m

Rather than pick a point in space and determine the fraction of time spent near that point, we determine the average displacement for one of the time intervals listed above and determine the fraction of time spent near that average displacement. The calculation proceeds as follows:

1. Choose the time interval to be used.
2. Calculate the mean displacement for that time interval.
3. Choose the distance threshold to be used.
4. Determine the fraction of time the displacement is within that distance of the mean displacement.
5. Repeat the process for all time interval - allowed distance pairs

Fortunately, the fraction of time results are much easier to interpret than those for persistence. Having separated the horizontal and vertical motions, we are dealing with one-dimensional random walk processes, and the mathematics that

deal with the deviation of a quantity from its average are well understood. Before presenting the mathematical approach we show the basic behavior of the data.

The fraction as a function of displacement for two wind speed ranges and the averaging times used are shown in Figure 27. The general behavior of the curves is the obvious one: The trajectory end spends a greater fraction of the time within large than within small distances. Note that, for longer times, the plume end spends a smaller fraction of the time within a given distance of the average position. This is due to the inclusion of lower frequency motions, meander, in longer time averages.

The dependence on wind speed can also be partially seen from Figure 27. Increased wind speed leads to larger trajectory lengths and increased displacement. This general behavior is modified by the decrease in turbulence intensity with increased wind speed. For longer averaging times, where meander becomes important, displacements definitely decrease with wind speed. The wind speed dependence shows enough variations that generalizations are not very useful. Thus we include no more figures to illustrate this behavior and refer to the tabulated results to be presented later in this section.

The differences in the vertical and horizontal fractions are illustrated in Figure 27. Vertical motions are seen to be less than the horizontal. This is due to the nearness of the trajectories to the ground and the suppression of vertical turbulence near the surface.

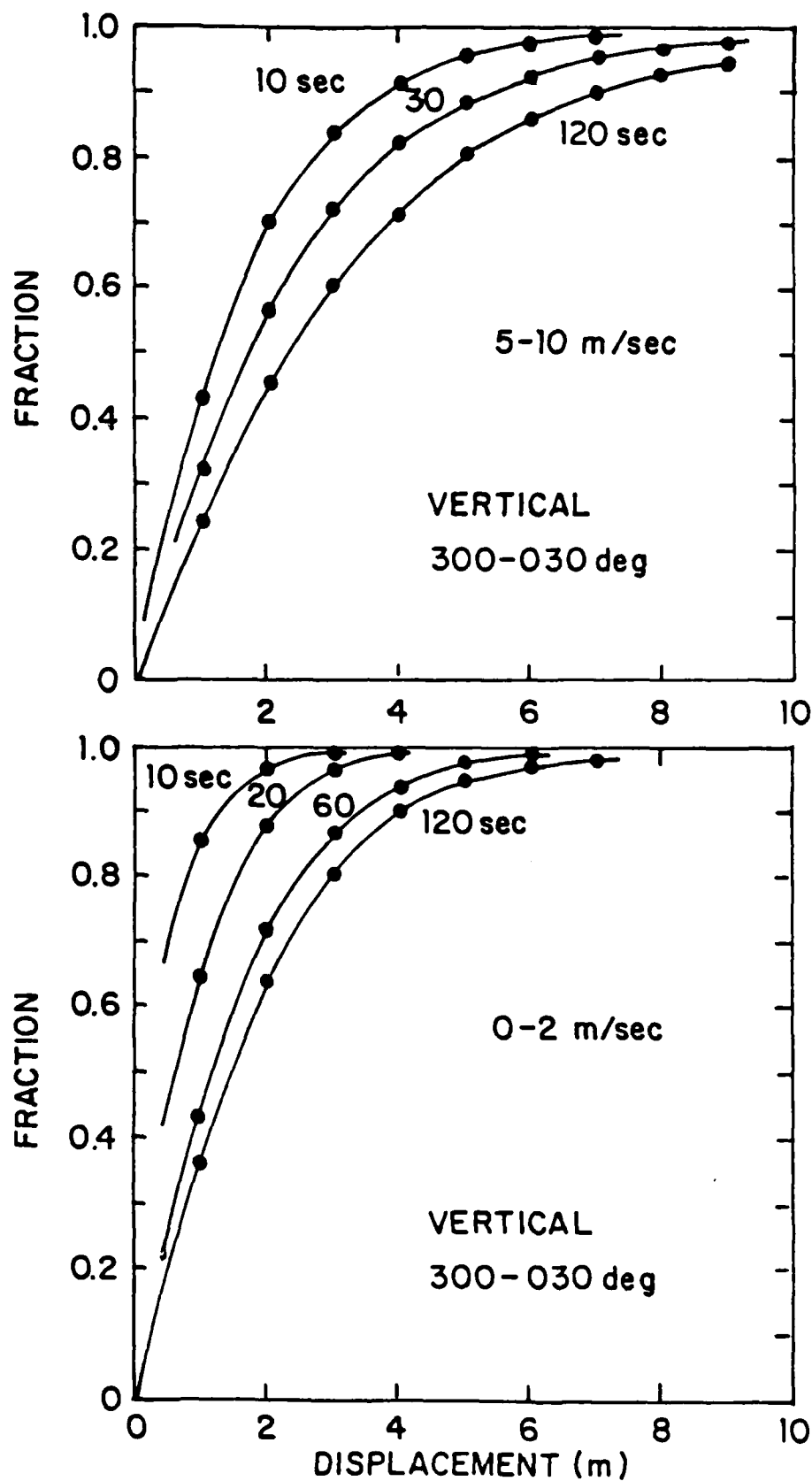


Figure 27. Fraction of the time that the plume end remains within a given displacement of its average position for the four averaging times. Two wind speed ranges are shown.

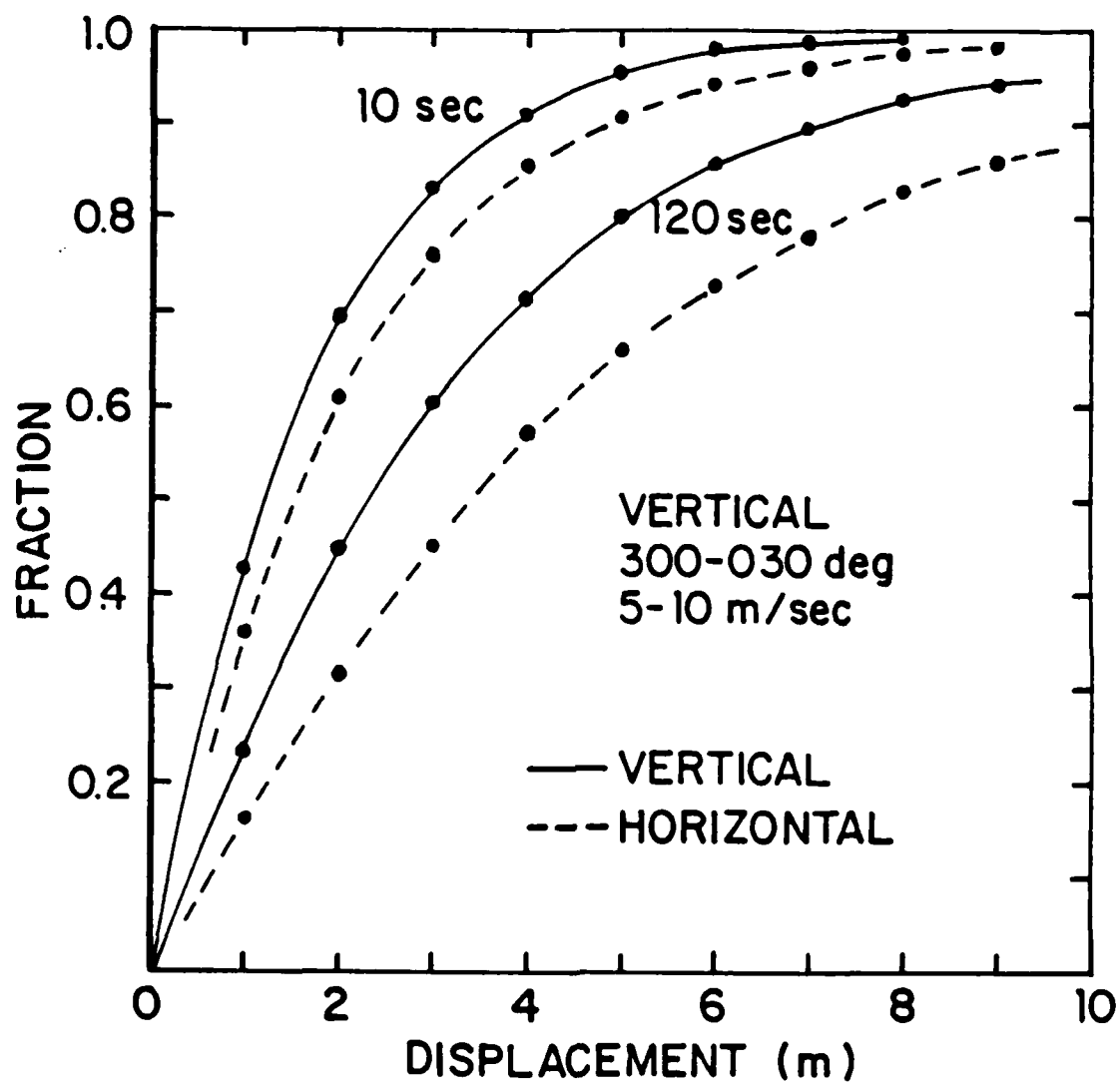


Figure 28. Fraction of the time the plume end remains within a given displacement of its average position for 10 and 120 sec averaging times for vertical and horizontal displacement.

As was stated above, the transverse motion of the end of the air parcel trajectory is a random walk process. If the motion is truly random, the distribution function for the displacement is the normal distribution.

$$F(y) = (1/\sqrt{2\pi} \sigma) \exp[-(y-\bar{y})^2/2\sigma^2], \quad (1)$$

where y is the cross wind displacement, \bar{y} the mean position and σ the standard deviation of the distribution. In this model the only two parameters needed to describe the motion are y and σ . In all that follows, we assume $y=0$ since all calculations are referred to an arbitrary mean position. The probability that the trajectory end will be found within $f\sigma$ of the mean position is

$$P(\text{within } f\sigma) = \int_{-f\sigma}^{f\sigma} F(y) dy. \quad (2)$$

Substituting $y=\sigma x$ gives

$$\begin{aligned} P(\text{within } f\sigma) &= (1/\sqrt{2\pi}) \int_{-f}^f \exp(-x^2/2) dx \\ &= \text{erf}(f) \end{aligned} \quad (3)$$

which is the well known error function. Values for the error function are presented in Table 3.

The probability to be within a given displacement can be directly related to our fraction of time. If the probability to find the trajectory within 3m is 25%, then, over a sufficiently long time, the fraction of time spent within 3m will be 25%. The time interval needed to ensure equality of the probability

and fraction is the averaging time. Table 3 shows that the trajectory end will spend 0.38 of the averaging time within 0.5σ of the mean position, 0.87 within 1.5σ , etc.

The shapes of the fraction curves shown in Figure 27 and 28 are quite similar to a plot of the error function. The error function can be fitted to the data by setting σ equal to the displacement for which the fraction is 0.68 (see Table 3). An example of such a fit is shown in Figure 29. It is easily seen that the fit to the data is fairly good, but not perfect. The data shows slightly higher probability for the occurrence of large displacements, indicating that the distribution is not truly random.

<u>f</u>	<u>erf(f)</u>	<u>Correcton</u>	<u>f</u>	<u>erf(f)</u>	<u>Correction</u>
0	0	0	1.5	.87	-.035
.25	.20	0	1.75	.92	-.033
.5	.38	0	2.0	.95	-.030
.75	.55	0	2.5	.988	-.023
1.0	.68	0	3.0	.997	-.015
1.25	.79	-.025			

Table 3. Error function and corrections to the error function fit to the fraction of time data as a function of the fraction of the standard deviation.

We have fit all fraction data with the error function, as described above and shown in Figure 29. The resulting standard deviations are presented in Table 4. Use of the standard

deviations and the error function will lead to about a 3% error at large displacements. If this error is significant for a particular application, a correction can be made. The needed corrections are listed in Table 3.

The use of the error function is quite simple:

1. For a given set of conditions, determine the standard deviation from Table 4.
2. Choose the displacement for which the fraction of time is wanted and determine what fraction, f , of the standard deviation that displacement is.
3. If the quantity wanted is the fraction of time the trajectory end will be within the displacement, look up the probability in Table 3. The correction may be used if desired.
4. If the quantity wanted is the fraction of time the trajectory end will be within some range, a_0 to b_0 , use

$$\begin{aligned} P(a_0 \text{ to } b_0) &= P(\text{within } b_0) - P(\text{within } a_0) \\ &= \text{erf}(b) - \text{erf}(a). \end{aligned} \quad (4)$$

The fraction of time depends on wind direction, as can be seen in Table 4. The fraction standard deviations as a function of wind direction range are shown in Figure 30. Horizontal and vertical displacements are shown separately and it is obvious that the horizontal are larger. There is a consistent pattern to the wind direction dependence. Winds from the Southeast and South have consistently low standard deviations, ranges 3 and 4, 070-140 deg and 140-200 deg. Northerly and northwesterly winds

produce the largest standard deviations. No explanation is offered for these dependences. Note that range 4 is shaded in Figure 30. This is due to a different plume length being used for that range since the impact of the South stack on the North stack is of interest. This change has no apparent effect on the results.

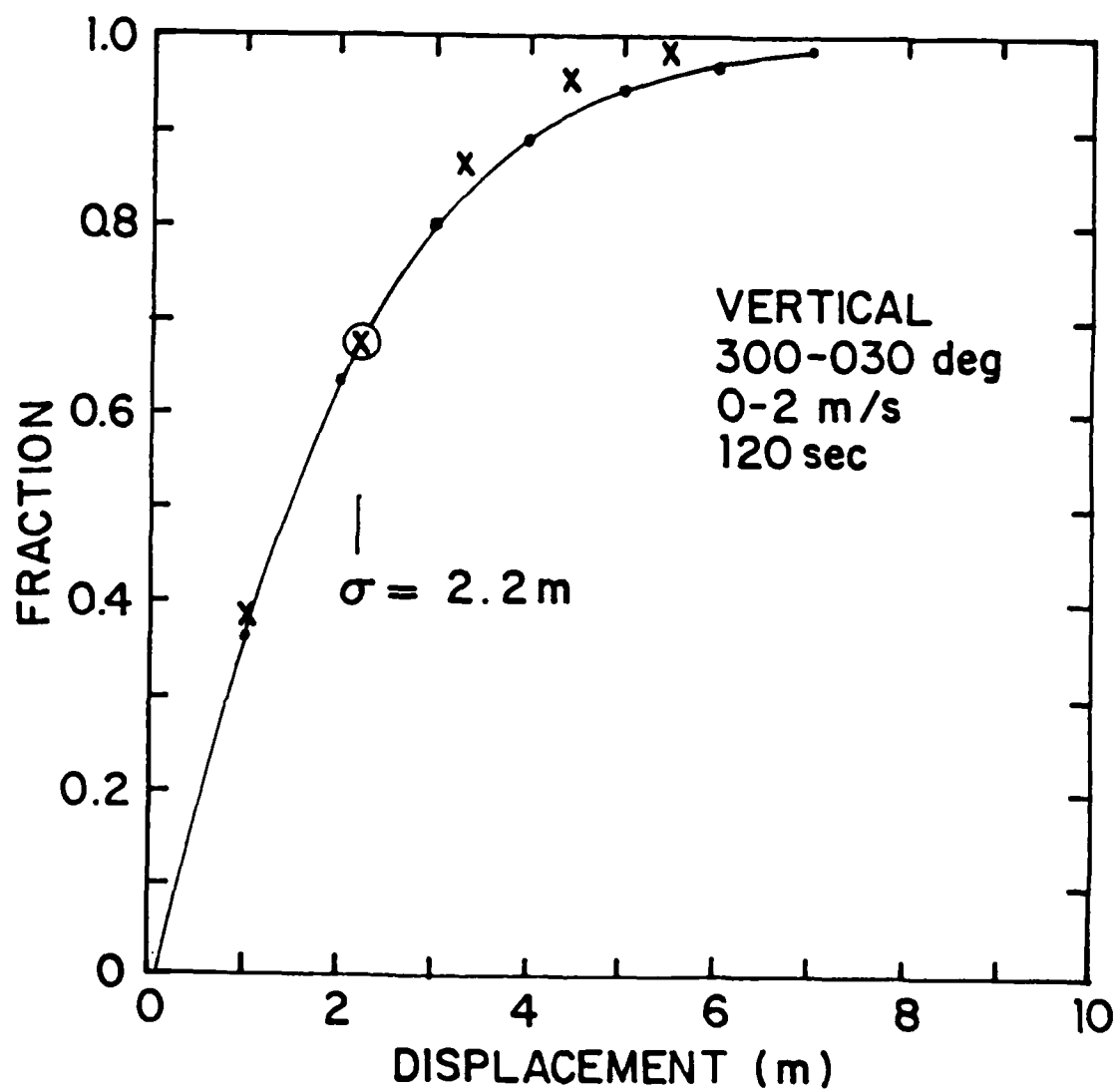


Figure 29. Fraction of time data (dots) and superimposed error function fit (crosses).

Fraction of Time Standard Deviation (m)

<Direction> Averaging Time	Vertical Wind Speed (m/sec)				Horizontal Wind Speed (m/sec)			
	0-2	2-5	5-10	10+	0-2	2-5	5-10	10+
<300-030>								
10	0.82	1.6	2.0	2.0	0.88	2.1	2.5	2.3
20	1.1	2.5	2.8	2.4	1.4	3.3	3.6	3.0
30	1.5	3.0	3.0	2.6	1.8	4.2	4.2	3.4
60	1.9	3.6	3.4	2.7	2.5	5.6	4.9	3.7
120	2.2	4.0	3.6	2.8	3.1	6.7	5.4	3.9
<030-070>								
10	0.81	1.3	1.8	1.8	0.90	1.8	2.3	2.3
20	1.2	1.9	2.6	2.1	1.6	2.9	4.0	2.8
30	1.3	2.3	2.9	2.2	1.9	3.7	4.5	3.0
60	1.8	2.7	3.2	2.3	2.7	4.6	5.3	3.2
120	2.2	2.9	3.4	2.4	3.5	5.3	5.7	3.4
<070-140>								
10	0.75	0.9	1.5		0.81	1.1	1.9	
20	0.87	1.2	2.0		1.2	1.8	2.7	
30	1.0	1.5	2.2		1.5	2.1	3.0	
60	1.3	1.7	2.4		2.0	2.5	3.4	
120	1.5	1.8	2.6		2.6	2.8	3.6	
<140-200>								
10	0.78	1.1	1.7	1.6	0.85	1.5	1.9	1.6
20	0.91	1.8	2.2	1.8	1.3	2.3	2.9	2.1
30	1.1	2.1	2.5	1.9	1.5	2.6	3.4	2.7
60	1.5	2.6	2.7	1.9	2.1	3.6	3.9	2.5
120	1.7	2.8	3.0	1.9	2.7	4.3	4.4	2.5
<200-300>								
10	0.9	1.4	2.0	3.5	0.92	1.5	2.6	4.6
20	1.4	2.2	3.0	3.8	1.6	2.6	4.4	5.5
30	1.7	2.6	3.2	4.8	2.0	3.2	5.0	6.4
60	2.1	3.3	3.8	4.8	2.8	4.3	5.9	6.7
120	2.6	3.7	4.0	4.9	3.6	5.4	6.5	7.4

Table 4. Fraction of time standard deviations as a function of wind speed and wind direction for averaging times of 10, 20, 30, 60, and 120 sec.

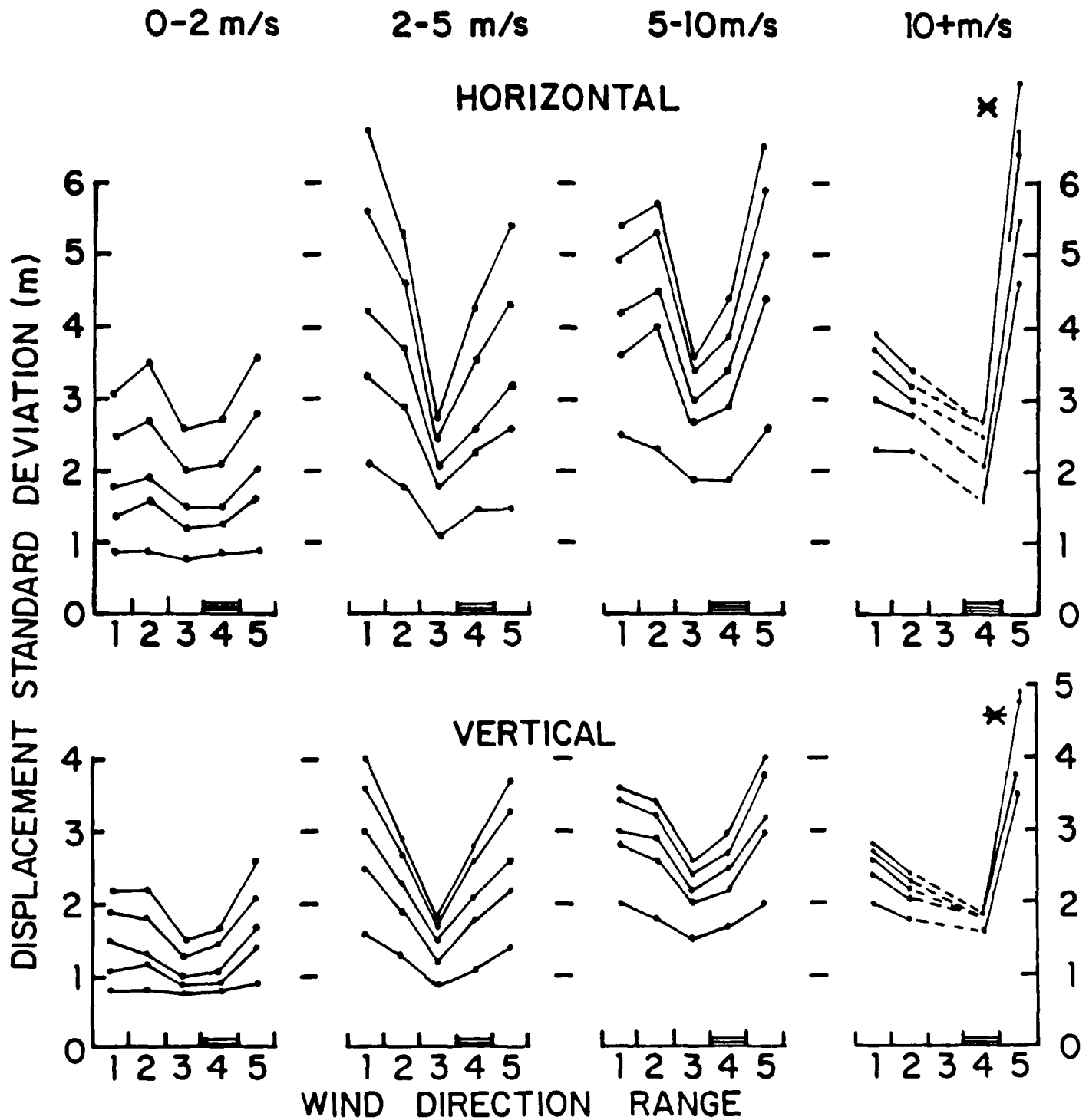


Figure 30. Displacement standard deviations as a function of wind direction range. Data for 10, 20, 30, 60, 120sec averaging time are shown with 10sec having the lowest and 120sec the highest standard deviations.

*Statistics are poor for this data set.

VIII. SPECTRAL ANALYSIS

The analyses described have all been in the time domain, relying on detailed time series calculations and on averaging. Spectral analysis is performed in the frequency domain, yielding average characteristics of the turbulence over the period of the Fourier transform. For this analysis, the averaging period was 10 or 20 min. Since the sampling period was 1 sec, the spectra contain frequencies from 1 Hz to ~ 0.001 Hz.

Spectral analysis does not add new information. Rather, a spectrum contains information about the average properties of the turbulence, from which some of the same quantities determined from time series analysis can be calculated. This gives a useful cross check on the results. We perform such a cross check by using the spectra to calculate vertical displacement.

In order to calculate displacement we must assume some model for the air motion and use the spectra to determine magnitudes for the model parameters. The model is straight forward; sinusoidal behavior of the turbulence motion and imbedded turbulence are assumed. This behavior is illustrated in Figure 31, where a schematic of a single eddy is shown. Idealized effects such eddies would have on the plume are shown in Figure 32 for two different size eddies.

Obviously, the behavior of the plume is the superposition of its response to a spectrum of eddies. In Figure 32, we see that the displacement of the plume is greater for the low frequency eddy, assuming the maximum vertical velocity is the same for each case, because of the longer time to respond.

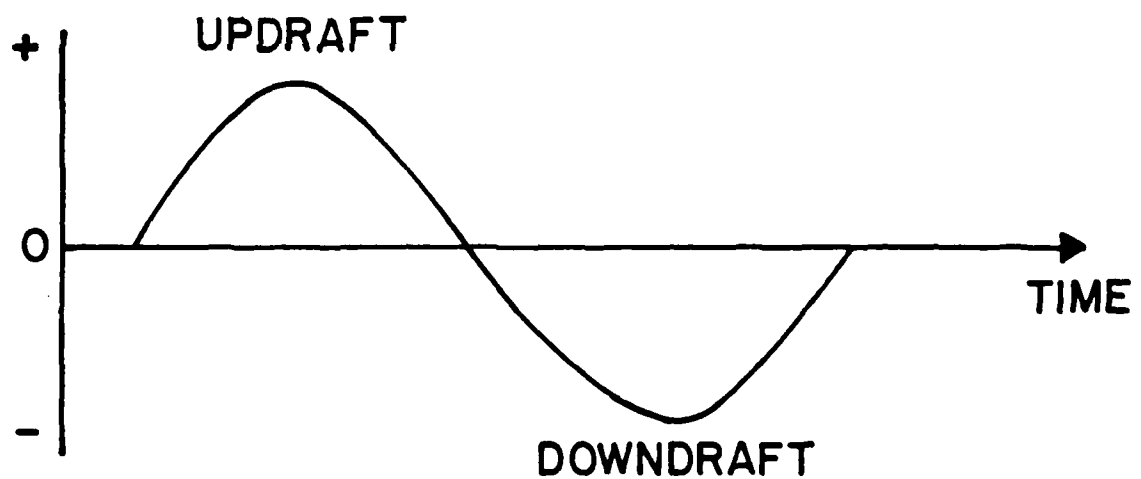
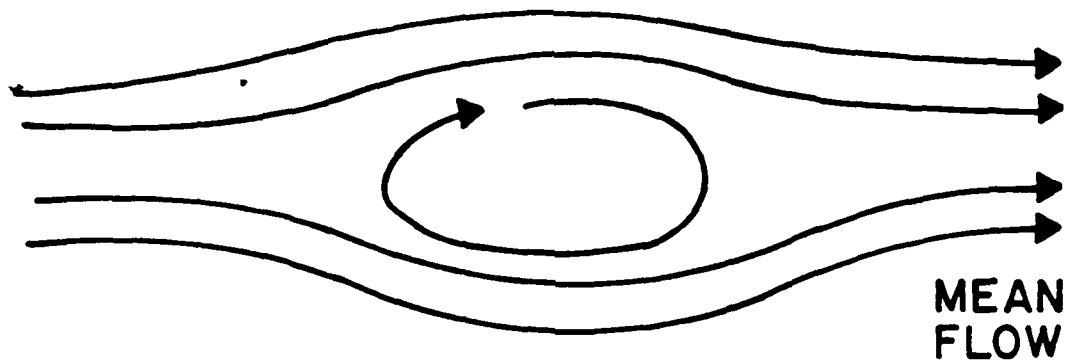
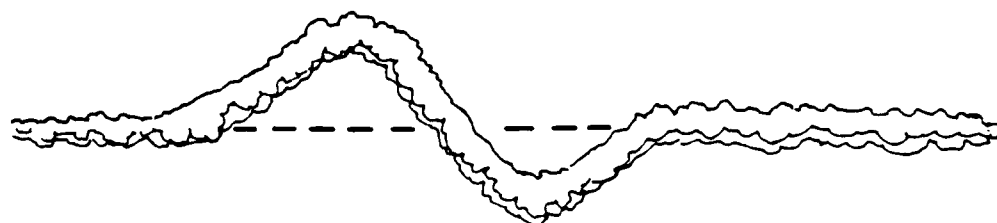
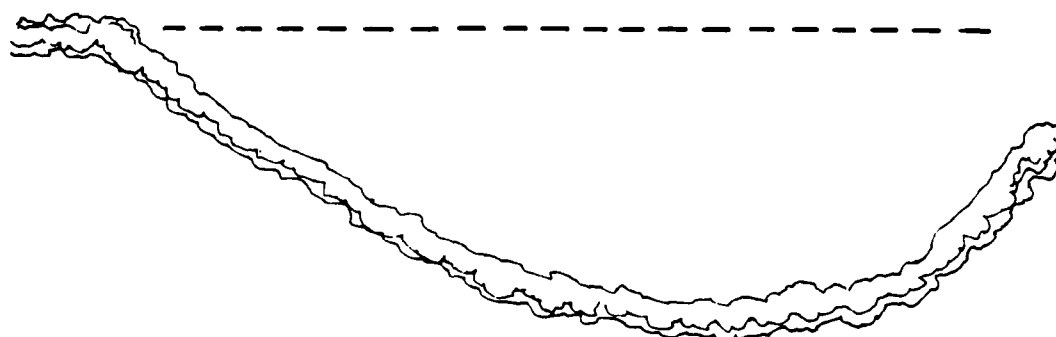


Figure 31. Schematic of a single turbulence eddy superimposed on the mean flow and the assumed sinusoidal behavior of the vertical velocity.



HIGH FREQUENCY EDDY



LOW FREQUENCY EDDY

Figure 32. Response of the plume to an idealized eddy for two different sized eddies.

The displacement of the plume depends on the rms vertical velocity and the time it acts on the plume.

$$D = WT, \quad (5)$$

where D is the displacement, W the rms velocity, and T the period of the eddy. W can be found from the power spectral density of the vertical velocity from

$$\overline{W^2(f)} = \int_{.62f}^{1.62f} (fS) df, \quad (6)$$

which is illustrated in Figure 33, the integral being the area shown. f is the frequency and S the spectral density. When the integral is evaluated we find

$$\overline{W^2(f)} = fS,$$

giving

$$\begin{aligned} D^2 &= fST^2 \\ &= S/f, \quad \text{for } T < L/U \end{aligned} \quad (7)$$

The time used to calculate the displacement cannot be longer than L/U, where L is the length of the plume and U is the mean wind speed. Thus

$$D^2 = fS(L/U)^2, \quad \text{for } T > L/U. \quad (8)$$

Use of the equations for D allows us to convert a power spectrum into a displacement function. This is illustrated in Figure 34. Note that what has been done is to assume that the full energy at a given frequency is contained in a single eddy.

The plume will not respond to a single eddy but a superposition of many eddies. We take this into account by finding W for several frequencies, being careful not to let the integrals overlap, and assuming that the eddies are randomly superimposed. The frequency range covered by a single integral is

$$1.62/0.62 = 2.6$$

The spectrum is approximately flat for approximately one decade. Thus

$$10/2.6 = 3.8 \approx 4$$

and we can assume that the spectrum contains about 4 independent eddies of the same amplitude. We find the "expected" displacement by assuming random walk response, so

$$\begin{aligned} \text{Dexp} &= (\text{Step Length}) \quad (\text{Number of Steps}), \\ &= D_{\max} \sqrt{4}, \\ &= 2 D_{\max}, \end{aligned} \tag{9}$$

where D_{\max} is found from the displacement function, Figure 34.

Two sets of vertical velocity spectra are shown in Figure 35. The results of applying the above analysis to these data, and the background conditions, are as follows:

Case 27.1	Daytime	Unstable	$U = 13$ kts
	$L/U = 15.6$ sec		
	$D_{\max} = 6.9$ m		
	$D_{\text{exp}} = 13.8$ m		
	$= 45$ ft		

Case 7.1 Nighttime Stable U = 4.5 kts

L/U = 22 sec*

Dmax = 6.4 m

Dexp = 12.8 m

= 42ft

*Unrealistic lifetime, use 15 sec

Dmax = 2.1 m

Dexp = 4.2 m

= 14 ft

These results are in good agreement with the time series analyses, adding validity to the approach.

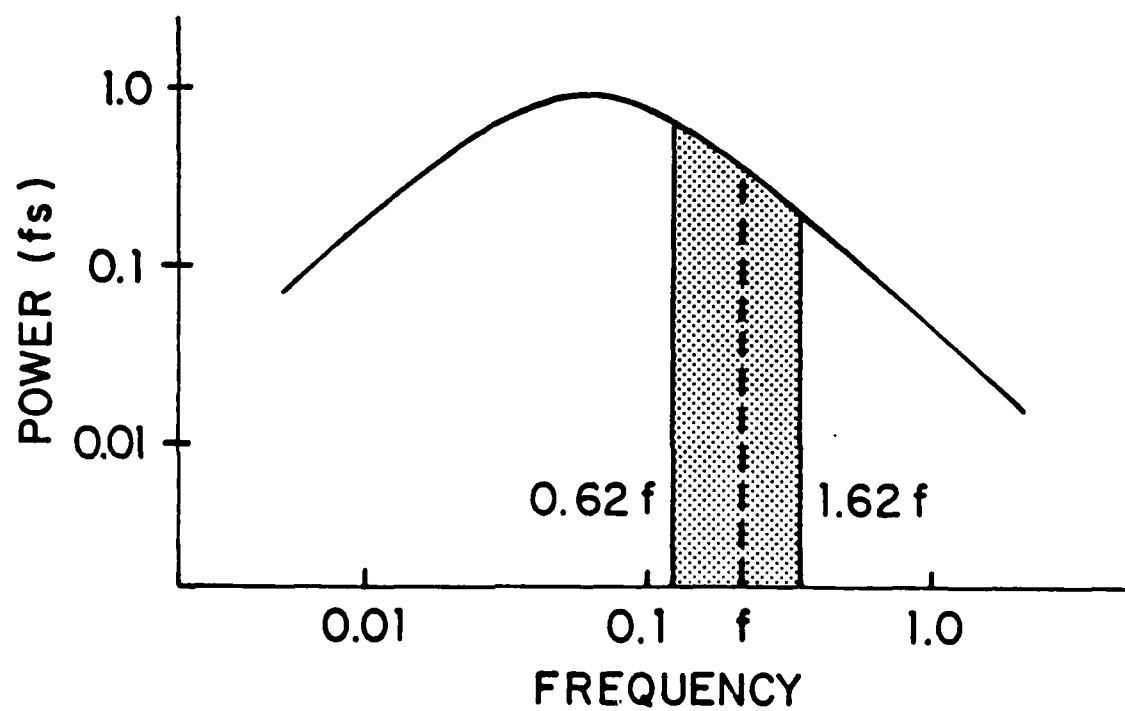


Figure 33. Schematic power spectral density of vertical velocity and the area used to determine the mean-square vertical velocity at frequency f .

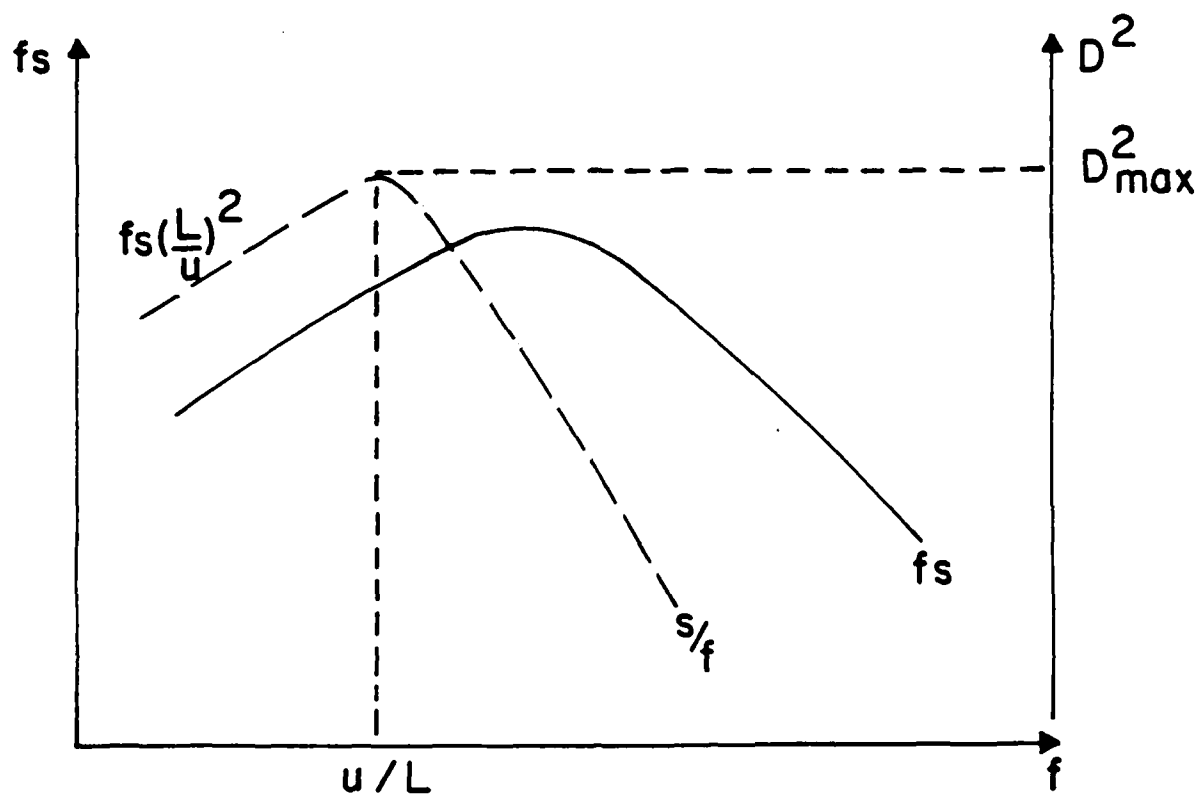


Figure 34. Conversion of a power spectrum into a displacement function. The dashed line is the power spectrum and the solid line the resulting displacement.

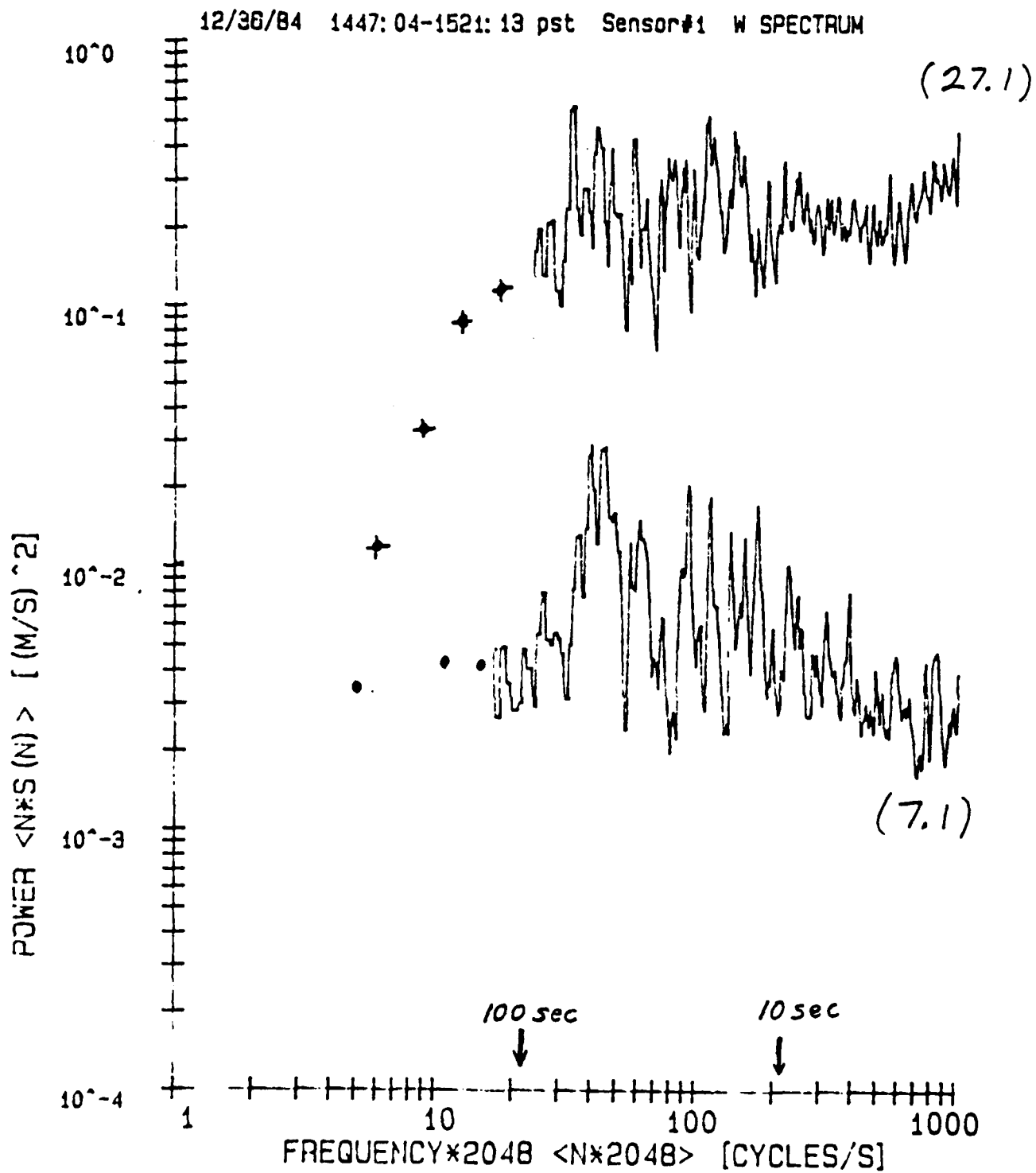


Figure 35. Example of power spectral density plots of vertical velocity.

IX. WIND CLIMATOLOGY

Since the severity of the hazard from the hydrogen flare is directly related to the wind direction, it is important to determine the frequency of occurrence of the direction. Results of this type already were presented in Section I where the wind speed was included as a parameter, and the data was taken at the flare stacks. The flare stack data was from a limited time period. The data presented in this section is from one full year of 15 min average wind measurements from Tower 301.

Monthly fractional occurrences of wind direction, in 20 deg bins, are shown in Figures 36. Note that no data is present for December due to equipment malfunction. It is apparent that the predominant wind direction is from the North. This is due to the predominant north westerlies being turned by the local coastal hills. This is a well known effect that appears in long term wind climatologies for the area.

Even though south winds are much less frequent than northerlies, the figures show that they do occur in all seasons. Since south winds represent a special hazard from the South flare stack impacting on the North, this wind direction receives special treatment. The probabilities that a south wind, when it occurs, will be at a particular time of day, are shown in Figure 37. These figures are not normalized, they only show relative probabilities.

The general conclusion to be reached from the South wind figures is that it can occur at almost any time with somewhat

AD-A162 520

AIR PARCEL MOTION AT THE VANDENBERG HYDROGEN FLARE
STACKS(U) NAVAL POSTGRADUATE SCHOOL MONTEREY CA
G E SCHACHER ET AL OCT 85 NPS-61-86-005

2/2

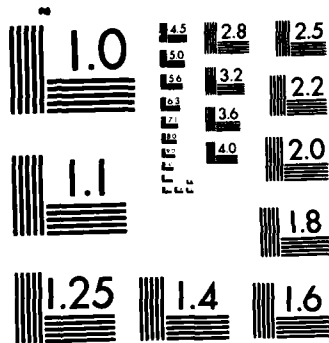
UNCLASSIFIED

MIPR-FV6168500914

F/G 19/1

NL





MICROCOPY RESOLUTION TEST CHART
NATIONAL BUREAU OF STANDARDS-1963-A

a preference for daytime periods. During the late spring and summer the occurrence is mainly during the morning. This is when the transition periods from land to sea-breezes occur, with the accompanying high and variable winds, often from the South.

An example of a full-day wind record from 1/23/85 is shown in figure 38. The data is the 10 min average wind direction as a function of time of day. S-N shows the direction for which the plume from the south stack impacts the northerly one. The figure shows a common diurnal cycle: Southerlies during the morning when no well established wind has developed, a transition before noon, afternoon westerlies due to a seabreeze, and evening land-breeze easterlies

It is reasonable to assume that south winds occur predominantly during transition periods, but we cannot present evidence for this here. The required detailed wind study, accompanied by synoptic analysis, is too lengthy and not appropriate for this study. Such a study will appear in the near future in a report to Air Force Space Division, and may be requested from these authors.

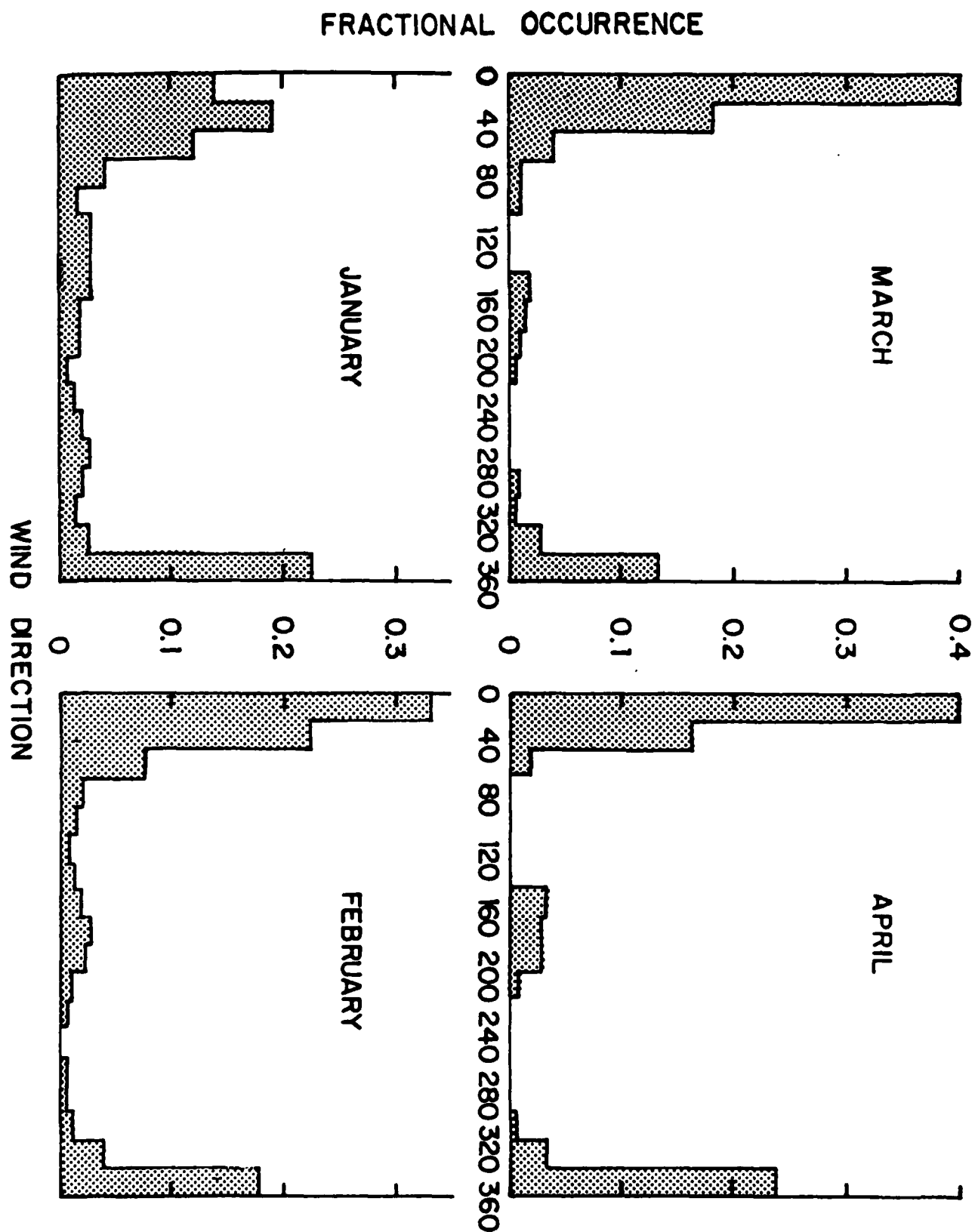


Figure 36a. Fractional occurrence of the wind as a function of wind direction for each month.

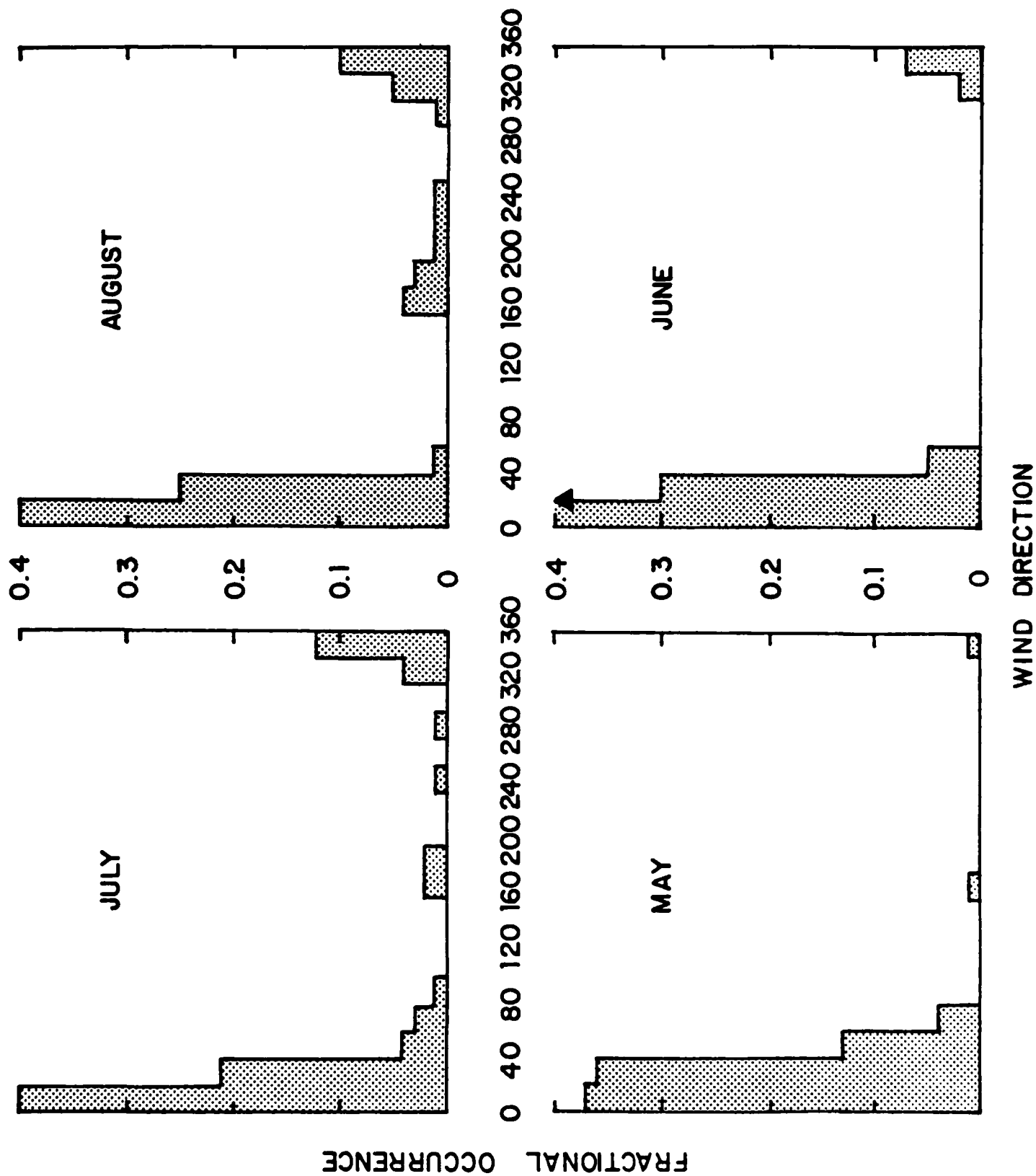


Figure 36b. Fractional occurrence of the wind as a function of wind direction for each month.

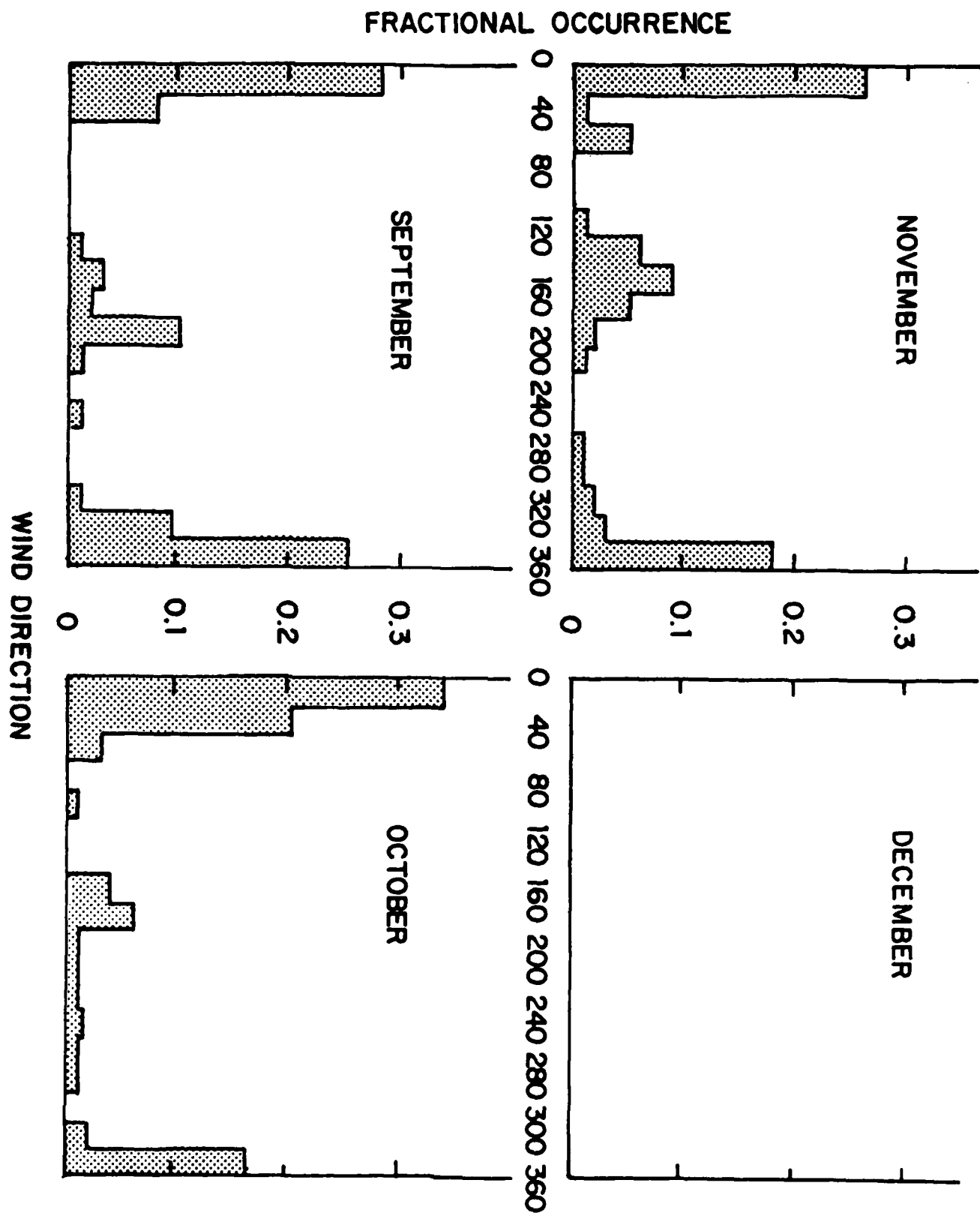


Figure 36c. Fractional occurrence of the wind as a function of wind direction for each month.

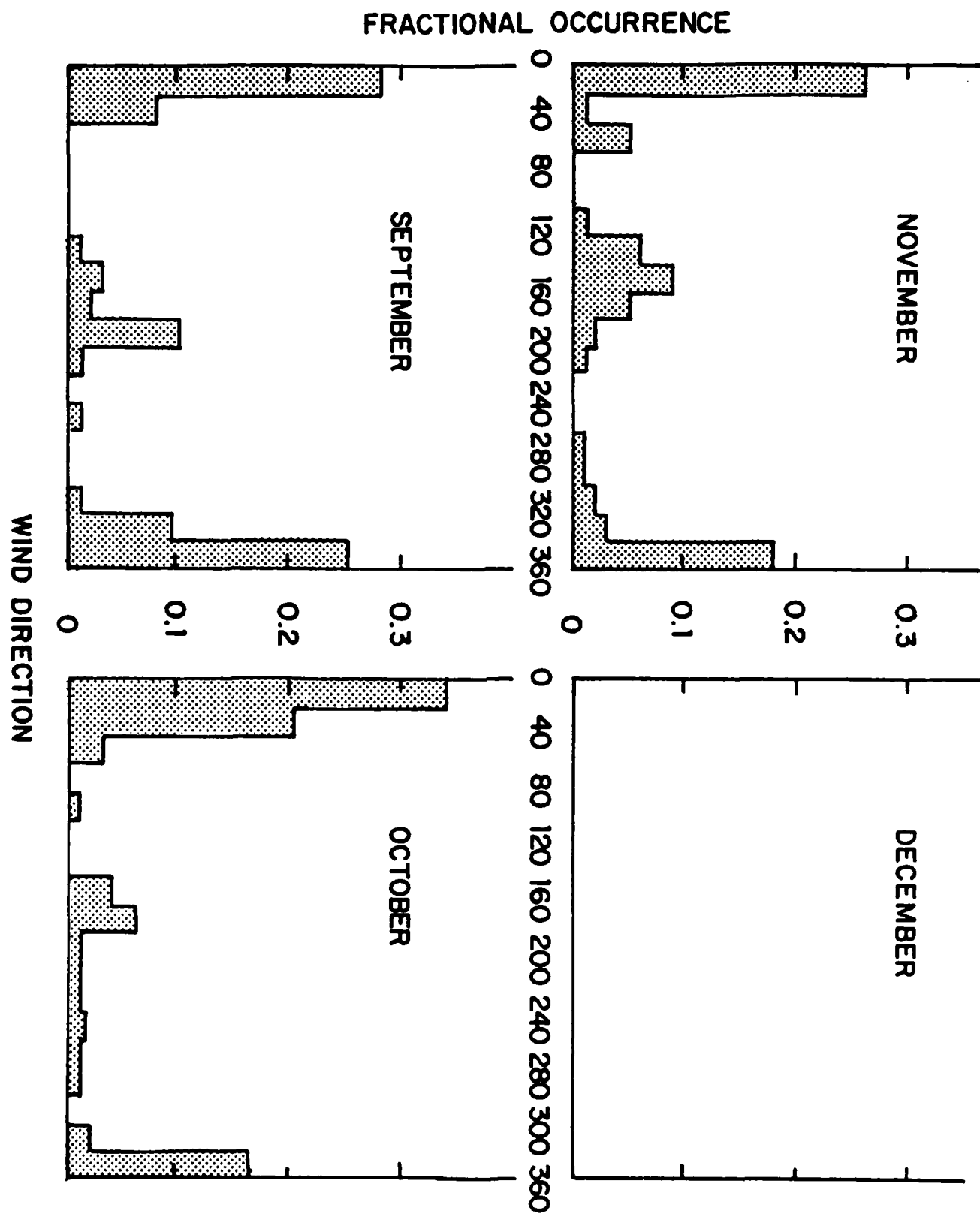


Figure 36c. Fractional occurrence of the wind as a function of wind direction for each month.

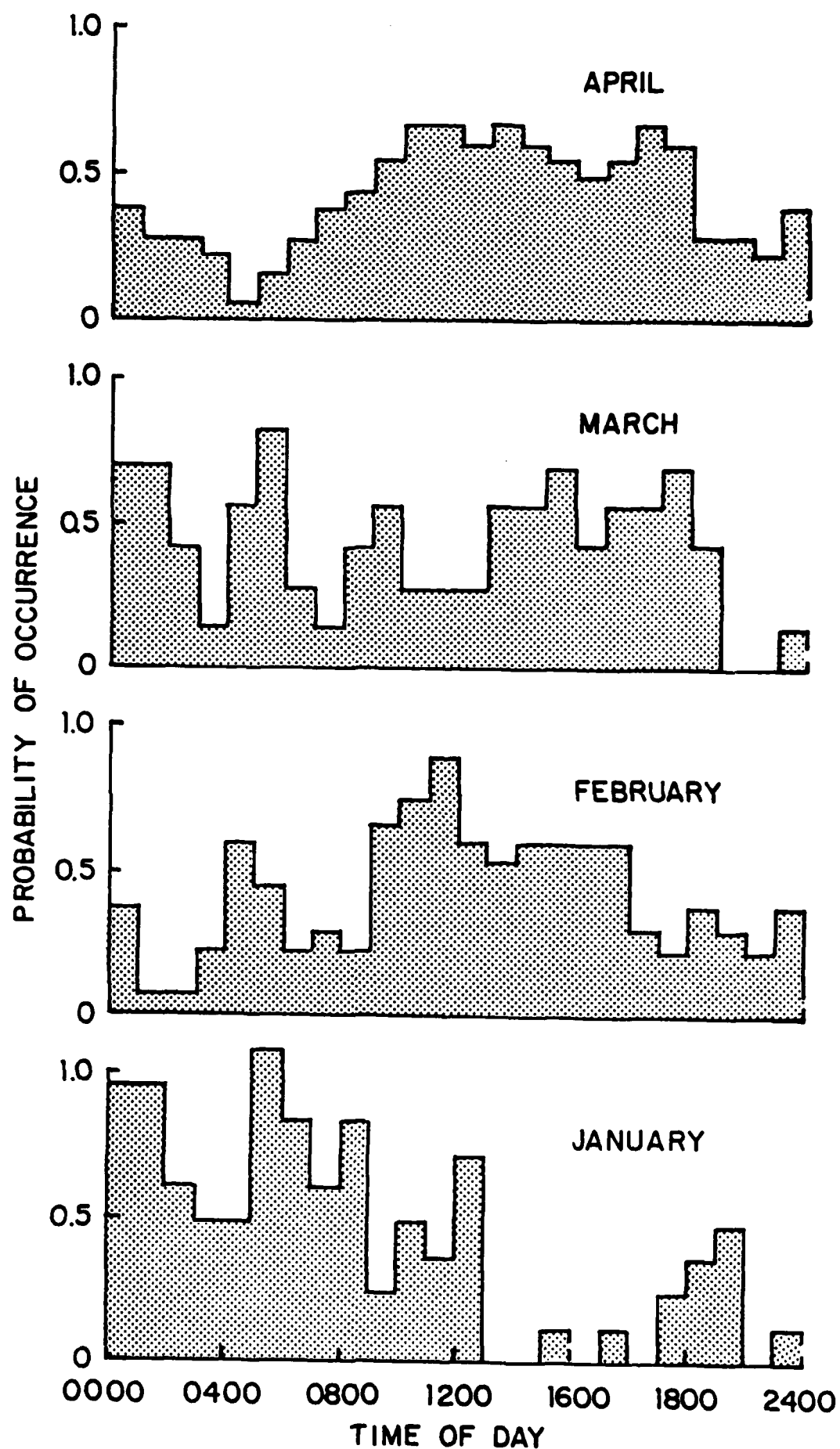


Figure 37a. Probability that a south wind, when it occurs, will be at a particular time of day (non-normalized).

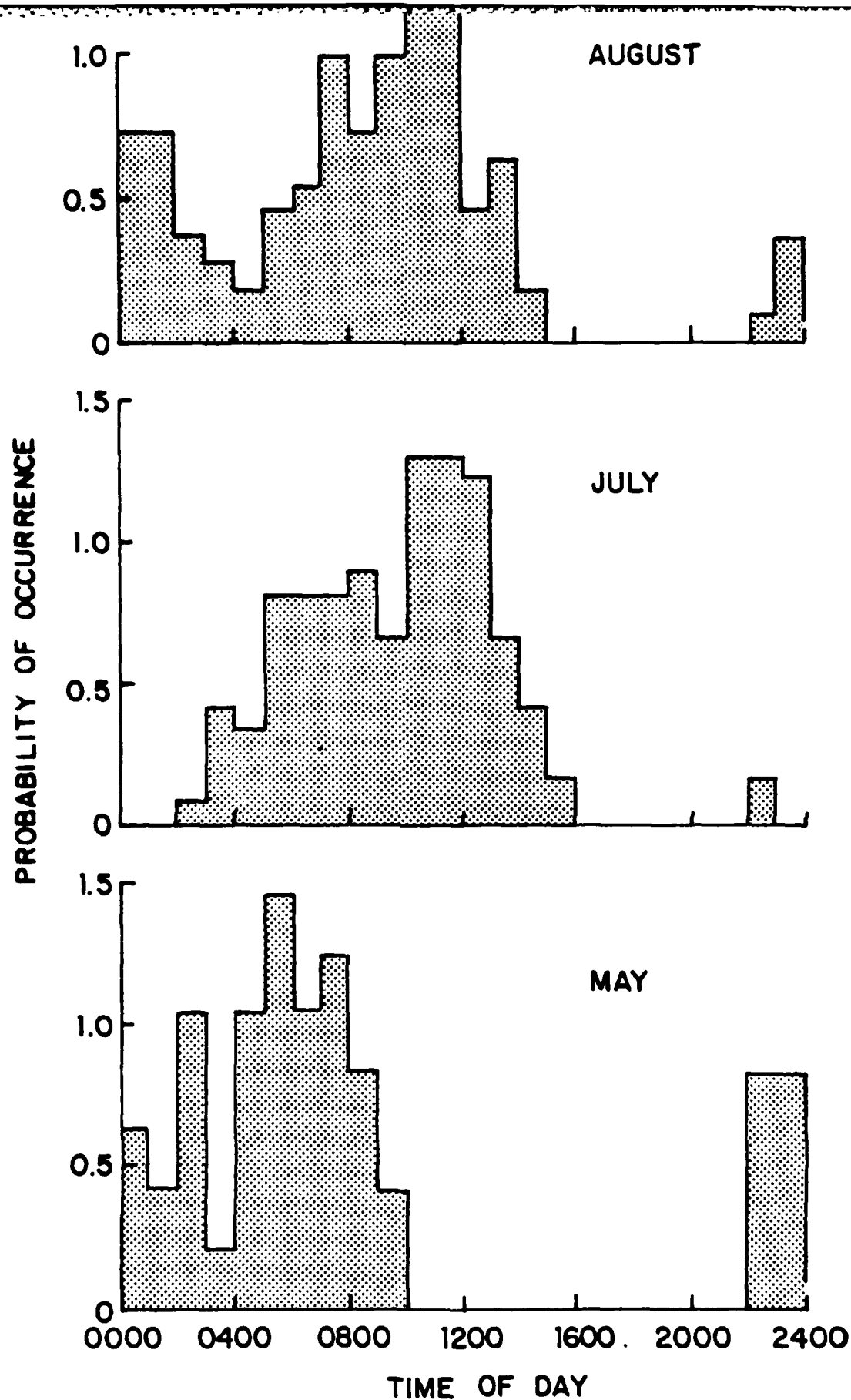


Figure 37b. Probability that a south wind, when it occurs, will be at a particular time of day (non-normalized).

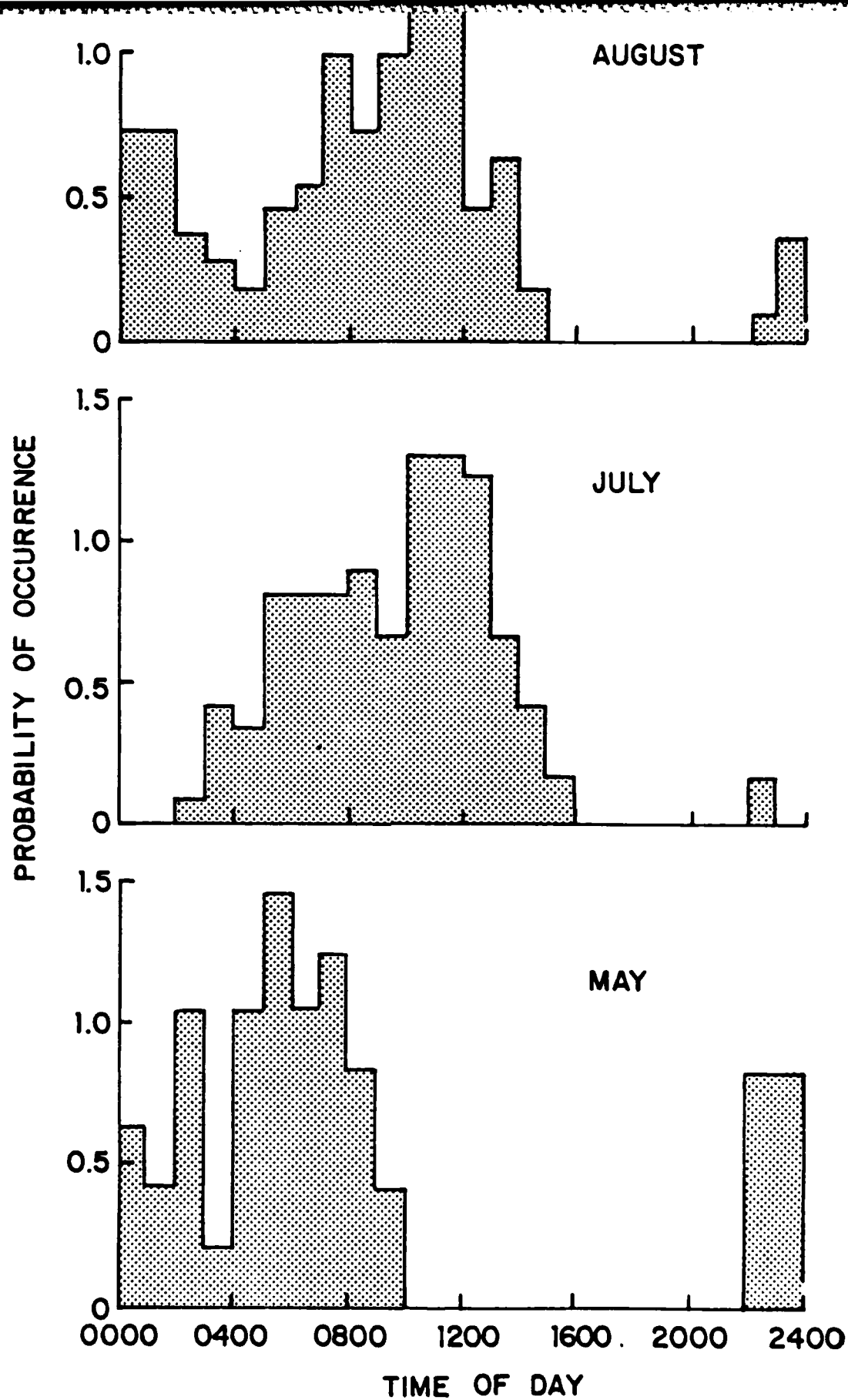


Figure 37b. Probability that a south wind, when it occurs, will be at a particular time of day (non-normalized).

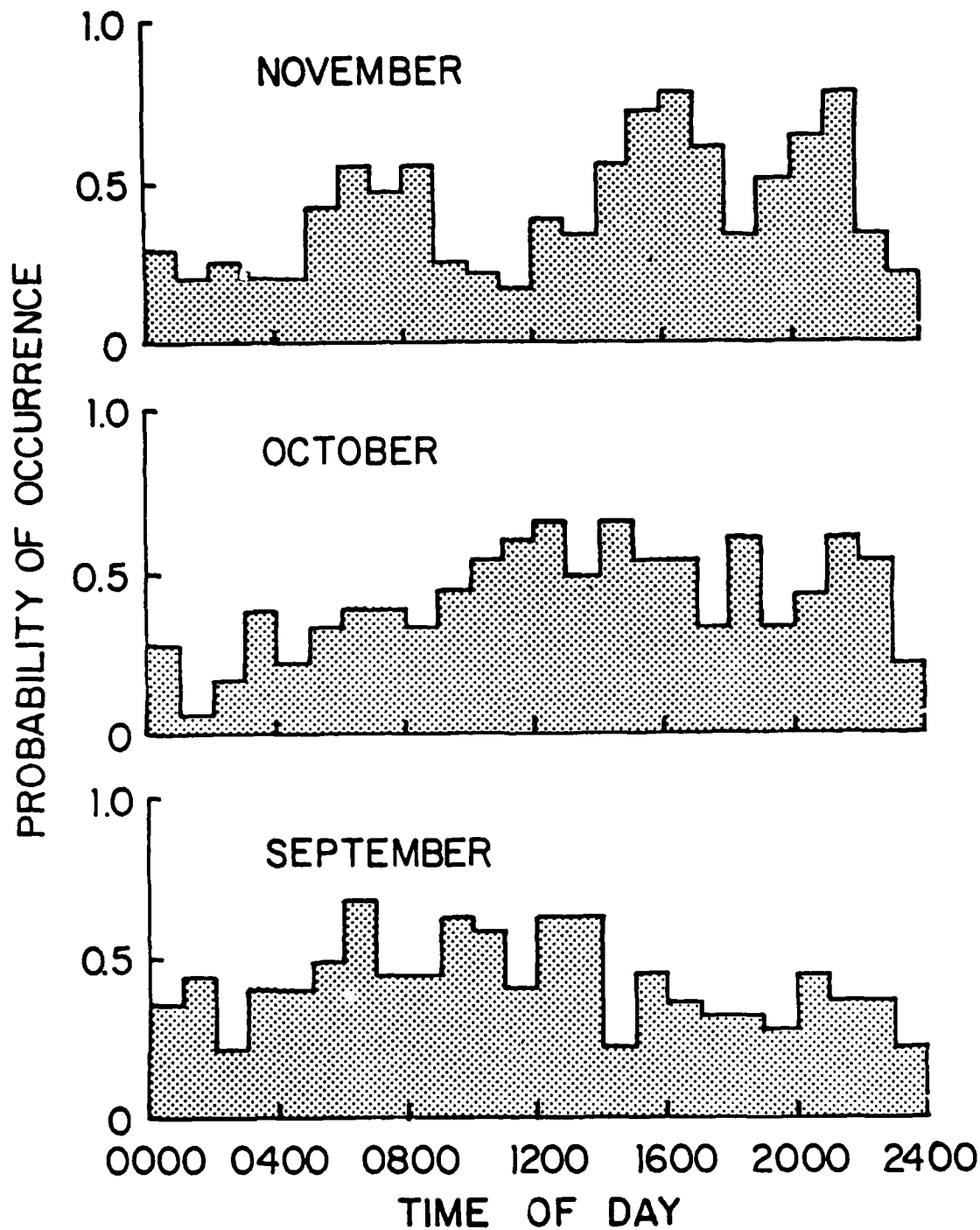


Figure 37c. Probability that a south wind, when it occurs, will be at a particular time of day (non-normalized).

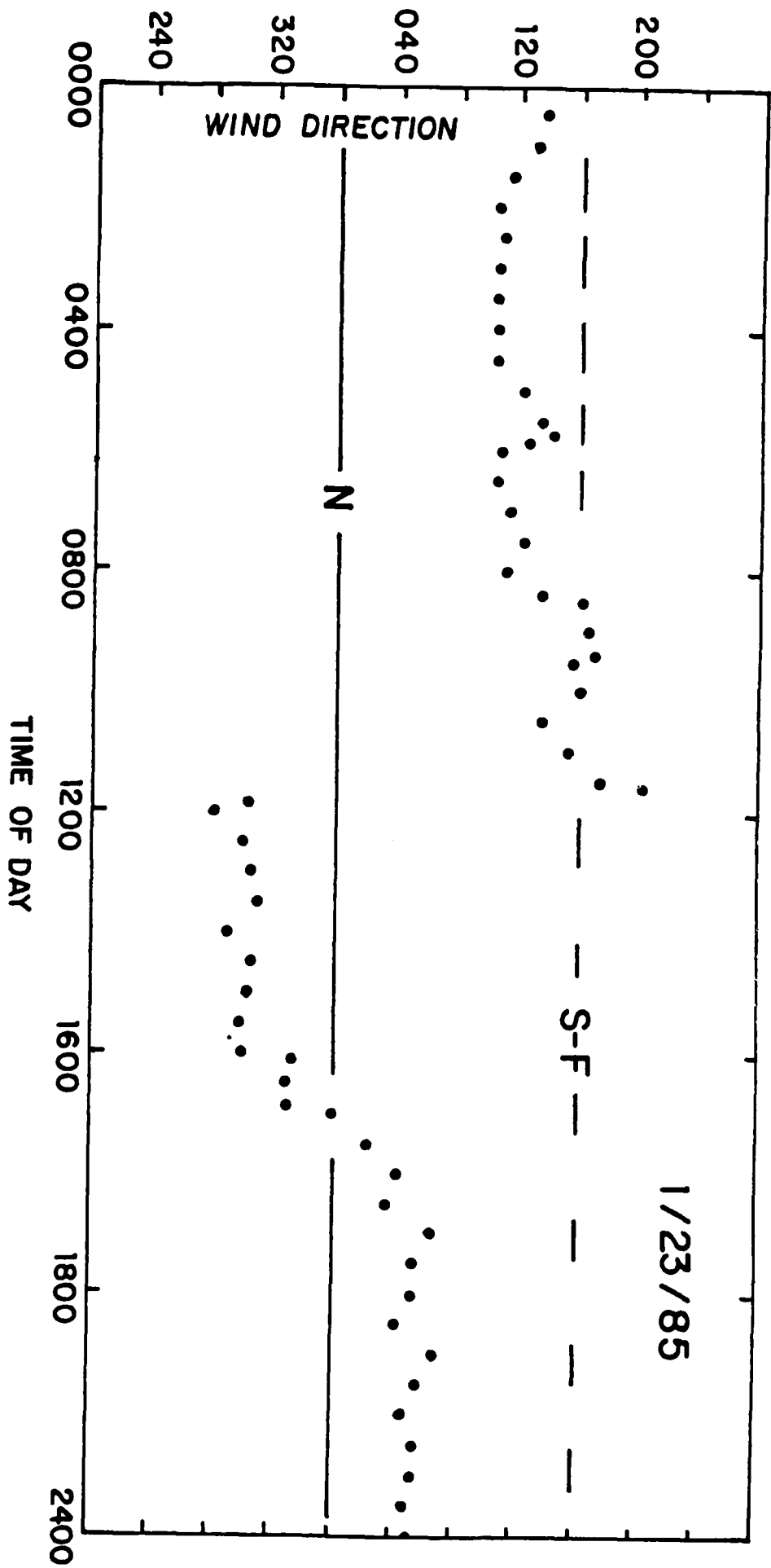


Figure 38. Flare stack wind direction as a function of time-of-day. S-F indicates the direction for which the flare from the South stack will impact on the North stack.

X. HEAT DEPOSITION CALCULATIONS

From the results of the analyses presented in this report, we have all that is needed to calculate the heat deposited by the flare, except the important quantities. This rather tongue-in-cheek statement is meant to impress the reader with the fact that we do not know some crucial parameters such as the hydrogen gas burn rate, plume temperature, plume size, etc. Thus, in what follows we have to treat many plume parameters as unknown symbols. It will be up to the engineers or flare modelers to supply the needed information.

In what follows, we will present methodologies for using our results to determine how much heat impacts an area due to the flow of hot gas over that area. The very important consideration of radiative heat transfer is not covered. Our basic assumption is that the heat produced by combustion (less radiative loss) is transported by the mean and turbulent flow to the impact point. The rate at which heat impacts a point is a direct function of the time the plume spends on that point. This time is the quantity that has been evaluated in this work.

1. General Considerations

In order to simplify our considerations, we will reduce the flare to as simple a set of parameters as possible:

F = flow rate

D = cross wind dimension

E = heat transfer efficiency

C = combustion rate
 L = heat loss rate (radiation)
 A = area on which heat is being deposited
 t = transit time from flare stack

Note that no attempt at rigor is being made here. We are ignoring the fact that some quantities are not constant with time and integration is needed. We merely wish to illustrate, in as simple a way as possible how the heat is created, spread out in the plume, and deposited. It is obvious that the person using our results will only use the very last of what we present: how the plume motion affects the heat deposition.

For a constant hydrogen flow rate, the gas is spread over a volume

$$V = \pi D^2 l, \quad (10)$$

where

$$l = U,$$

since one second of gas emitted is spread over a length equal to the wind speed. The total gas in the volume is

$$\text{amount of gas} = F.$$

The amount of heat contained in this volume is

$$Q = (C-L)t. \quad (11)$$

with

$$(Ct)_{\max} = F.$$

The rate at which this gas crosses a plane in space is

$$\begin{aligned}
 r &= Q/\text{time} \\
 &= Q/(l/U) \\
 &= Q.
 \end{aligned} \quad (12)$$

This is obviously true since the total amount of heat in the volume passes the plane in one second. The fraction of this heat that impacts the critical area is

$$\text{fraction} = A/\pi D^2. \quad (13)$$

Thus, the amount of heat which impacts the area each second is

$$R = (C-L)tA/\pi D^2. \quad (14)$$

The total heat transferred per sec is simply RE , and the total heat absorbed is RET :

$$H = [EAt(C-L)/\pi D^2]T, \quad (15)$$

where T = the amount of time the flame remains on area A .

For our considerations, we treat everything in the square brackets as engineering parameters, not to be discussed here. Note that the flow rate, does not appear unless the combustion rate is such that the total amount of hydrogen emitted has been oxidized during transit time t . Also, the wind speed does not appear because of the way the emitted gas is spread longitudinally.

Wind speed is an important parameter because it strongly influences D and T . D is due to relative diffusion of the plume about its centerline, and diffusion depends on the wind speed. The way in which T depends on wind speed can only be seen by examining what follows and the results presented in former sections.

The former sections deal with the motion of the centers of mass of air parcels, ignoring that the parcel has spatial extent.

This makes the determination of T not straight forward. The basic problem is that both the heat and hazard location are areas in space and the heat deposited depends on the overlap between these areas. This is illustrated in Figure 39. Also shown in the figure is the overlap area as a function of the separation between the centers of the areas. It does not matter which diameter is larger, the plume or hazard areas, the considerations are the same.

There may be cases where the location within the hazard area impacted by the heat is important. Such considerations are beyond the scope of this work. We will only deal with the overlap area in what follows and assume that the dashed line linear fit to the variation of the area with separation in Figure 39 is a reasonable approximation.

2. Use of Fraction of Time

The fraction of time allows one to calculate the total heat deposited over a period of time. Equation 15 can be rewritten as

$$H = K(A/\pi D^2)T, \quad (16)$$

which allows one to identify the area ratio and the deposition time as connected quantities. K is everything else in the square brackets in Equation 15. Assuming that the separation S_i exists for time T_i one can rewrite Equation 16 as

$$H = K(d^2/D^2) \left[\sum_i f(S_i) T_i \right], \quad (17)$$

where $f(S_i)$ is the fraction of the area πd^2 represented by the overlap area.

The T_i for a given S_i can be found from the fraction of time results. For a given set of meteorological conditions,

- a. determine σ , the fraction of time standard deviation
- b. $f = S_i/\sigma$ is the fraction of σ to be used in Table 3 for the error function to find
- c. $P(\text{within } f\sigma) = \text{erf}(f)$
- d. Then $T_i = [\text{erf}(S_{i-1}\sigma) - \text{erf}(S_i\sigma)]T$

$$= F(S_i)T \quad (18)$$

Using the above, Equation 17 can be rewritten as

$$H = KT(d/D)^2 \sum_i f(S_i)F(S_i) \quad (19)$$

As the final step in this approach, $f(S_i)$ can be easily found from Figure 39. Thus

$$H = KT(d/D)^2 \left[\sum_0^{D-d} F(S_i) + \sum_{D-d}^{D+d} (1 - [S_i - D + d]/2d) F(S_i) \right] \quad (20)$$

$$\begin{aligned} f(S_i) &= 1 & 0 < S_i < (D-d) \\ &= (1 - [S_i - (D-d)]/2d) & (D-d) < S_i < (D+d) \\ &= 0 & S_i > (D+d) \end{aligned} \quad (21)$$

Equation 20 can be rewritten as an integral by using the normal distribution. Also, the way d and D are utilized can be changed depending on the application. We leave the development at this point.

3. Use of Persistence Time

The use of the persistence time is simple if the overlap area does not change. Then one can use Equation 17 directly to obtain

$$H = K(d/D)^2 f(S) T_p, \quad (22)$$

where T_p is the persistence time. If $f(S)$ is changing the treatment is somewhat more complicated. Normally, one is

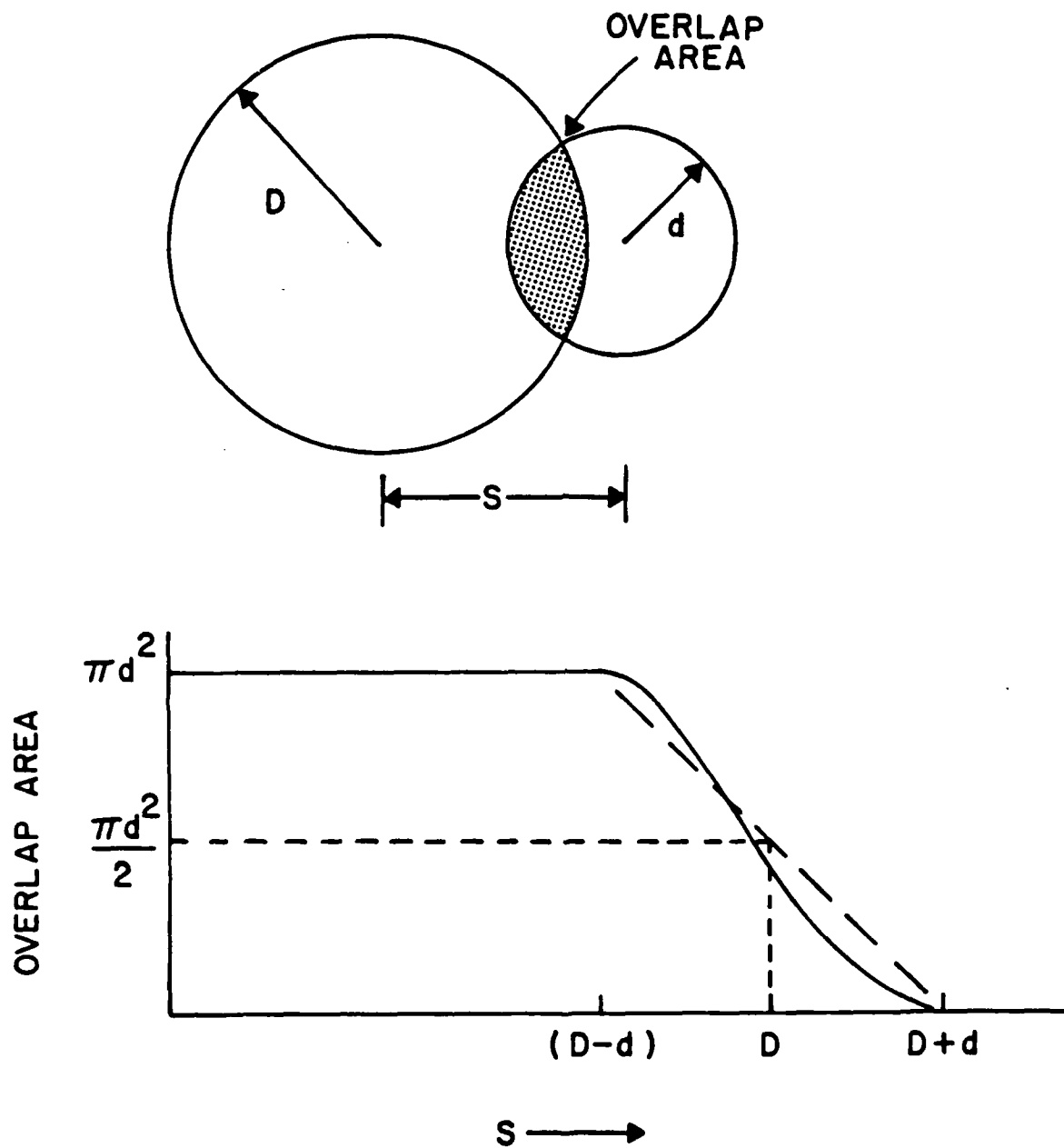


Figure 39. Geometrical picture of overlap between plume and hazard areas and overlap area versus center separation.

interested in the persistence of constant conditions because that is the meaning of persistence.

If a special situation must be addressed where the overlap changes, Equation 15 must be used in a piecewise fashion. Such a situation could be encountered when the area of interest is of unequal size in the horizontal and vertical directions. The extension of Equation 22 to such cases is obvious. A given situation, S , will persist for a time T_p , and one merely sums the cases up to the desired total S .

4. Non-Uniform Heat Deposition

For a large hazard area it may be of interest to know the heat deposition distribution on the area, not just the total heat. This is fairly simple to do using fraction of time. Also it may be done, independently, for either the horizontal or vertical directions. The error function approach, Equation 4, can be used to generate a heat distribution profile

$$H(S_a \rightarrow S_b) = KT(d/D)^2 [f(S_a) - f(S_b)], \quad (23)$$

where we have assumed that the overlap is constant for the direction under consideration. It is not valid to construct a profile from the error function if the overlap is changing since, in that case, the deposition is controlled by the overlap area.

It is also possible to construct a continuous heat deposition profile using the normal distribution, Equation 1. All that is needed to use the equation is to look up the appropriate standard deviation, σ . Care must be taken to insure that the heat is

properly normalized; the integral of the distribution must yield the total heat.

As an example of this procedure, we use a particularly important situation: South wind impact of the South flare stack on the North flare stack.

wind direction 140-200 deg.

wind speed 8 kts, 4 m/sec, 2-5 m/sec range

Vertical σ = 1.8 m for 20 sec from Table 4

Horizontal σ = 2.3 m for 20 sec from Table 4

We have arbitrarily chosen 20 sec as the time period of interest. It may be that this time is not the optimum one to use for damage to the north stack. It is necessary to separate the horizontal and vertical motions.

Horizontal Motion:

The stack is approximately 6 ft in diameter, which defines the horizontal hazard length. At this point there is a choice to make; either the fraction of time or persistence can be used. The normal procedure would be to use fraction of time in order to be consistent with the treatment to be used for the vertical motion. If the persistence method is used, a new time period, the horizontal persistence time for overlap of the plume and stack to go to zero (or near zero), will be found and should be used as the averaging time for the vertical fraction of time.

The diameter of the stack is 1m. For σ = 2.3 m the fractions of σ for 1 m and 2 m displacement, the error functions, and needed parameters are

<u>S_i</u>	<u>f</u>	<u>erf(f)</u>	<u>F(S_i)</u>	<u>f(S_i)</u>
1m	0.43	0.33	0.33	0.50
2m	0.98	0.61	0.28	0.19
3m	1.3	0.81	0.20	0

Recall that $F(S_i)$ is the difference in the error functions.

In order to obtain $f(S_i)$, the fraction of the plume area represented by the overlap of the plume and stack, we have arbitrarily taken the plume diameter to be 6 ft. This may be too small in which case the overlap will be smaller.

Using Equation 19, the total heat deposited in 20 sec is

$$H = K(20 \text{ sec})(1)[(0.5)(0.33) + (0.19)(0.28) + 0] \\ = 4.4K$$

This total heat is distributed in the vertical direction, up and down the stack, with approximately a normal distribution.

Vertical motion:

Rather than use the error function approach, it is easier to simply use the normal distribution function, Equation 1:

$$H(2) = (1/\sqrt{2\pi}\sigma)(4.4K)\exp[-(z-h)^2/2\sigma^2], \quad (24)$$

where $\sigma = 1.8$ m from above, h is the height on the stack where the plume impacts, and the constants in front insure the total heat deposited is 4.4K.

Impact Area:

Note that the above considerations can be used to determine the total area impacted by the plume. The normal distribution as

for both horizontal and vertical motion can be used to define an area within which the flare will spend 68% of its time. 95% of the time will find it within 2σ , which can reasonably be used to define the spread of the centerline position. Plume width due to dispersion is still needed.

XI SUMMARY

The purpose of this section is to summarize the more important results from this study. No attempt will be made to cover all of the results, for that the reader must examine the individual sections. We will mention results which deal generally with the flow and turbulence in the area and also results that are significant when assessing the hazard from the flare.

1. The predominant flow at the stacks is from the North due to influence from nearby hills. Preferred wind directions are almost exactly aligned with the North-South flare stacks line and with the direction from the stacks to the hydrogen dewar.
2. The elvation angle of the flow approximately follows the slope of the immediate terrain. This confirms that the mean flow will maintain the plume at approximately a constant height above the ground.
3. Wind direction fluctuations are of sufficient magnitude to drive air parcels a significant distance off the mean flow. The parcels can be driven to ground level about 5% of the time.
4. The end of the air parcel trajectory will spend about 70% of its time within 2-3 m of its average position.
5. Plume end statistics are closely approximated by the normal distribution.

6. The persistence of the trajectory end on a point follows a very regular behavior. Universal curves have been determined which relate persistence times for various displacements and are valid for both vertical and horizontal displacement, all wind speeds, and all wind directions.
7. Persistence times are of the order of 5 sec for 1 m displacement, 10 sec for 2 m displacement, etc.
8. Air trajectory fluctuations are highly dependent on wind speed and more weakly dependent on wind direction. Vertical and horizontal displacements are roughly the same, with horizontal being slightly larger.
9. Methodologies have been developed which allow heat deposition calculations to be made using simple equations and data tables from this report. Many of the engineering parameters needed to complete these calculations are not available here.
10. The heat deposition calculations described here are designed to determine the total heat transferred to a specific area. The general results presented in the report can also be used to determine how large an area will be impacted by the plume. This was briefly described in the section on non-uniform heat deposition.

DISTRIBUTION LIST

	No. of Copies
1. Prof. G. E. Schacher, Code 61Sq Department of Physics Naval Postgraduate School Monterey, CA 93943	10
2. Mr. Chuck Skupniewicz, Code 61 Department of Physics Naval Postgraduate School Monterey, CA 93943	20
3. Defense Technical Information Center Cameron Station Alexandria, VA 22314	2
4. Library, Code 0142 Naval Postgraduate School Monterey, CA 93943	2
5. Prof. K. L. Davidson, Code 63Ds Department of Meteorology Naval Postgraduate School Monterey, CA 93943	1
6. Dr. Torben Mikkelsen Department of Meteorology Naval Postgraduate School Monterey, CA 93943	1
7. LT Betty Hagan SD/CFAT Headquarters Space Division P.O. Box 92960 Worldway Postal Center Los Angeles, CA 90009	1
8. Dr. Ray Bernberg, M5-592 The Aerospace Corporation P.O. Box 92957 Los Angeles, CA 90009	1
9. Dr. Ron Bywater, M4-965 The Aerospace Corporation P.O. Box 92957 Los Angeles, CA 90009	1

10. S. B. Belknap, VAFB 1
The Aerospace Corporation
P.O. Box 92957
Los Angeles, CA 90009
11. Mr. S. Lewis, M5-592 1
The Aerospace Corporation
P.O. Box 92957
Los Angeles, CA 90009
12. D. Moody, M4-967 1
The Aerospace Corporation
P.O. Box 92957
Los Angeles, CA 90009
13. E. Ndefo, M4-964 1
The Aerospace Corporation
P.O. Box 92957
Los Angeles, CA 90009
14. D. Nelson, M4-967 1
The Aerospace Corporation
P.O. Box 92957
Los Angeles, CA 90009
15. T. B. Rehder, VAFB 1
The Aerospace Corporation
P.O. Box 92957
Los Angeles, CA 90009
16. J. R. Smith, M4-907 1
The Aerospace Corporation
P.O. Box 92957
Los Angeles, CA 90009
17. G. F. Widhopf, M4-965 1
The Aerospace Corporation
P.O. Box 92957
Los Angeles, CA 90009
18. LT COL R. R. Babcock, Jr. 1
DET 30, 2WS
Vandenberg AFB, CA 93437-5000
19. CPT Mike Buell 1
DET 30, 2WS
Vandenberg AFB, CA 93437-5000
20. LT R. Johnson 12
SATAF-EN
Bldg. 8500 ANNEX
Vandenberg AFB, CA 93437

21. Dr. E. S. Takle 1
Climatology/Meteorology
310 Curtiss Hall
Iowa State University
Ames, IA 50011
22. Dr. C. W. Fairall 1
Dept. of Meteorology
Walker Building
Pennsylvania State University
University Park, PA 16802
23. Dr. S. E. Larsen 1
Met-Physics Department
RISO National Laboratory
DK-4000 Roskilde
DENMARK
24. CPT J. Betchart 1
SD/CFAT
Headquarters Space Division
P.O. Box 92960
Worldway Postal Center
Los Angeles, CA 90009
25. Research Administration 1
Code 012
Naval Postgraduate School
Monterey, CA 93943

END

FILMED

2-86

DTIC

END

FILMED

2-86

DTIC